TAMPEREEN TEKNILLINEN YLIOPISTO
TAMPERE UNIVERSITY OF TECHNOLOGY

JANNIKA PAULAMÄKI

THE EFFECTS OF INHIBITING MECHANOTRANSDUCTIVE CELL SIGNALLING PATHWAYS IN HUMAN BONE MARROW STROMAL CELLS IN 2D VS. 3D CULTURE

Master of Science Thesis

Examiner: Assistant prof. Oommen P. Oommen and PhD Nick Walters
Examiner and topic approved on 9th of August 2017

ABSTRACT

JANNIKA PAULAMÄKI: The Effects of Inhibiting Mechanotransductive Cell Signaling Pathways in Human Bone Marrow Stromal Cells in 2D vs. 3D Culture
Tampere University of Technology
Master of Science Thesis, 80 pages, 0 Appendix pages
September 2017
Master's Degree Program in Bioengineering
Major: Tissue Engineering
Examiner: Assistant Professor Oommen P. Oommen and PhD Nick Walters

Keywords: mechanotransduction, stem cell, focal adhesion kinase, mitogen-activated protein kinase kinase, RhoA associated protein kinase, focal adhesions, stress fibers, non-muscle myosin II, inhibition

Mechanotransduction is the process of mechanical information transfer between a cell and its surroundings into biochemical responses. Involved in mechanotransduction are several components: extracellular matrix (ECM), transmembrane integrin receptors, focal adhesion protein complexes, and actin stress fibers. Through these complex interactions, cells can exert contractile forces and migrate, proliferate, change morphology and differentiate in the case of stem cells. It has been suggested in the literature that mechanotransductive effects vary between two-dimensional (2D) and three-dimensional environments (3D).

Objectives: In this study, four inhibitors were tested to determine the critical points (concentrations) affecting mechanotransduction. The used inhibitors were PF-562271, a focal adhesion kinase (FAK) inhibitor, PD98059, a mitogen-activated protein kinase kinase (MEK) inhibitor, Y-27632, a Rho-associated protein kinase (ROCK) inhibitor and (-)-Blebbistatin, a non-muscle myosin II (NMMII) inhibitor. Although all four inhibitors have previously been studied, critical concentrations at which these inhibitors affect human bone marrow stromal cell (hBMSC) survival is unclear. In addition, the effects on morphology and viability are poorly reported, both in 2D and 3D.

Methods: The critical points of four inhibitors were assessed based on two aspects: viability and morphology. Various concentrations of the inhibitors were applied to cell cultures for 24 h or 48 h. After the exposure time in 2D and 3D models, cells were imaged for morphological changes (n=2) and tested for their viability (n=5 and n=3, respectively). Tissue culture plastic/glass and rat collagen I hydrogel were used as a 2D and 3D models, respectively.

Results: IC50 was successfully calculated for FAK inhibitor in both 2D and 3D model (3.5 µM and 5.2 µM, respectively) and for Blebbistatin in 2D (28.5 µM). ROCK inhibitor had little effect on viability, but based on morphological changes IC50 of 6 µM was estimated. MEK inhibitor had no clear effect on viability or morphology of the cells.

Conclusion: Based on the results achieved in the present study, new information was obtained concerning all four inhibitors. In addition, the results correlate the hypotheses of the present study and the mechanotransductive signaling pathway hierarchy.

TIIVISTELMÄ

JANNIKA PAULAMÄKI: Mekanotransduktiivisten signalointipolkujen inhiboimisen vaikutukset luuytimen kantasoluissa 2D vs. 3D malleissa
Tampereen teknillinen yliopisto
Diplomityö, 80 sivua, 0 liitesivua
Syyskuu 2017
Biotekniikan diplomi-insinöörin tutkinto-ohjelma
Pääaine: Kudosteknologia
Tarkastaja: Apulaisprofessori Oommen P. Oommen ja tohtori Nick Walters

Avainsanat: mekanotransduktio, kantasolut, fokaaliadheesio kinaasi, mitogeeni-aktivoituva proteiinikinaasi kinaasi, RhoA proteiinikinaasi, fokaaliadheesio, aktiini-stressisäikeet, ei-lihasperäinen myosiini II, inhibointi

Mekanotransduktio on mekaanisen informaation muuntamista biokemialliseksi vasteeksi solun ja sen ympäristön välillä. Prosessissa on osallisena useita komponentteja: soluväliaine (ECM), integriinit, fokaaliadheesio proteiinikompleksit ja aktiini-stressisäikeet. Näiden yhteyksien kautta solu muodostaa solunsisäisen jännitteen ja kykenee liikkumaan, jakautumaan, muuttamaan morfologiaa sekä erilaistumaan kantasolujen tapauksessa. Kirjallisuuden mukaan mekanotransduktiiviset vaikutukset poikkeavat toisistaan kaksi- (2D) ja kolmiulotteisessa (3D) ympäristössä.

Tässä työssä pyrittiin määrittelemään kriittinen piste, konsentraatio, neljälle inhibiittorille, jotka vaikuttavat solun mekanotransduktion signalointipolkuihin. Valitut inhibiittorit olivat fokaaliadheesio kinaasi (FAK) -inhibiittori PF-562271, mitogeeni-aktivoituva proteiinikinaasi kinaasi (MEK) -inhibiittori PD98059, RhoA proteiinikinaasi (ROCK) -inhibiittori Y-27632, ja ei-lihasperäinen myosiini II (NMMII) -inhibiittori (-)-Blebbistatin. Kyseiset inhibiittorit ovat laajalti tutkittuja, mutta niiden kriittinen konsentraatio, joka vaikuttaa luuytimen kantasolujen selviytymiseen, on toistaiseksi selvittämättä. Lisäksi inhibiittorien vaikutuksista solujen morfologiaan ja elävyyteen on raportoitu vähäisesti niin 2D- kuin 3D-soluviljelymalleissa.

Neljän inhibiittorin kriittistä pistettä tutkittiin kokeellisesti tarkkailemalla solujen elävyyttä ja morfologiaa. Soluviljelmiä altistettiin useille inhibiittorikonsentraatioille 24 tai 48 tunnin ajan.). Altistumisajan jälkeen solujen morfologinen muutos kuvattiin (n=2) ja solujen elävyys mitattiin, niin 2D- kuin 3D-mallissakin (n=5, n=3). Soluviljelymuovia ja -lasia käytettiin materiaalina 2D-mallissa ja rotan kollageeni I hydrogeeliä 3D-mallissa.

Kriittinen piste määritettiin onnistuneesti FAK-inhibiittorille sekä 2D- että 3D-mallissa (3.5 µM ja 5.2 µM). Konsentraatio määriteltiin myös Blebbistatinille 2D-mallissa (28.5 µM). ROCK-inhibiittorilla ei havaittu olevan vaikutusta solujen selviytymiseen, sen sijaan solujen morfologia muuttui merkittävästi. Tämän perusteella kriittiseksi pisteeksi arvioitiin 6 µM. MEK-inhibiittori ei vaikuttanut merkittävästi elävyyteen eikä morfologiaan. Suoritetuilla tutkimuksilla tuotettiin uutta informaatiota kaikista käytetyistä inhibiittoreista. Lisäksi tulokset korreloivat työn hypoteeseja ja mekanotransduktiivisten signalointipolkujen hierarkiaa.

PREFACE

This Master of Science thesis was carried out between September 2016 and 2017 for the Adult Stem Cell group of BioMediTech Institute of Biosciences and Medical Technology, University of Tampere, Finland. I would like to thank Docent Susanna Miettinen and PhD Nick Walters for providing me this opportunity to do my thesis in this group.

My warmest gratitude goes to the “Mese group”. The academic research world was an intriguing but intimidating world to step into and you have all made it feel like home. A special thank you to Anna-Maija Honkala, Miia Juntunen and Laura Hyväri, who always had time for my questions and helped me through the laboratory work. I would also like to thank Kaisa Vuornos for providing the hydrogel material and for guiding me through the process.

I want to thank my family for their love and support through my degree and this thesis. They have always both inspired and encouraged me to perform to the best of my abilities and beyond. I couldn’t have done this without you.

Last but not least, there have been two extraordinary people by my side through the thick and thin of the past year. Hermanni, you have brought so much joy and happiness into my life and been so calm and strong through all the long nights and weeks. Thank you for being there for me. Henriikka, you are the best “partner in crime” anyone could ever hope for. Thank you for all the years we spent together at the university, all the long and longer projects written side by side, and thank you for keeping the both of us laughing when it was all that was left to do.

Tampere, 20.09.2017

Jannika Paulamäki

CONTENTS

LIST OF FIGURES

LIST OF TABLES

LIST OF ABBREVIATIONS

2D	Two-dimensional
3D	Two-dimensional
ATP	Adenosine triphosphate
BM	Basic medium
Col-I	Collagen Type I
DAPI	4',6-diamidino-2-phenylindole
ECM	Extracellular matrix
ERK, MAPK	Extracellular signal regulated kinase, AKA mitogen-activated protein kinase
ERM	Ezrin-radixin-moesin
ESC	Embryonic stem cell
FA	Focal adhesion
FAK	Focal adhesion kinase
FAT	FAK C-terminal focal adhesion targeting
FERM	FAK N-terminal 4.1 ezrin-radixin-moesin-domain
FN	Fibronectin
HA	Hyaluronic acid
hASC	Human adipose stromal cells
hBMSC	Human bone marrow stromal sell
hMSC	Human Mesenchymal Stromal Cell
iPSC	Induced pluripotent stem cell
LIMK	Lim kinase
MEK, MAPKK	Mitogen-activated ERK kinase, AKA mitogen-activated protein kinase kinase
MeMaHA	Methacrylate malemide hyalyronic acid
MLC	Myosin light chain
mMPC	Murine mesenchymal progenitor cell
mMSC	Murine mesenchymal stromal cell
MSC	Mesenchymal stromal cell
MyoD	Myogenic differentiation transcription factor
NMMII	Non-muscle myosin II
OCCC	Ovarian clear cell adenocarcinoma
OM	Osteogenic medium
PEG	Poly(ethylene glycol)
PPARγ	Peroxisome proliferator-activated receptor gamma
ROCK	Rho-associated protein kinase
Runx2	Runt-related transcription factor 2
siRNA	Small interfering RNA
Sox9	SRY-related high-mobility group box 9 transcription factor

TAZ	Transcriptional coactivator with PDZ-binding motif
TCP	Tissue culturing plastic
TE	Tissue engineering
WJ-MSC	Wharton's jelly mesenchymal stromal cells
YAP	Yes-associated protein

1. INTRODUCTION

The transfer of physical information concerning the extracellular matrix (ECM) to cells via biochemical signaling is called mechanotransduction. This information, connection and signaling takes part in regulating cellular behaviors such as homeostasis, migration and differentiation. Regenerative medicine and tissue engineering (TE) applications could, therefore, take advantage of this interaction by altering the physical properties of a culturing material and, hence, manipulate stem cell behavior. However, stem cell differentiation activating properties of ECM remain mostly unknown.

The mechanotransductive chain of complexes is connected to signaling pathways regulating cell behavior and fate. Among those signaling proteins are focal adhesion kinase (FAK), Rho-associated protein kinases (ROCK) and mitogen-activated protein kinase kinase (MEK), taking part in cytoskeletal organization, apoptosis and focal adhesion (FA) formation. These components regulating cell function and mechanotransduction can be inhibited using pharmacological, transient and reversible substrates.

The inhibitors affecting mechanotransduction were chosen from several stages of various mechanotransductive pathways: upstream activator FAK, downstream signaling protein MEK and ROCK, which are also key regulators of stress fibers, and structural factor Non-Muscle Myosin II (NMMII), controlling intracellular tension and contraction. The inhibitors are widely used and demonstrated in the literature. However, a critical point or an effective concentration at which cell survival and/or morphology is significantly altered has not been stated clearly. In addition, the results on the effects on viability, especially that of stem cells, have not been fully reported. Moreover, the morphological changes have not been stated for all the inhibitors.

To date, the majority of information concerning cell behavior and signaling has been gathered through two-dimensional (2D) experiments. However, in living tissues, the cues guiding the cells and mechanotransduction are typically provided in three-dimensional (3D) microenvironments. The two models provide very different environments for cells to grow and, therefore, the information taken from 2D experiments might not be translatable into TE and tissue culture applications. Hereby, experiments performed in two different models might vary in response.

The objectives of this study were as follows:

I. To determine the effects of various concentrations of inhibitors of mechanotransductive pathways on human bone marrow stromal cell (hBMSC) viability, following 24 or 48 h exposure.
II. To determine the effects of various concentrations of inhibitors of mechanotransductive pathways on hBMSC morphology, following 48 h exposure.
III. To compare the effects on viability and morphology between two different models 2D and 3D.

The aim of the objective I is to find a critical point where there is a significant change in the viability of the cells. This is executed by using various concentrations, selected in order to cover the range of reported concentrations in previous studies. The hypothesis is that a critical point affecting the viability of the cultures will be found for each inhibitor. The aim of the second objective is to use the same concentrations as in the objective I and to assess the morphological changes. The hypothesis of this study is that, since the signaling pathways are induced by mechanotransductive processes, morphological changes will be observed and recorded in the range of the critical point determined in objective I. Objective III uses two different models to study the difference between the dimensionality of provided mechanotransductive cues. It is hypothesized that there will be a difference between the two models on how the cells respond to the inhibitors and expected that the critical concentration is higher for the 3D model due to inhibitor diffusion.

This thesis includes a literature review on stem cells, mechanotransduction and connected signaling pathways. In addition, a comprehensive report is given on the previous studies performed using the chosen inhibitors. Here, the expected responses are also stated. Next the materials and methods are explained and the results are given. Finally, the discussion explores the results and their possible causes are speculated upon.

2. STEM CELLS

Stem cells are partially or completely undifferentiated cells with the capability to divide indefinitely and to produce progenitors with the potential to differentiate [1]. Due to these abilities, scientists have been highly interested to use stem cells for drug discovery, immunotherapy and regenerative medicine [2]. The potential of stem cells can be divided into three stages: totipotent, pluripotent and multipotent. Totipotent cells can divide and differentiate into all types of cells and can only be found in zygotes and early blastomeres. Pluripotent cells, such as embryonic stem cells (ESC) can generate all three germ layers and lineages: ectoderm, mesoderm and endoderm. These three germ layers are called multipotent and are more restricted in their path of differentiation. [1]

Mesenchymal stromal cells (MSC) have mesodermal origin and are multipotent. They were first discovered by Friedenstein and co-workers in 1968 [3]. These cells can be found in several somatic tissues: bone marrow (BMSC) [3], adipose tissue (ASC) [4, 5], Wharton's jelly in the umbilical cord (WJ-MSC) [6], dental tissue [7] and placenta [8], to name a few. Harvested MSCs have proven to be promising experimentally for TE applications and show potential to differentiate according to the mesodermal lineage *in vitro*. In other words, several experiments demonstrate the potential of MSCs to differentiate into adipogenic [9, 10], osteogenic [9, 10], myogenic [11] and chondrogenic [9] cells. These lineages and their tissue-specific protein expression, in addition to tissue-specific elasticity, are illustrated in Figure 1. In addition to their differentiation potential, MSCs are abundantly available in several adult tissues and therefore are readily available and free of the ethical issues concerning ESCs. There have also been reports over MSC transdifferentiation into ectodermal and endodermal lineages, showing differentiation potential towards neuronal cells [12], hepatocytes [13] and pancreocytes [14]. These results are highly interesting in terms of regenerative medicine and stem cell therapy, not to mention tissue engineering (TE).

Some of the activators of the signaling pathways leading to MSC differentiation remain uncertain. In the literature, differentiation *in vitro* has been simulated mostly by using chemical inducement but also through mechanotransduction, as chemical inducement might not be translatable to the *in vivo* situation, and could have carcinogenic effects. Several characteristics have been connected with fate commitment. Osteogenic differentiation is most commonly confirmed through the expression of runt-related transcription factor 2 (Runx2) [2, 5], whereas adipogenic fate commitment is characterized by the expression of peroxisome proliferator-activated receptor gamma (PPARγ) [15], among other indicators presented in Figure 1. In addition, chondrogenesis and myogenesis are positively characterized by the expression of SRY-related high-

mobility group box 9 transcription factor (Sox9) [2] and myogenic differentiation (myoD) [4], respectively.

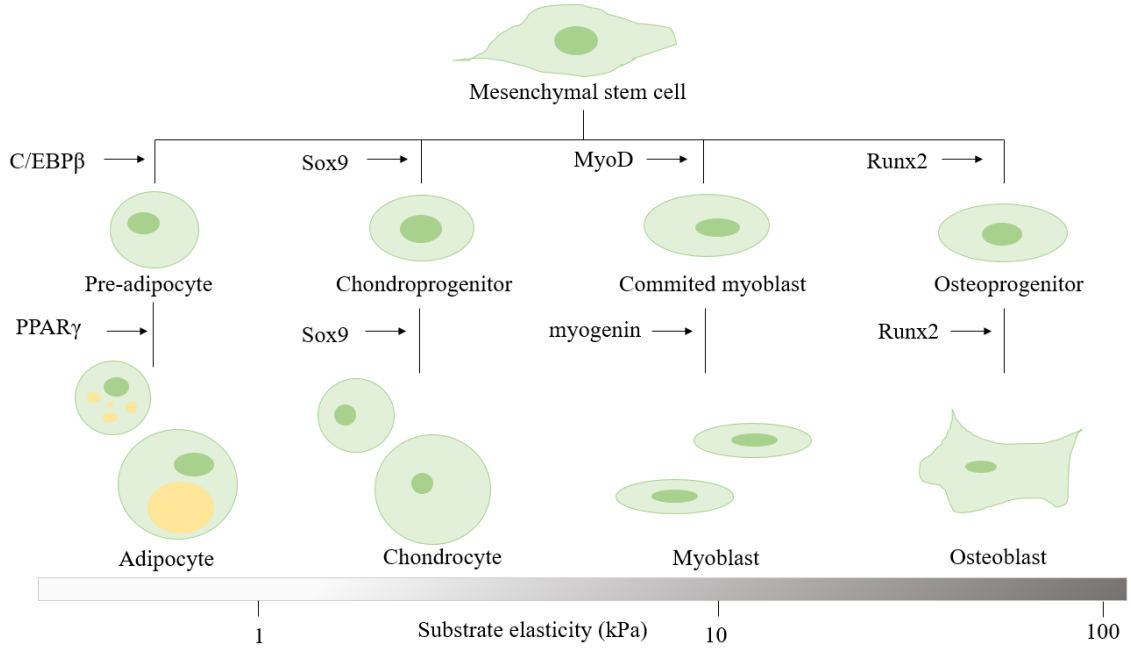

Figure 1. *Differentiation lineages of mesenchymal stem cells, their respective transcription factors and tissue-specific substrate elasticity. Adapted from [16].*

The fate commitment of stem cells has also been connected to morphological changes in 2D *in vitro* experiments. A flat and spread morphology is typically associated with osteogenic differentiation [17], whereas rounding of the cells is linked with adipogenic commitment [18]. As a contrast, cells committing towards neurogenic differentiation appear dendritic, with several protrusions [19]. In 3D, however, conflicting data exists as to whether these morphological indicators are directly translatable. This was demonstrated in a study by Clements et al. in which MSCs had a round morphology both in 2D and 3D hydrogel cultures (on top of and encapsulated within hydrogels), but showed significant signs of osteogenesis only in 3D cultures [20].

3. MECHANOTRANSDUCTION

Mechanotransduction is a bidirectional process of information transfer between a cell and its surroundings. In this process, mechanical stimuli provided by the environment are transferred into biochemical responses and behavioral changes within the cell. [21] The environment of the cell affects gene expression and subsequent behaviors via complex linkages, involving transmembrane proteins, numerous adaptor proteins and actin stress fibers. The biochemical response is delivered through several different signaling cascades, both in the cytosol and the nucleus. Mechanotransduction affects the cell's behavior in proliferation, migration, polarity and apoptosis. In addition, mechanotransduction is involved in the differentiation of stem cells. [22]

3.1 Extracellular matrix

ECM is the non-cellular material surrounding the cell. The ECM provides a physical scaffold for the cell to attach to and acts as a reservoir for biochemical cues such as growth factors and cytokines, which are required, for example, for homeostasis. The most common components of ECM are water, proteins and polysaccharides. For each tissue type there is a unique and specific composition and structure to the ECM that provides the ideal platform for tissue development and maintenance. The biophysical properties of ECM can vary in terms of its stiffness, elasticity and dynamic properties, such as stress relaxation. The dynamic properties provide the cells the possibility to remodel their environment either enzymatically (e.g. via matrix matalloproteinases, collagenases and hyaluronidase) or non-enzymatically, via hydrolysis. [23] For example, collagen and fibronectin, natural ECM proteins, are reported to be rearranged by the cells and usually align along the axis of the applied force. [24] Hence, it can be said that cells react to the extracellular cues received through mechanotransduction and remodel their environment.

In addition to remodeling the matrix, cells respond to mechanotransductive information by adapting to their environment. The mechanical properties of the ECM regulate tissue functions. For example, a sudden stiffening of the ECM has been reported to cause malignancy in the cells. Therefore, the tension and the elasticity of ECM, or scaffolding matrixes in tissue engineering, have been particularly well studied. One major focus of recent research has been the differentiation of MSCs, solely as a response to the matrix stiffness, independently from growth factors. [25]

Cells sense their ECM by applying force to it through attachments. The response is detected both in stress and in strain. For a rigid ECM, the response to the intracellularly applied force is followed by increased tension and little elasticity, which is detected by

the intracellular complexes, as the ECM does not yield in distance. For a softer matrix, the ECM deforms and therefore the intracellularly applied force responds slowly and elasticity is detected as a greater change in distance. [25]

For tissue engineering and regenerative medicine purposes, more translatable *in vitro* experiments are needed before ECM stiffness properties can be used in stem cell therapies. Polymeric biomaterials such as natural semi-synthetic hydrogels have been studied to provide scaffolds that better resemble the ECM of *in vivo* situations. The stiffness and porosity of these materials can be altered by varying cross-linking density. [26] Hydrogels are a novel interest of study, which could enable researchers to move away from the dominating practice of *in vitro* tissue culture plastic (TCP) use in cell culturing experiments in 2D. Hydrogels have been used both as coating materials to substitute TCP and to create 3D scaffolds, in which cells can be grown in a truly 3D environment. Some examples of 3D hydrogel materials that have been used include collagen I (Col-I) [27, 28] and hyaluronic acid (HA) [29]. In addition, synthetic biodegradable polymers, such as poly(ethylene glycol) (PEG) [30, 31] and poly(lactic acid) (PLA) [32] have been used to develop tissue engineering scaffolds [33].

3.2 Proteins implicated in cell-ECM interactions

The cellular proteins that take part in ECM-cell signaling and therefore participate in mechanosensing, can be divided into three subgroups: integrins; adaptor proteins in FAs, such as vinculin and talin; and actin stress fibers. Cells are attached to the ECM through integrins, which in turn are attached to adaptor proteins inside the cell. The adaptor proteins connect with stress fibers and the signaling proteins. All components are essential for a fully functioning process of mechanotransduction. The interactions are illustrated in Figure 2 and explained in the following chapters.

3.2.1 Integrins

Integrins are a family of cell surface receptors, composed of two non-covalently associated transmembrane glycoprotein subunits, α and β. Their expression is dominant in animal cells [34] in charge of sensing ECM properties and translating the information into intracellular signals that regulate cell growth, survival, migration and gene expression. [25, 35] The attachment of integrins on to the ECM proteins depends on the ECM properties and integrins' connection to the cytoskeleton.

The subunits of integrins have several isoforms and their combinations vary, depending on the ECM protein the cell attaches to. [21] Eight different integrins are capable of binding to fibronectin (FN), including for example α5-β1, whereas laminin is recognized by five integrins, including α7-β1. There are altogether nine β and 24 α isoforms. The

most common β isoform is β1, which forms dimers with up to 12 α isoforms. [34] Col-I is recognized by α2-β1 [36, 37].

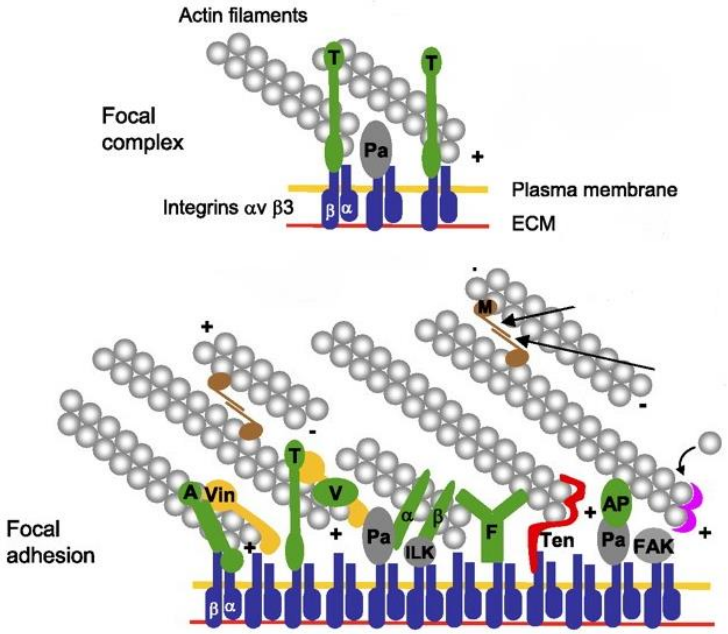

Figure 2. *A focal complex and a focal adhesion. Integrins presented in blue; adaptor proteins: vinculin (yellow), α-actinin, talin (green), paxillin and focal adhesion kinase (grey); stress fiber components: actin filaments as chains of pearls and myosin II in brown. Modified and reproduced with permission from ref. [38]), © American Physiological Society*

The binding of integrin to ECM ligands results in a conformational change in the cytoplasmic tail of the beta subunit, enabling it to bind with intracellular adaptor proteins. Actin subunits subsequently bind to the adaptor proteins and polymerize into stress fibers. [34] Clustering of integrins leads to the formation of FAs [35]. In order to function actively, integrins need to interact with intracellular stress fibers to bind strongly to the ECM. This connection is usually ensured by binding to bundles of actin filaments through FAs. However, the interaction with the ECM remains dynamic with a low binding affinity. This keeps the cells from binding too strongly to their surroundings and enables migration in addition to matrix remodeling. [34]

Integrin–ECM adhesion is not only required for cell attachment; the subsequent mechanotransductive processes in turn influence proliferation, cytoskeletal remodeling, migration and differentiation. Integrins bind to the ECM proteins and provide a platform for the cells to execute force-dependent processes, such as cell division. The initial binding affinity might be low, but when force is applied, either externally or internally,

integrins transition to high affinity conformation. Through this binding affinity adaptation, integrins have a major role in sensing the stiffness of the ECM. [25]

The role of integrin subunits in sensing matrix stiffness and differentiation was studied by Shih et al. by experimenting with α2 subunits. They demonstrated that cells in stiffer matrices had increased expression of integrin subunit α2. The group also tested the effects of α2 knockdown, which lead to a decrease in osteogenic expression. In addition, the study also reported downregulation of pFAK, pERK1 and pERK2, which demonstrates the connection between integrins and activated signaling proteins. The roles of ERK and FAK are explained later. [39]

3.2.2 Focal adhesion complexes

FAs are protein complexes formed on the intracellular side of the cell membrane after integrin attachment to the ECM. After binding to the ECM, the cytoplasmic tail of β subunit binds with FA proteins, including talin, tensin, paxillin and α-actinin. Some of these proteins then bind with vinculin, FAK, zyxin and filamin, which in turn lead to actin recruitment, stress fiber formation and cross-linking via α-actinin. [34] The tension in the integrin-ECM binding promotes the recruitment of cytoskeletal proteins to reinforce the integrin-actin connection [25]. There is a dynamic fluctuation in the complexes, which is mediated by the stiffness of the ECM.

Focal adhesion complexes can be divided into three groups: nascent adhesions, focal complexes and focal adhesions. Nascent adhesions are formed immediately after integrin receptors engage with the ECM. They are located at the leading edge of a migrating cell and have a fast turnover, either diminishing or evolving into focal complexes. [40] Focal complexes are small circular formations, about 2 µm in diameter, which can mature into FAs. [24] However, the maturation requires several adjacent integrins to bind to the ECM and cluster, in order for the adaptor proteins to be situated close enough to one another to interact [26]. FAs are more mature, larger and more elongated structures, with a width of 2µm and length of 3-10 µm [24].

FAs translate physical tension into intracellular biochemical signaling and are also involved in migration. First, extensions of the leading edge and nascent FAs are formed. Next, the maturation of FAs takes place and the cell body is translocated. Finally, FAs are disassembled and the rear of the cell retracts. [40]

Talin also binds with integrins and cytoskeleton. It is required to reinforce the linkage and the assembly of FAs in response to external force. The head domain of the protein binds directly with the cytoplasmic tails of some α and β isoforms of integrins. In addition, talin binds with FAK, the importance of which is explained later. Talin not only performs as a

link between the cytoskeleton and the ECM, but also increases the attraction between ECM and integrins. [38]

Paxillin is an adaptor protein family with three isoforms. It binds with vinculin and FAK. The protein also has a direct association with β1-integrin tail. Paxillin has several phosphorylation sites mediating cell migration and FA turnover. Its most important function is its implication in the efficient migration and motility of the cell. [41]

Vinculin is an actin filament binding protein. It has an auto-inhibition system, whereby the head interacts with the tail and masks the binding site for actin filaments. The activation and therefore the exposure of the binding site occurs when it binds with other FA proteins, such as talin and α-actinin. [38]

α-actinin is a homodimeric protein which crosslinks actin fibers into bundles. They are detected throughout the stress fibers, but they also interact with β-integrin tail and vinculin. They take part in controlling the stiffness of the fibers and transmit contractile forces. [38]

3.2.3 Stress fibers

The stress fibers are formed by bundles of actin filaments attached together by α-actinin and non-muscle myosin II (NMMII) [38]. Actin filaments form bundles of approximately 10–30 at a time. Unlike muscle cells, other cells do not present inherent polarity of the filament, meaning that there is not always a plus or 'barbed' end, and a minus or a 'pointed' end alternating in the bundle. However, the majority of motile cells have a uniform organization of barbed ends pointing outside. This means that the cells always depolymerize from the tail and polymerize at the leading edge during migration. [42] An actin depolymerizing factor, cofilin, attaches to the pointed end of the actin filament and changes its structure, leading to depolymerization of the pointed end. This also promotes the polymerization at the barbed end of the filament and, hence, regulates actin-based motility. [38]

There are three types of stress fibers: ventral and dorsal stress fibers and transverse arcs. Ventral stress fibers are the most common and attach to the integrin-rich FAs, which in 2D cultures with a high density of FAs are located at the bottom of the cell. Dorsal stress fibers attach to FAs at only one end, leaving the other end loose. Transverse arcs are located at the cell surface and connect with the dorsal loose end. [42] Given that this theory applies to planar 2D cell cultures, it may not directly translate into 3D systems, in which the cell is surrounded by a uniform matrix on all sides.

Non-muscle myosin II (NMMII) is a motor protein attached to actin filaments. [39] It pulls on the filaments through crosslinking and generates contractile force through the

actin bundles [21, 26]. The motion is driven by hydrolysis energy of adenosine triphosphate (ATP). The tension and contractile forces applied by NMMII are not only essential for sensing matrix and shear stress, but also necessary for embryonic survival, cytokinesis and intracellular stiffness generation. [39]

NMMII can be divided into three subgroups. NMMIIA is widely expressed across different tissues and has the highest rate of ATP hydrolysis. NMMIIB is mostly present in cardiac and neural tissues and has the highest adenosine diphosphate (ADP) affinity, giving it the longest period of binding. NMMIIC exists in epithelial cells. [39]

3.3 Effects of mechanotransduction on differentiation in 2D

Matrix properties and their effects on stem cell differentiation have been studied from various perspectives. The most common approach is to study differentiation based on the size, shape and/or stiffness of the provided substrate. Through size control, the cells are affected by limited area available for growth, whereas through shapes and geometrical patterns the formation of FAs are controlled by the density and localized arrangement of ligands available for attachments. In 2D, the stiffness of the surface affects the cells by the tension created between the ECM and the cells, which also affects their morphology. In 3D, stiffness also appears to have an important role, though it is less consistently associated with specific morphologies.

McBeath et al. studied the effect of 2D culture substrate area on hMSC morphology and differentiation. They found that when limited space was provided, the cells adopted a round shape and expressed proteins associated with adipogenesis. On the other hand, when space was provided in excess, the cells spread extensively and expressed proteins associated with osteogenesis. The study also stated that the highly-spread hMSCs showed more prominent stress fibers than the rounded ones. [18]

Kilian et al. studied the effect of geometric patterns on MSCs in 2D. The area of adhesive “islands” on an otherwise non-adhesive substrate was kept as a constant, but the aspect ratios of rectangles varied. As a result, osteogenesis was more dominant as the aspect ratio grew. Next, a pentagonal shape was experimented with variation in curvature, ranging from a star shape into a flower. The flower shape drove the cells towards adipogenic differentiation, whereas on the star shapes the MSC preferred osteogenic fate. It was also noted, that on star shapes FAs and stress fibers were larger than on flower shapes. [43] These geometries generally correspond to the level of spreading or polarization of cells undergoing differentiation down the corresponding lineages.

The effect of the stiffness of 2D culture surfaces was studied by Engler et al. hMSCs were plated on polyacrylamide gels varying in elasticity. Surfaces with three different elastic moduli were synthesized, mimicking brain tissue (0.1–1 kPa), muscle (8–17 kPa) and

collagenous bone (25–40 kPa). When cultured on these gels, the hMSCs showed both tissue-specific differentiation and morphology. [44]

3.4 Effects of mechanotransduction on differentiation in 3D

The effects of cellular microenvironment on differentiation in 3D remain unclear. Information on cell signaling and the effects of ECM stiffness have been widely studied in 2D, but with 3D cues the environment is much more complex. This was demonstrated by Kubow et al., who showed that not all 3D model FA characteristics, such as FA protein composition, can be seen in 2D models [45]. To date the key factors in 3D experiments have been the material compliance/stiffness, ligand presentation and degradation properties.

Huebsch et al. tested the effects of matrix rigidity on murine MSCs (mMSC) encapsulated in RGD-presenting alginate hydrogels. They detected that one week after encapsulation, the cells cultured in 11–30 kPa gels expressed osteogenic commitment, whereas the cells cultured in softer matrices (2.5–5 kPa) differentiated towards adipogenic fate. This, however, does not correlate directly, but is in line with the tissue specific elasticities. [46] Pek et al. demonstrated accordingly with PEG-silica hydrogels that hBMSC fate could be mediated through matrix stiffness. They also reported that the presence of RGD in the stiffer gels increased osteogenic commitment by 13 %. [47]

Khetan et al. experimented on the effect of compliance and degradation on hMSC fate commitment. They demonstrated that when a compliant matrix was provided, the cells would spread and undergo osteogenic commitment, whereas in non-compliant matrix the cells would remain round and signs of adipogenesis would increase. However, they also found that the non-degradable cross-linking combined with cell spreading lead to adipogenesis. This indicates that the morphology or spreading of the cells is not essential in fate decision in 3D, whereas the degradability and compliance of the ECM are. [29]

Jung et al. prepared composites, encapsulating not only hMSCs in four-arm PEG hydrogels, but also ECM proteins, Col-I, laminin-111 or FN, hereby providing hMSCs ECM proteins presenting ligands naturally. The differentiation experiments were coupled with 2D cultures provided with ECM protein coatings in addition to chemically induced differentiation. It was detected that, in general, adipogenesis increased in all composites. They also reported that, after 28 days, the Col-I composite significantly induced osteogenesis, adipogenesis and chondrogenesis when compared to both chemically induced and 2D coating cultures. The preference for adipogenesis could be explained by the stiffness of provided materials, a very soft modulus of only 0.9 kPa. The ECM protein-free PEG hydrogels failed to maintain expression of both adipogenic and osteogenic differentiation markers after 14 days. In addition, it was reported that viability in the ECM

protein-free PEG hydrogel was as low as 60 %. It could therefore be argued that the differentiation markers in those samples might be associated with apoptosis. As a conclusion, 3D composites induced differentiation in all but cardiomyogenic differentiation, but that this was only statistically significant in Col-I composites. [30] Thus the experiment highlights the importance of both stiffness and the presented ligands.

4. SIGNALING PATHWAYS

4.1 Focal adhesion kinase pathway

Focal adhesion kinase (FAK) is a tyrosine kinase located at integrin-enriched cell adhesion cites within FAs [48]. This protein takes part in several cellular functions through various signaling pathways, including migration [48, 49], cytoskeletal regulation [48], stem cell differentiation [16], proliferation and survival [49, 50]. The protein is composed of three functional domains: N-terminal 4.1 ezrin-radixin-moesin (FERM) domain, kinase domain and C-terminal focal adhesion targeting (FAT) domain. [48, 51] The structures, their targets and functions are listed in Table 1.

The FERM domain of FAK presents a structure similar to other cytoskeletal proteins, including talin and ERM proteins [48, 49], but also signaling molecules, such as JAK family of tyrosine kinases [49]. The FERM domain also binds with the cytoplasmic tail of integrin β1 and various growth factor receptors [49], including platelet-derived growth factor receptor (PDGFR) and epidermal growth factor receptor (EGFR) [48]. It has been hypothesized that the FERM domain of FAK could inhibit the activity of the FAK kinase domain. This has been supported by the enhanced activity of FAK kinase domain after the removal of FERM domain. [48, 49]

When the kinase or catalytic domain of FAK is phosphorylated, a structure is formed which is recognized by several SH2 domain-containing proteins. These proteins include Src-family kinases (SFKs), phospholipases Cγ (PLCγ), suppressor cytokine signaling (SOCS), growth factor receptor-bound protein 7 (GRB7), the Shr adaptor protein, p120 RasGAP and p85 subunit of phosphatidylinositol 3-kinase (PI3K). [48] The binding of FAK-Src leads to several tyrosine phosphorylations at multiple sites in FAK [48, 52, 53]. One phosphorylation target of the FAK-Src complex is p130Cas. The downstream signaling result of p130Cas phosphorylation is the increased activity of Rac, the regulator of membrane ruffling, lamellopodia formation and cell motility promotor [48, 51].

FAK-Src complex also phosphorylates tyrosines in the FAT domain. The phosphorylation of paxillin, an FA protein, occurs through this path. The phosphorylation of paxillin regulates FA turnover and migration [41]. The FAT domain phosphorylation also binds p190 RhoGEF, a Rho-family GTPase activator. RhoA is activated by p190 RhoGEF and, hereby, FAK has a direct link to RhoA signaling pathways. [48, 54] The other important protein, which binds to FAK after phosphorylation, is growth factor receptor-bound 2 (GRB2). This binding leads to activation of the Ras-Raf-MEK-ERK pathway. [48]

Table 1. *FAK domains, targets and functions.*

Domain	*Targets and downstream effectors (if known)*	*Function*	*Reference*
FERM	ERM proteins EGFR PDGFR	Activation through integrin contacts Suppression of kinase domain activation	[48, 49]
Kinase domain	Src	Phosphorylation of FAK at several cites	[48, 52, 53]
	p120RasGAP	Activation of Ras	[48]
	GRB7	Migration	[48, 51]
	p130Cas - Regulation of Rac	Membrane ruffling Lamellopodia Migration	[48, 51]
	p190 RhoGEF	RhoA-ROCL pathway regulation Stress fiber regulation Cell migration	[48, 54]
	N-WASP - ARP2/3 complex	Actin polymerization in the leading edge of a migrating cell	[51]
FAT	Talin	Focal adhesion activation	[55]
	Paxillin	Focal adhesion turnover Regulation of migration	[41]
	GRB2	Ras-Raf-MEK-ERK pathway regulation	[48]

4.2 Ras-Raf-MEK-ERK pathway

The Ras-Raf-MEK-ERK is a signaling cascade that transfers signals from the cell membrane to the nucleus [56, 57]. The pathway is implicated in cell cycle progression, proliferation, apoptosis [56-58] and differentiation [56, 59]. The cascade is regulated through several other interacting signaling pathways and is thought to have different effects, depending on the cell lineage [56].

The cascade starts with the activation of Ras, a small GTP-binding protein, which is an upstream molecule for several signaling pathways [57]. Ras is activated upon stimulation of Shr-Grb-SOS complex, which is coupled after the binding of cytokines, growth factors or mitogens to appropriate receptors in the cell membrane. Four Ras proteins have been identified: Ha-Ras, N-Ras, Ki-Ras 4A and Ki-Ras 4B. It has been suggested that the proteins have different abilities in activating the Raf-MEK-ERK cascade. For example, Ki-Ras appears to be a stronger inducer than Ha-Ras. [56]

Downstream kinase Raf is activated through a series of events, including recruitment to the plasma membrane through an interaction with Ras, dimerization and phosphorylation at several sites [57]. There are three members of the mammalian Raf gene family: A-Raf, B-Raf and Raf-1 (C- Raf). Ras and Src activity is required for maximal activation of A-Raf and Raf-1, but it seems that B-Raf is not dependent on Src. In addition, it is reported that B-Raf is more prone to mutations that take part in human cancers than A-Raf and Raf-1. When it comes to the signaling cascade of Ras-Raf-MEK-ERK, B-Raf is the most potent in activating MEK. It has also been suggested that B-Raf might take part in Raf-1 activation. The Raf-MEK-ERK signaling pathway is regulated positively and negatively by additional transduction pathways such as the Ras/PI3K/PTEN/Akt pathway. [56]

Mitogen-activated ERK kinase (MEK), which is also known as mitogen-activated protein kinase kinase (MAPKK) [59], is positively induced by Raf [56, 57]. MEK1 and MEK2 are the two recognized forms of MEK. [57] Together, they are the only dominant upstream activators of ERK. [56, 59]

Extracellular signal regulated kinase (ERK), or mitogen-activated protein kinase (MAPK) [59] is activated by dual phosphorylation on tyrosine and threonine residues, separated by a glutamate residue [59]. As a result of activation, two forms of ERK are met: ERK1 and ERK2. The difference in targets *in vivo* of the two molecules are yet rather poorly understood. However, it would seem that ERK2 drives more proliferative effects, whereas ERK1 has more anti-proliferative effects. [56]

Activated ERKs affect various cellular behaviors via phosphorylation of several transcription factors, such as Ets-1, c-Jun, NF-κB, AP-1 and c-Myc [56]. It has been reported that these phosphorylated transcription factors induce the expression of genes

related to cell cycle progression, including Cdks, cyclins and growth factors, in addition to preventing apoptosis. [57] ERKs are also responsible for the activation of $p90^{Rsk}$ through phosphorylation, causing the activation of cyclic AMP-responsive element binding protein (CREB) [56, 57], a transcription factor which regulates the CAMP signaling pathway. In addition, it takes part in signal transduction induced by Ca^{+2}, growth factors and stress signals. [57]

ERK also has an effect on apoptosis by regulating post-translational phosphorylation of apoptotic regulatory molecules Bad, Bim, Mcl-1, caspase 9 and Bcl-2. [56] The signaling pathway can inactivate Bad by phosphorylation at residue S112, which enables Bcl-2 to form homodimers and leads to an anti-apoptotic response. An anti-apoptotic response is also achieved by phosphorylation of Mcl-1. On the other hand, through phosphorylation of the pro-apoptotic Bim, apoptosis is inhibited, as the protein is dissociated from Bcl-2 and Mcl-1 and targeted to proteasomes. Hereby Bcl-2 and Mcl-1 bind with Bax, preventing it from forming homodimers and inhibiting apoptosis.

It has been suggested that ERK regulates Runx2-mediated gene transcription alongside JNK. This is explained by the signaling coupling with transcriptional coactivator with PDZ-binding motif (TAZ) and Yes associated protein (YAP), which are stimulated by stiff ECM, leading to their co-localization to the nucleus and subsequent osteogenic differentiation. TAZ and YAP are effector proteins in the Hippo signaling pathway, which affects proliferation, tumorigenesis and stem cell self-renewal [58]. In addition, studies have shown that ERK phosphorylates PPARγ and therefore restricts adipogenesis [59].

Abnormal activation of Raf-MEK-ERK has been associated with some human cancers. This is due to mutations at upstream membrane receptors Ras and B-Raf or in the interacting transduction pathways (eg. Ras/PI3K/PTEN/Akt) which regulate Raf activity. According to the literature, the malfunction of Raf-MEK-ERK pathway can have various affects depending on the cell lineages. For example, in hematopoietic cancers, the signaling pathway promotes proliferation, but it is inhibited in several prostate cancer cases. The varying effects could be explained with coupling protein mutations such as PTEN and p53 pathway. Abnormal function of the signaling pathway has also been reported to cause drug resistance. [56]

4.3 RhoA-ROCK pathway

RhoA is part of Rho family of small GTPases, which is activated through G protein-coupled receptors (GPCR). Activators, such as lysophosphatidic acid (LPA) or sphingosine-1 phosphatase (S1P), stimulate guanine nucleotide exchange factor (GEF), which leads to an active GTP-bound Rho. [42, 60].

RhoA activates Rho-associated protein kinases (ROCKs) through Rho-binding domain (RBD) [60, 61]. The kinases can also be activated by arachidonic acid and caspase-3 [61]. ROCKs have been found to be involved in several cellular responses, such as cellular growth, migration, metabolism and apoptosis, through actin cytoskeleton assembly, disassembly and contraction [60, 61]. ROCKs are naturally inhibited in the cells by RhoE, Gem and Rad [42].

The ROCK family can be divided into two subgroups: ROCK1/ROCKbeta and ROCK2/ROCKalpha [61] ROCK1 is reported to be ubiquitous, but with higher expression levels in non-neuronal tissues such as liver, lungs and testis. ROCK2 is also widely expressed, but occurs at higher levels in cardiac, brain [60] and muscle tissues [61].

The regulation of actin cytoskeleton by ROCKs takes place through phosphorylation of myosin light chain (MLC) phosphatases. ROCKs phosphorylate myosin phosphatase-targeting subunit 1 (MYPT1), which decreases the activity of MLC phosphatases and increases the amount of phosphorylated MLC. This leads to interactions between myosin and F-actin, causing cell contraction and FA reinforcement. [61]

Actin stress fiber formation is also controlled through LIM kinases (LIMK). Cofilin is an actin binding and actin depolymerizing protein, which controls the turnover of actin filaments. ROCK1 phosphorylates LIMK1 and LIMK2, which in turn phosphorylate cofilin [60, 61], inhibiting its action and therefore increasing the number of stress fibers. ROCK2 is necessary for phagocytosis and cell contraction. It phosphorylates ezrin-radixin-moesin (ERM) proteins, which leads to the disruption of a head-to-tail association of the proteins and causes actin cytoskeletal reorganization and crosslinking with transmembrane proteins. [61]

In the literature, there are several references to ROCKs being the dominant regulator of cell polarity. ROCKs impair the formation of protrusions and extensions of the membrane all but in the leading edge of the cell. This has been explained by the phosphorylation of PAR3, which is a component of the PAR polarity complex. The phosphorylation by ROCKs indirectly prevents the formation of extensions by Rac. [61]

The abnormal behavior of RhoA-ROCK signaling has been connected to cardiovascular diseases. In the vascular wall, ROCK mediates smooth muscle contraction through actin cytoskeletal organization, cell adhesion and motility. Therefore, it can be said that increased ROCK activity leads to tumor metastasis and overexpression of activated ROCK causes tumor invasion. [60]

5. INHIBITION

5.1 FAK inhibitor - PF-562271

In the literature, several molecules have been reported to inhibit FAK. One of these is PF-562271, which shows effective inhibition of the kinase activity of FAK with a high degree of selectivity. PF-562271 shows significant promise in tumor therapy. The inhibitor has been reported to cause tumor stasis in mouse models of prostate, breast, colon, lung, glioblastoma and pancreatic cancers. The tumors show an increase in apoptotic cells. [54] In 2012, PF-562271 was the first FAK inhibitor to have been tested in phase I clinical trials. [62]

By description of the manufacturer and other reports, PF-562271 is a potent ATP-competitive reversible inhibitor of FAK and Pyk2, achieving an IC50 of 1.5 nM and 13–14 nM, respectively, in cell-free studies. [63-65] IC50 is a concentration of an inhibitor causing 50 % of the maximum effect. However, when tested in a cell culture environment, the IC50 values range from 0.277–49.89 μM, depending on the cell line. [63] hMSCs were not listed among the tested cell lines.

PF-562271 treatment abrogates proliferation and decreases viability. Roberts et al. exposed human prostate cancer cell line PC3-M to PF-562271 for 48 hours and detected significant G1 cell cycle inhibition at a concentration of 3.3 μM [64]. On the other hand, Yoon et al. applied several concentrations of PF-562271 to ovarian clear cell adenocarcinoma cell line OCCC and reported 50 % loss of the cultures lowest at 3–6 μM and highest at 6–12 μM concentrations. [66] It should be noted, that the cells were induced with a copy number gain of *FAK* gene to study overexpression. This disturbance both in proliferation and viability could be explained by a lack of FAs, as the key mediator in assembling was inhibited. The decrease in FAs both disrupts the necessary tension needed for cell growth in cell cycle and in cytokinesis. Moreover, without FAs the anchorage-dependent cells would die due to anoikis. The details of some 2D *in vitro* studies of PF-562271 are listed in Table 2.

As PF-567221 has been used in clinical trials, several studies have been implemented *in vivo* instead of *in vitro*. Roberts et al. provided several different doses of the inhibitor to human glioblastoma-bearing mice. They reported an IC50 of 93 ng/mL. In addition, the study described a significant increase in apoptosis of lung cancer tumor xenografts after treatment with 25 mg/kg twice, daily, for three days. [64] Sun et al. reported tumor suppression both in local implants and xenograft models after being given five doses per week for up to two weeks in mice. [65] It is argued that the primary mechanism of tumor suppression with PF-562271 is anoikis. Bleomycin-induced lung fibrosis mice were

treated with PF-562271 (15 mg/kg, twice daily) and showed similar structure to the control lungs with little tissue fibrosis or abnormality in pulmonary structure after 21 days. The abrogation of lung fibrosis achieved in a comparative test with small interfering RNA (siRNA)-mediated FAK knockdown. [62] Some *in vivo* studies of PF-562271 are listed in Table 3.

Table 2. *2D in vitro studies of FAK inhibitor PF-562271.*

Cell type	*Concentrations*	*Time-point*	*Outcomes*	*Reference*
PC3-M	3.3 µM	48 h	G1 cell cycle inhibition	[64]
OCCCs	0–50 µM	72 h	50 % decrease in viability at 3–6 µM or 6–12 µM	[66]
HUVECs	10 µM	30 min	Decrease of pFAK	[67]

The probable responses to inhibitor exposure can also be predicted based on other FAK-related experiments, such as those involving genetically modified mice or the use of siRNA. The role of FAK's kinase domain was studied by injecting HUVECs with FAT-containing C-terminus of FAK, without the kinase domain. The FAT sequence was delivered with GST-beads and performed through competitive binding, inhibiting FAK entry into FAs. It was detected that the endogenous FAK in FAs decreased, but did not affect the localization of other FA proteins such as vinculin and talin. Therefore, it was suggested that FAK might work as a signaling protein due to the formation of FAs, rather than performing as a mediator in their assembly. However, it was recognized that the inhibition of FAK prevents cell cycle progression and that FAK supports the survival of adherent cells. [68]

Table 3. *In vivo studies of PF-562271.*

Cell type	*Concentrations*	*Time-point*	*Outcomes*	*Reference*
Tumor xenografts	25 mg/kg daily doses	3 days	Significant increase in apoptosis	[64]
Tumor xenografts	25 mg/kg, 5 doses a week	2 weeks	Tumor suppression, local implants and xenograft models	[65]
Mice, bleomycin-induced lung fibrosis	15 mg/kg twice daily	3 weeks	Attenuation of fibrosis	[62]

Salaznyk et al. transfected hBMSCs with FAK siRNA. After eight days of culture, the relative Runx2 phosphorylation was quantified. In osteogenic medium (OM)-treated cultures there was a significant difference between the control and siRNA-treated cells, showing decrease of Runx2. The same was detected after the tissue culturing plastic was coated with either FN, Col-I or vitronectin. Moreover, the phosphorylation of ERK decreased after FAK siRNA treatment. The siRNA treatment blocked Osterix transcriptional activity and prevented osteogenic differentiation. These results indicate that FAK has a role in osteogenic differentiation. [69]

Mouse embryos with either wild-type FAK+/+, FAK+/- or FAK-/- expression were compared in terms of size and other visible changes after E8.0 (embryos aged 8.0 days old). The embryos with FAK+/- and FAK-/- expression appeared smaller in size than those with FAK+/+ expression. The FAK-/- embryos did not survive beyond day E9.0, and after E11 the FAK+/- became indistinguishable from those with FAK+/+. The knockout cells also showed multiple and fragmented nuclei. However, there was no evidence of changes in actin expression. In addition, the same group studied the dependence between FAK and p53. After seven days' growth, FAK-/- embryos showed stronger expression of p53 than the two other genotypes. Moreover, the knockout of p53 increased the proliferation of FAK-/- significantly. The relation was also tested with human fibroblasts and it was detected that after short hairpin RNA (shRNA)-treatment targeting FAK, the expression of p53 increased. Therefore, it was concluded that FAK controls human fibroblast proliferation and p53-dependent apoptosis. [53]

Castillo et al. compared two types of primary immortalized osteoblastic clonal lines expressing either wild type FAK or FAK-/- mutation. No difference in actin cytoskeleton was detected but the mean number of FAs per cell area was significantly lower in FAK-/- cultures. [55] Some other experiments on FAK activity are summarized in Table 4.

Table 4. *Reported experiments on other FAK disruption.*

FAK disrupting format	*Model*	*Format*	*Time-point*	*Outcomes*	*Reference*
FAK provided without kinase domain	2D	HUVECs	2 h	Decrease in proliferation	[70]
FAK +/+ vs. FAK +/- vs. FAK -/-	2D	Mouse embryos	7 days	Multiple and fragmented nuclei in cells	[53]
FAK shRNA	2D	Human fibroblasts	72 h	Increase in p53 expression	
FAK siRNA	In vivo	Bleomycin-induced lung fibrosis	N/A	Decrease in FAs	[62]
FAK+/+ vs. FAK-/-	2D	Fibronectin-coated coverslips	24 h	FAs/cell area decreased significantly	[55]

5.2 MEK inhibitor - PD98059

The targeting of MEK is advantageous as it is the upstream dominant kinase of ERK. Hence, the inhibition of MEK blocks several downstream signaling pathways of ERK, preventing the activation of several transcription factors. In other words, MEK serves as a bottleneck in cell signaling which, when interrupted, can have a knock-on effect on multiple pathways. [56] In the literature, many MEK inhibitors are mentioned and in the present study PD98059 was used. The manufacturer reports an IC50 of 2 μM in a cell-free assay, but presents several studies using concentrations in the range of 2–100 μM. PD98059 inhibits MEK activation of ERK1 and ERK2, but does not interrupt ERK directly. It should be noted that the inhibitor does not affect Raf-1 phosphorylated MEK1. [71] Successful ERK inhibition has not been reported. As there are two known ERK molecules, ERK1 and ERK2, with indication to different targets, specific ERK inhibitors could be useful in the future, when it comes to treatment of diseases. [56]

Roberts and Der discussed the possibilities of MEK inhibitors in cancer treatment in 2007 and suggested that the potential is great due to the signaling cascade's major role in a normal cell's proliferation, survival and differentiation [72]. However, in the literature there is very little reported on experiments concerning the viability or morphological changes of PD98059 treated cells. The differentiation potential of MEK inhibitor-treated

cells, on the other hand, is quite well demonstrated. Several studies concerning the differentiation of PD98059-treated cells are summarized in Table 5.

Jaiswal et al. cultured hBMSCs in 2D in OM conditions, resulting in an even ratio between osteogenesis and adipogenesis. When a culture was exposed to 50 µM of the inhibitor, adipogenesis increased in a dose-dependent manner after 16 days. The results were confirmed both histologically and biochemically. Hereby, it was concluded that ERK has an important role in osteogenesis. [59] Concurring results were presented by Salaznyk et al. However, the group used ECM protein-coated culture surfaces and demonstrated significant decrease in the expression of osteogenesis indicator Runx2 after 8 days. [69] Liu et al. demonstrated that these results also applied to hASCs, the alkaline phosphatase activity of which decreased after exposure to 50 µM of the inhibitor after 14 days. However, they did not manage to show adipogenic commitment, except when OM was provided with Dex. [73]

Table 5. *Summary of studies on differentiation with PD98059.*

Cell type	*Model*	*Concentrations*	*Time-point*	*Outcomes*	*Reference*
hBMSC	2D, OM	10, 25, 50 µM	16 days	Adipogenesis in dose-dependent manner	[59]
hBMSC	2D, FN, VN, Col-I	50 µM	8 days	Decrease in Runx2 expression	[69]
hBMSC	2D, Col-I, mechanical strain	50 µM	5 days	Strain-induced calcium phosphate levels decreased, adipogenesis upregulated	[74]
hASC	2D, OM	10, 25, 50 µM	14 days	Decrease in osteogenesis, adipogenesis only after OS CI and Dex	[73]
hMSC	3D, Col-I	50 µM	7 days	Enhanced expression of osteogenic gene markers, hydrogel compaction	[75]

Ward et al. investigated an additional factor by applying mechanical strain to Col-I-coated culture surfaces. They also reported on other differentiation pathways. Upon application of strain, the BMSCs showed increased osteogenic expression, whereas adipogenesis, chondrogenesis and neurogenesis decreased and myogenesis fluctuated over several time-points up to five days. A concentration of 50 μM of MEK inhibitor had the opposite effect and reduced calcium phosphate levels, an indicator of osteogenesis, and induced non-osteogenic expression, such as adipogenesis, neurogenesis and myogenesis. [74]

The 2D studies presented so far contrast with the results by Lund et al. under 3D conditions. In this study, MSCs were cultured in Col-I hydrogels and conditioning with 50 μM inhibitor enhanced the expression of osteogenic markers significantly when measured after 7 days, with a concurrent lack of adipogenic marker expression. [75]

There have been several studies of the inhibitors' effects on cell cycle and proliferation from previous years. Liu et al. exposed human osteosarcoma cells to the inhibitor at 50 μM, which induced an anti-proliferative effect after 24 hours. This was confirmed by following G1 and G2/M phase arrest through both protein and mRNA expression levels of G1 phase. [73] The results were aligned with a separate study from Cui et al. with human dermal fibroblasts. They reported decrease in proliferation after four days. [76] Studies on proliferation involving PD98059 are summarized in Table 6.

Table 6. *Summary of studies on proliferation with PD98059*

Cell type	*Model*	*Concentrations*	*Time-point*	*Outcomes*	*Reference*
Human osteosarcoma cells	2D	50 μM	24 h	Proliferation arrest	[73]
Human dermal fibroblasts	2D	50 μM	4 days	Proliferation decrease	[76]

Based on previous studies presented here, two conclusions can be drawn. First, the inhibitor concentrations used vary very little and therefore it would be useful to study a wider range of concentrations. In the literature, it was mentioned that a concentration of 10 μM decreased the phosphorylation of ERK after 30 min, and therefore lower concentrations should also be experimented on. [67] Second, most of the previous studies concentrate on the changes in differentiation behavior after inhibitor exposure. ERK has, however, been shown to be affected by integrin activity and mechanotransduction. For both of these reasons, the effects on viability and morphology should be studied and a broader range of concentrations should be used.

5.3 ROCK inhibitor - Y-27632

According to Amano et al., inhibiting ROCK results in three visible changes that can be detected in cell cultures: disturbed stress fiber formation, lack of cell polarization and abnormalities in cytokinesis. As ROCK is responsible for the maintenance of stress fibers and contractility via MLC phosphorylation and LIMK activation, the use of inhibitors is expected to lead to disorder of stress fibers. The polarity of a cell is essential for migration, and since ROCK controls the polarization and leaves a cell with only one leading edge, inhibition would most likely cause random protrusion formation, leading to multiple leading edges. Tension and contraction are both key elements for cell division, especially in cytokinesis, when a cell is divided into two daughter cells by an actomyosin-based contractile ring, the assembly, stability and disassembly of the cleavage furrow. The inhibition does not, however, arrest cytokinesis, but causes delays in division and abnormalities in cultured cells. [61]

There are two reported ROCK inhibitors in the literature, Y-27632 and Fasudil, but on several occasions, the overexpression of dominant negative mutants of ROCKs has also been used as an approach to inhibit the pathway. These inhibition tactics for ROCK have resulted in loss of stress fibers and focal adhesion complexes. [61, 77] In the present study, Y-27632 was chosen as the inhibitor of ROCK and will be later on referred to as ROCK inhibitor. The manufacturer describes the inhibitor as a selective ROCK1 inhibitor with the potential to also inhibit ROCK2. However, no IC50 is given. Instead, the binding affinity (K_i) of the ROCK1 and ROCK2 inhibitors are stated as being 140 and 300 nM, respectively. [78]

There are several reports on morphological changes and protrusion formations in cell cultures after Y-27632 treatment. Ishizaki et al. cultured Swiss 3T3 cells with 10 µM of the inhibitor and detected actin fiber dissolution after 30 min of exposure. After 24 hours of treatment, thin F-actin bundles reappeared, but thin processes were visible in the cultures. The processes were compared to long neurite-like processes, composed of microtubules and intermediate filaments. The cause of process growth was explained by the loss of tension in ROCK-mediated contractile actomyosin filaments. [79] Worthylake et al. treated human primary monocytes with several concentrations of the inhibitor and reported morphological abnormalities in a dose-dependent manner. The cells showed detectable tails with doses as low as 1 µM. The tails were more apparent and longer when the concentration was increased. [80] Images presented in the report of Arnsdorf et al. show protrusion or tail formation compared to the control, even though this is not discussed in the study. The results were achieved with 10 µM treated mouse mesenchymal progenitor cells after one hour. The study does, however describe the cells as being stellate, with ruffled edges. [81] In contradiction, McBeath et al. reported no change in the morphology of 10 µM-treated hMSCs. [18]. Novozhilova et al. exposed human neural

precursor cells to 5 µM of the inhibitor and recorded their in-growth to a rat brain slice tissue over two weeks. By morphology, the neurite length was longer and elongated processes were detected. In addition, the cells' somata were elongated. [82] Maldonado exposed human induced pluripotent stem cells (hiPSC) to several concentrations of the inhibitor up to 50 µM for 36 hours. The cells responded by increasing in cell area, but by decreasing in actin intensity when the concentration was increased. [83] In Table 7, the experiments are summarized in more detail.

Table 7. *Summary of morphological studies in 2D using Y-27632.*

Cell type	*Concentrations*	*Time-point*	*Outcomes*	*Reference*
Swiss 3T3	10 µM	30 min	Dissolution of actin fibers	[79]
		24 h	Thin processes, thin actin bundles, neurite processes	
Human primary monocytes	1–10 µM	45 min	Detectable tail starting from 1 µM, increased in length and numbers with increasing concentration	[80]
mMPC	10 µM	1 h	Lack of actin fibril organization and ruffled edges	[81]
Human neuronal precursor cells	5 µM	2 week	Migration into the explant, two-fold increase, elongated processes, elongated cell somata	[82]
hIPSC	0–50 µM	36 h	Increase in cell area, decrease in actin intensity	[83]

Ishizaki et al. also studied the effect of Y-27632 on G1-S transition and cytokinesis. By exposing Swiss 3T3 cells to 10 µM and 100 µM of the inhibitor, G1-S transition was delayed by one and four hours, respectively. This indicates that ROCK may not be a critical component in the transition, but causes delays when its action is interrupted. The role of ROCK in cytokinesis was also tested on HeLA cells after four hours of exposure. Inhibition of cytokinesis was detected at 30 µM, but this was not statistically significant below a concentration of 100 µM. This further indicates that ROCK might not have a key role in proliferation. On the other hand, a compensatory mechanism could take over in the absence of ROCK. One possible effector could be citron kinase, which is also present

in the cleavage furrow during cytokinesis. This kinase is more resistant to Y-27632. [79] Wu et al. exposed marmoset iPSCs to several concentrations of the inhibitor and followed colony growth after seven days. In the study, growth was detected at concentrations up to 20 µM. The colony growth was, however, significant only up to 10 µM. In addition, 10 µM exposure decreased levels of caspase-3, a key factor in cell apoptosis, significantly after three days. Moreover, levels of Bax and Bcl-2 remained the same. The results suggest that the inhibitor could increase the survival rate of stem cells by preventing caspase-3 mediated apoptosis. [84] The experiments are summarized for comparison in Table 8.

Table 8. *Summary on proliferation and viability studies performed in 2D using Y-27632.*

Cell type	*Concentrations*	*Time-point*	*Outcomes*	*Reference*
Swiss 3T3	10 µM	-	1 h delay in G1-S transition	[79]
	100 µM	-	4 h delay in G1-S transition	
HeLa cells	10, 30, 100 µM	4 h	Inhibition of cytokinesis detected at 30 µM, significant at 100 µM	
Marmoset iPSC	5, 10, 20 µM	7 d	Colony percentage increased significantly at 5–10 µM	[84]

There are several reports on stem cell fate abrogation due to the use of Y-27632 in 2D models. McBeath et al. detected that 10 µM of the inhibitor was enough to abrogate constitutively active RhoA-induced osteogenesis in hMSCs after one week [18]. Arnsdorf et al. cultured mouse mesenchymal progenitor cells on fibronectin-coated glass slides. In comparison to the control, the cells exposed to 10 µM decreased in Runx2 expression by three-fold after one hour. Moreover, Sox9 expression increased twofold, which indicates that by limiting tension through inhibition, cells might derive towards chondrogenic fate. [81] Geometrical cues were provided to hMSCs, varying in curvature of a pentagon, by Kilian et al. When the cultures were exposed to 2 µM of the inhibitor, a star-shape induced osteogenesis was abrogated and all shapes were derived towards adipogenic fate, independently of the shape. [43] Shih et al. cultured hBMSCs with 5 µM of the inhibitor. They followed osteogenic expression over a three-week period. Type I collagen and osteocalcin expression decreased significantly after two weeks and even more after three

weeks. The study also tested the effect of inhibition on other signaling proteins and recorded downregulation of pFAK and pERK1/2 after three days of exposure. [85]

A further study by Hwang et al. suggested that Rho activation is important for stiff matrix-induced osteogenic activation. hMSCs were plated on acrylamide and bis-acrylamide mixture hydrogels with varying stiffnesses. A stiffness of 4.47 kPa induced osteogenic differentiation in the controls. Nevertheless, as the cultures were treated with 50 µM of Y-26732, a decrease in osteogenic gene expression was detected. In addition, TAZ nuclear localization was abrogated, along with targeting gene expression after 12 hours of treatment. [58] The results indicate that ROCK is an important mediator of stiff matrix-induced osteogenesis. The studies on differentiation performed in 2D with Y-27632 are summarized in Table 9.

Table 9. *Summary of differentiation studies performed in 2D with Y-27632.*

Cell type	*Model*	*Concentrations*	*Time-point*	*Outcomes*	*Reference*
hMSC	2D	10 µM	1 week	Constitutively active RhoA-induced osteogenesis abrogated	[18]
mMPC	2D	10 µM	1 h	Runx2 expression decreased threefold, twofold increase in SOX9	[81]
hMSC	2D, geometric cues	2 µM	1 week	Shape-induced osteogenesis abrogated	[43]
hBMSC	2D, stiffness variations	5 µM	3 days	Downregulation of pFAK and pERK	[85]
			1–3 weeks	Downregulation of osteogenic expression	
hBMSC	2D, stiffness variations	50 µM	12 h	Decreased osteogenic gene expression	[58]

Several studies have been performed with Y-27632 in 3D models. Maharam et al. cultured mouse MSCs in a 3D environment in the form of a silk fiber scaffold. In this scaffold, the control cells adopted an elongated morphology along the fibers and expressed tenogenic

differentiation. To study the role of ROCK in this setup, the culture was treated with 10 µM of the inhibitor for seven days. The results showed a decrease in elongated morphology and tenogenic mRNA expression, including genes such as *Scx*, *Col1a1*, *Nfatc4* and *Nst*. [86] On the other hand, Khetan et al. cultured hMSCs encapsulated in methacrylate malemide hyalyronic acid (MeMaHA) hydrogels. The cells were exposed to 10 µM of Y-27632, daily. After seven days, cells exposed to the inhibitor had deformed the matrix less than the control, but the spreading was visibly similar. However, the cytoskeletal organization had decreased. After 14 days, the cells showed no change in morphology when compared with the control, even though minimal actin expression was detected. Adipogenic differentiation was detected and extensive lipid droplet formation was visible. [29] The reported studies with Y-27632 in 3D are summarized for comparison in Table 10.

Table 10. *Summary of 3D studies performed with Y-27632.*

Cell type	*Concentrations*	*Time-point*	*Outcomes*	*Reference*
Human foreskin fibroblasts	10 µM	1 h	Long protrusions compared to the control	[27]
hMSC	10 µM, daily doses	7 days	Decrease in matrix deformation	[29]
		14 days	Decrease in gel deformation, adipogenesis, lipid droplet formation, minimal actin expression	
mMSC	10 µM	7 days	Decrease in elongated morphology	[86]

5.4 Non-muscle myosin II inhibitor - (-)-Blebbistatin

When compared to the other used inhibitors, Blebbistatin, a NMMII inhibitor, has only recently been reported in the literature. The role of NMMII has been widely discussed and reviewed, although Blebbistatin has received less attention. "(-)-Blebbistatin" is presented as an inhibitor for NMMII ATPase by the manufacturer, with an IC50 of 2 µM in cell-free assays. The usage of the inhibitor should inhibit contraction, but not disable mitosis or contractile ring assembly. It can, nevertheless, inhibit cytokinesis. [87] Reported studies often use Blebbistatin in addition to F-actin disrupting inhibitors. Several studies can be found investigating its effects on both morphology and differentiation, but not viability.

The morphology of Blebbistatin-treated cells are reported to change drastically. Arnsdorf et al. exposed mMSCs with 50 µM of the inhibitor, leading to stellate cells with ruffled edges. They also described lack of fibril organization. [81] This was confirmed by Ngo et al. by using several concentrations up to 50 µM. After 48 hours of exposure to 50 µM the hBMSCs showed a complete change in morphology by rounding. They also reported reduced cell area and total contractility arrest at 10 and 50 µM after 24 hours, respectively. [88] The reduction in spreading and increasing in roundness was also demonstrated by Caliari et al. with 50 µM conditioning of hBMSCs after seven days. [89] However, Sharman et al. conditioned WJ-MSCs using only 5 µM Blebbistatin, causing major changes in cell size and spreading. This major change after only exposure to such a low concentration could be due to the conditioning time of two passages. [90] The changes in morphology seem to be in alignment between 2D and 3D culture environments. This was confirmed by Maharam et al. in mMSC cultured in silk scaffolds. The cells showed a decrease in elongation after exposure to 50 µM of the inhibitor for seven days. [86] Morphology studies involving Blebbistatin are summarized in Table 11 for comparison.

In addition to morphology, the proliferation of a cell seems to be affected by Blebbistatin. The inhibitor causes a decrease in contraction and therefore disrupts cytokinesis. This can be seen in the form of multi-nucleated cells, as demonstrated by Straight et al. in HeLa cells, in a dose-dependent manner, with concentrations in the range of 0–150 µM [91]. Sharman et al. reported the slowing down of proliferation of WJ-MSCs after conditioning using 2.5–10 µM Blebbistatin, for several passages. A concentration of 10 µM resulted in almost total arrest of proliferation. This was confirmed by following the change in population doubling time. [90] The studies are listed in Table 12 for comparison.

The loss of tension and contraction in the cells affects the fate commitment. A concentration of 50 µM inhibitor abrogated RhoA- [18] and stiffness- [44] induced osteogenesis, after seven days and 48 hours, respectively. The stiffness variation with polyacrylamide gels caused Blebbistatin not only to halt fate commitment towards osteogenic lineage but also myogenesis and neurogenesis. [44] Arnsdorf et al. conditioned mMSC with 50 µM of Blebbistatin and flow, leading to a threefold increase in Sox9 expression, a marker of chondrogenesis [81]. Interestingly, geometrically induced osteogenesis was halted by only 1 µM Blebbistatin in hMSCs. Moreover this combination led to adipogenesis. [43] This result was supported by Khetan et al. with 3D MeMaHa hydrogel cultures. After 14 days of hMSC culturing with 50 µM of the inhibitor, cellular traction decreased, osteogenesis was reduced and adipogenesis was increased. [29] Differentiation studies concerning Blebbistatin are listed in Table 13.

Table 11. *Summary of studies on morphology performed with Blebbistatin.*

Cell type	*Model*	*Concentrations*	*Time-point*	*Outcomes*	*Reference*
hBMSC	2D, Col-I	10, 50 µM	24 h	Decrease in contraction in dose-dependent manner	[88]
		50 µM	48 h	Complete morphological change, no change in viability	
mMSC	2D	50 µM	1 week	Stellate cells, ruffled edges	[81]
hWJ-MSC	2D	5 µM	2 passages	Major changes in morphology, cell size increased	[90]
mMSC	3D	50 µM	7 days	Decrease in elongated morphology	[86]

NMMII has only been described as a downstream effector in mechanotransduction. However, its inhibition could have effects on upstream signaling proteins, leading to several other effects. Ngo et al. exposed hBMSCs to 5 or 10 µM of the inhibitor chronically through several passages. As a result, the expression of NMMIIA/B were both increased. They therefore concluded that either the concentrations used were too low or that secondary mechanisms take effect after longer exposure times. [88] Caliari et al. used 50 µM Blebbistatin for seven days and measured the expression of ROCK and pERK1/2. Both were decreased, suggesting the loss in contraction and tension inside the cell regulates the expression of upstream proteins. [89]

Table 12. *Summary of proliferation assays with Blebbistatin.*

Cell type	*Model*	*Concentrations*	*Time-point*	*Outcomes*	*Reference*
HeLa	2D	0–150 µM	N/A	Multi-nucleated cells increased in DDM	[91]
hWJ-MSC	2D	2.5, 5, 10 µM	P1-P5	Proliferation slowing in dose-dependent manner	[90]

Table 13. *Summary of differentiation assays with Blebbistatin.*

Cell type	*Model*	*Concentrations*	*Time-point*	*Outcomes*	*Reference*
hMSC	2D	50 µM	7 days	RhoA induced osteogenesis abrogated	[18]
hMSC	2D, stiffness variation	50 µM	48 h	Stiffness induced differentiation abrogated	[44]
mMSC	2D	50 µM	N/A	Chondrogenic differentiation	[81]
hMSC	2D geometric cues	1 µM	1 week	Shape induced osteogenesis abrogated, adipogenesis	[43]
hMSC	3D	50 µM	7 days	Reduced cellular tractions and osteogenesis, slightly increased adipogenesis	[29]

Based on the results found in the literature it can be expected that the morphology of the cells will change, at least with a concentration of 50 µM. In addition, the proliferation may be affected and multi-nucleated cells should be visible in high concentration cultures. The viability experiments in the present study should provide new information, as very little has been described in previous studies. It could be speculated that as the tension and contractility is lost in the cells, the rounding will lead to the decrease in FAs and might therefore lead to anoikis.

6. MATERIALS AND METHODS

6.1 Cell culture

Primary human bone marrow stromal cells (hBMSC) from an anonymous female donor (referred to as "5/16") born in 1929 (aged 87 at the time of harvesting) were obtained through a medical operation performed at Tampere University Hospital. The donor weighed 74 kg and was 160 cm tall, with no history of osteoporosis or diabetes type I or II. The cells were verified by fluorescence-activated cell sorting and showed the propensity to undergo both osteogenic and adipogenic differentiation. Cells were thawed at passage four (P4) and seeded for experiments at P5, with the exception of standard curves for the metabolic assay, which were seeded at P6. Prior to experimentation, cells were cultured in basic medium (BM), consisting of minimum essential medium alpha (MEM α, Gibco, Thermo Fisher Scientific) supplemented with 5 % human serum (HS, Lonza/BioWhittaker) and 1% penicillin-streptomycin (10.000 U Penicillin/ml, 10.000 U Streptomycin/ml, Lonza/BioWittaker). During cell maintenance, but not during experimentation, BM was supplemented with 0.005 % human fibroblast growth factor-2 (hFGF-2, Miltenyi Biotec), in order to maintain the multipotency of the hBMSC. The cells were maintained at 37 °C, 5 % CO_2 and 95 % relative humidity.

6.2 Immunocytochemistry

Samples were fixed with 0.2 % Triton-X-pFA for 10 min and were then washed with Dulbecco's phosphate-buffered saline (D-PBS, Gibco, Thermo Fisher Scientific). Fixed samples were then treated with a blocking agent consisting of 1 % BSA in D-PBS and incubated for 1 h at 4 °C. The primary monoclonal antibody, rabbit anti-vinculin (Invitrogen, Thermo Fisher Scientific) was diluted in blocking solution (1:100), applied to the samples and incubated overnight at 4 °C. After four washes with D-PBS, the secondary antibody, Alexa Fluor 488 donkey anti-rabbit IgG (Invitrogen, Thermo Fisher Scientific), was diluted in blocking solution (1:800). Phalloidin-tetramethylrhodamine B isothiocyanate (phalloidin-TRITC, Sigma-Adrich) was added to the same solution (1:500) and the samples were incubated for one hour. The samples were washed three times with 0.5 mL of D-PBS. Next, 4',6-diamidino-2-phenylindole (DAPI) was diluted in D-PBS (1:2000) and incubated for 5 min. The samples were then washed twice with deionized water.

6.3 Microscopy and image processing

Bright field images were acquired using a Nikon eclipse TE2000-S light microscope with 20X air objectives.

Immunostained fluorescent imaging was performed using a Zeiss Axio Scope.A1 with 63X oil immerse objective. Filters of 395 nm, 495 nm and 560 nm were used to visualize DAPI, vinculin and phalloidin-TRITC, respectively.

Confocal imaging was executed with a Zeiss LSM700 laser scanning confocal microscope with 40X air objective. DAPI, vinculin and phalloidin-TRITC were visualized using solid state diode lasers: 405 nm, 488 nm, and 555 nm, respectively.

The fluorescence microscope images were edited with Adobe Photoshop CS4. The black and white images obtained through microscopy were colored and three images from different filters were stacked. The confocal z-plane images were stacked using ImageJ.

6.4 Experiments in 2D

6.4.1 Viability and proliferation

A range of inhibitor concentrations of interest was determined, based on the literature, and covering concentrations above and below the reported IC50 value. In the first round of experiments, a two-fold dilution series was performed on each inhibitor to achieve eight concentrations (n=5). In the second round, concentrations were prepared at specific intervals, rather than through serial dilutions. Since the inhibitors were supplied in a dimethyl sulfoxide (DMSO) solution in order to solubilize them, experiments included two controls: DMSO+ and DMSO- (containing only BM without growth factors). The concentration of DMSO (Sigma-Aldrich) was set to a constant 1.28 % throughout the experiment for all inhibitors and samples, excluding the DMSO- control and several samples in which the inhibitor concentration exceeded 100 μM. The inhibitors, all obtained from Selleckchem, were: PD98059 (MEK inhibitor), Y-27632 (ROCK inhibitor), (-)-Blebbistatin (NMMII inhibitor) and PF-562271 (FAK inhibitor). Inhibitors were applied in several concentrations according to Table 14.

Table 14. *Inhibitor concentrations used in the 1st and 2nd rounds of 2D viability and proliferation experiments.*

Inhibitor		*Concentrations (µM)*
FAK		0.1, 0.2, 0.4, 0.8, 1.6, 3.2, 6.4, 12.8
MEK	1st	0.5, 1, 2, 4, 8, 16, 32, 64
	2nd	5, 10, 20, 30, 40, 50, 60, 70
ROCK	1st	0.5, 1, 2, 4, 8, 16, 32, 64
	2nd	20, 30, 40, 50, 60, 70, 80, 90
Blebbistatin	1st	0.5, 1, 2, 4, 8, 16, 32, 64
	2nd	20, 30, 40, 50, 60, 70, 80, 90

Cells were plated in a 96 well plate at a concentration of 16,600 cells/cm^2, and cultured for 24 hours, prior to inhibitor exposure, followed by a further 24 or 48 hours of exposure. At each time-point, the inhibitor-containing medium was removed and cultures were treated with Cell Counting Kit-8 (CCK-8, Dojindo Molecular Technologies, Inc.) diluted 1:10 in D-PBS and incubated for 3 h at 37 °C and 5% CO_2. CCK-8 is a colorimetric assay that uses water-soluble tetrazolium salt 8 (WST-8) to measure the mitochrondrial metabolic activity of a cell, turning from a pale pink to a measurable yellowish hue upon metabolism. After incubation, absorbance at 450 nm was measured using a plate reader (Viktor 1429 Multilabel Counter). Every experiment was run in parallel with five fresh standards prepared in two-fold dilutions of cell concentration (n = 5), which were used to form a standard curve in order to extrapolate the viable cell count.

6.4.2 Morphology

For the 2D morphology assessment, cells were plated on a 24 well plate on sterilized glass coverslips at a concentration of 2,000 cells/cm^2, and cultured for 24 hours prior to inhibitor exposure, followed by a further 48 hour period of exposure. Inhibitor concentrations were decided based on the results obtained during the viability experiment (n=2). The same DMSO- and DMSO+ controls were included. The chosen concentrations are presented in Table 15. The samples were imaged with a brightfield microscope, before being fixed and immunostained.

Table 15. *Inhibitor concentrations used in 2D morphology estimation.*

Inhibitor	*Concentrations (μM)*
FAK	2, 5, 7, 10
MEK	10, 30, 60
ROCK	10, 40, 90, 200
Blebbistatin	10, 30, 60

6.5 Experiments in 3D

6.5.1 Preparing the cell-collagen solution

The collagen I solution was prepared as instructed by the manufacturer [92]. In relation to the volume of collagen, 0.025 % of sterile 1 N sodium hydroxide (NaOH) was suspended with 10 % D-PBS (10X) (Gibco, Thermo Fisher Scientific) on ice. Rat tail collagen I (Gibco, Thermo Fisher Scientific) was then added slowly as a thin ribbon and suspended well for three minutes on ice, in order to adjust the pH of the solution. Next, the suspension was applied to a cell pellet at a concentration of 1,000,000 cells/mL. The solution was kept on ice for the encapsulation.

6.5.2 Viability and proliferation – 3D

For the viability assay 50 µL samples from the cell- collagen solution were pipetted into a 96 well plate (n=3). The gelation occurred as the gel warmed both at room temperature and at 37 °C upon transfer to the incubator. The warming of the solution was aided by applying pre-warmed BM on to the gel in droplets. The cells were encapsulated for 24 hours prior to inhibitor exposure, followed by a 48 h period of exposure. Upon experimentation, the inhibitor-containing medium was removed and cultures were treated with CCK-8 diluted 1:10 in D-PBS and incubated for 3 h at 37 °C. After incubation, absorbance at 450 nm was measured using a plate reader. Every experiment was run in parallel with five fresh standards prepared in two-fold dilutions of cell concentration (n=3), which were used to form a standard curve in order to extrapolate the viable cell count. The used inhibitor concentrations investigated are listed in Table 16.

Table 16. *Inhibitor concentrations used in 3D viability assays.*

Inhibitor	*Concentrations (µM)*
FAK	2, 5, 7, 10
MEK	10, 30, 50, 70, 100, 200
ROCK	25, 50, 100, 200
Blebbistatin	10, 20, 40, 80

6.5.3 Cell morphology

The 50 µL 3D cell morphology assay samples from the cell-collagen solution were pipetted on pre-warmed sterile glass coverslips as droplets (n=2). The gelation occurred upon warming, as previously described. The cells were encapsulated for 24 hours, prior to inhibitor exposure, followed by a 48 hour period of exposure. The inhibitor concentrations used are listed in Table 17. The samples were fixed and immunostained as previously described.

Table 17. *Inhibitor concentrations used in 3D morphology assessment.*

Inhibitor	*Concentrations (µM)*
FAK	10
MEK	100, 200
ROCK	100, 200
Blebbistatin	80

6.6 Experimental flow-chart

In Figure 3, the experimental workflow is illustrated.

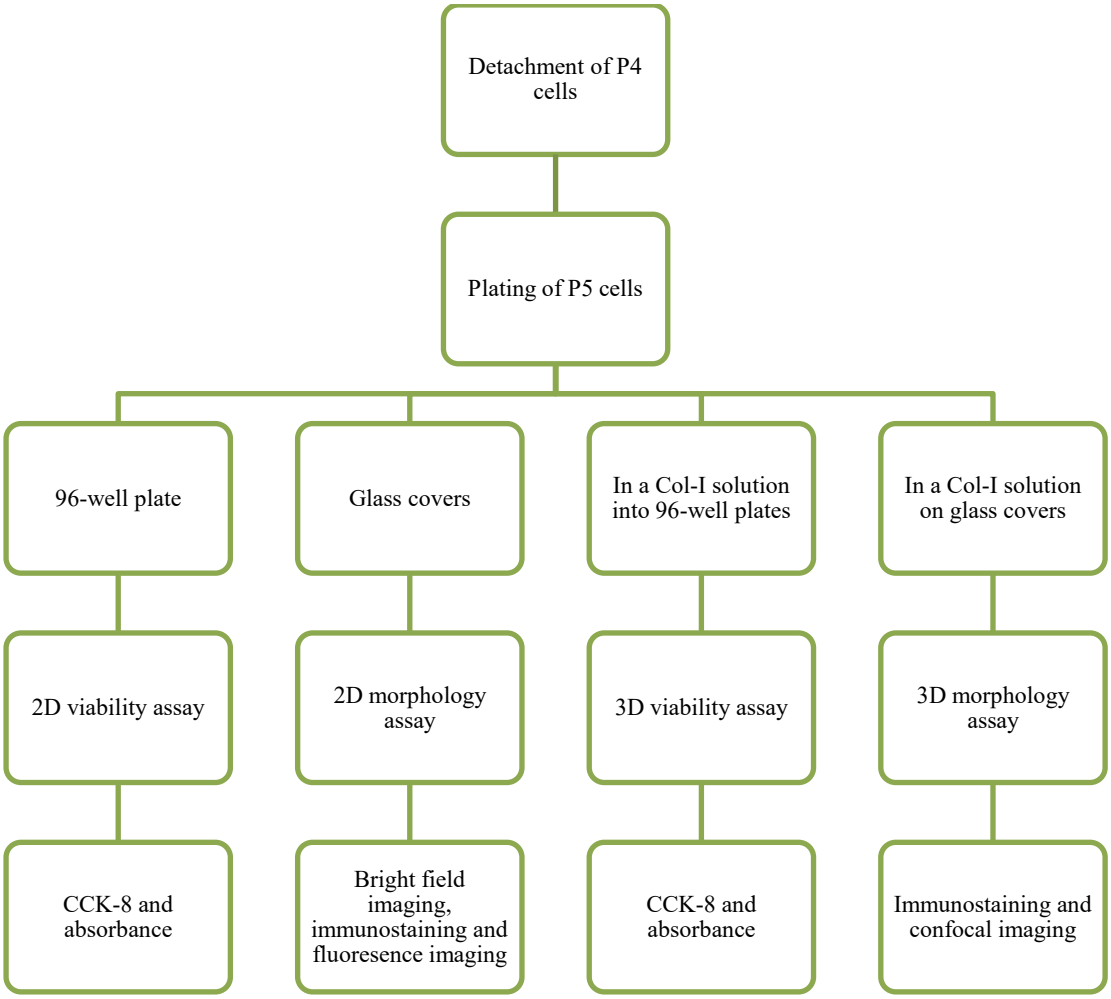

Figure 3. *Illustration of the work-flow, providing information on the seeding material and executed experiments.*

7. RESULTS

7.1 MEK inhibitor results were inconclusive

Several experiments were performed with MEK inhibitor in the viability assay to optimize the culture density, time-point and number of dosages. All of the trialed combinations, but not all results, are presented in Figure 4. The results of the 2D assay are presented as mean values (n=5) with standard deviations, whereas the results of the 3D assay are presented with individual data points for each replicate, due to their wide standard deviation. All results were normalized relative to the DMSO+ control (100 %). In addition, the DMSO- control is provided as a reference. The 24 hour time-point was rejected with the 48 hour time-point of two doses. Instead a half-way was chosen; 48 hours with one dose was considered to provide the maximum effect with minimum disruption of the culture. This set-up was used for all inhibitors both in the viability assay and for the morphological assessments. In the MEK inhibitor 2D assay, no correlation between the different results could be seen. In addition, the 48 hour assay with only one dose was considered unsuccessful, as no twofold dilutions could be made.

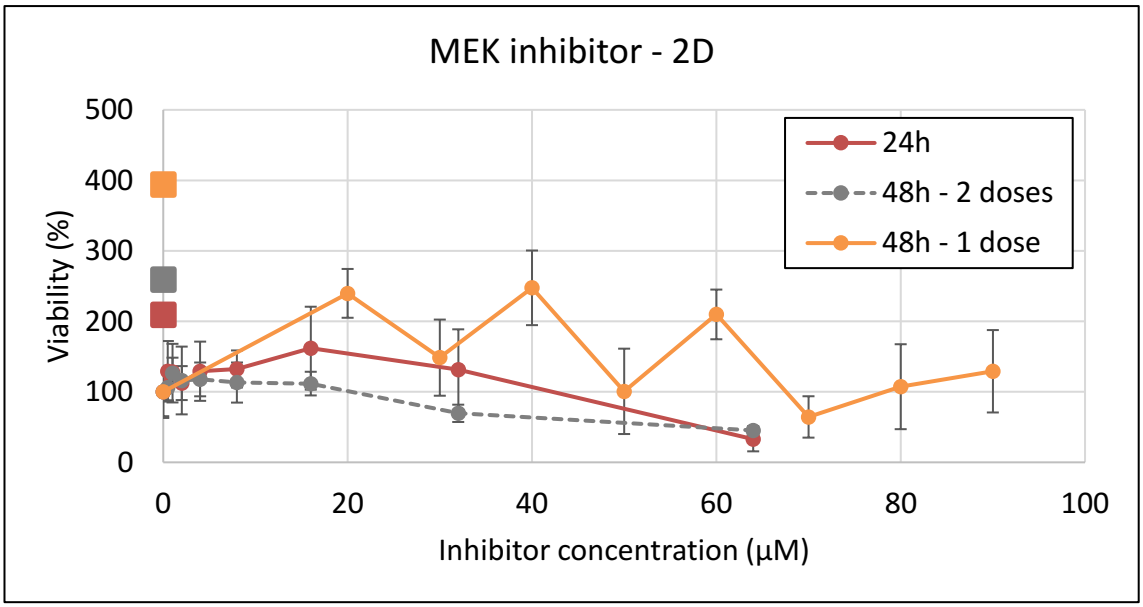

Figure 4. *MEK inhibitor viability results. CCK-8 assay results presented as percent viability vs. inhibitor concentration. Given results vary in time-point and number of medium changes. The DMSO+ control is taken as a comparison (100 %) and DMSO- is presented as a mean value, a color coordinated square. Values are presented as mean values (n=5), with error bars representing standard deviation.*

Considerably higher concentrations of inhibitors were used in the 3D assay, in order to achieve maximum effect. The results from 3D viability assay are presented in Figure 5. The results are provided as stand-alone and compared to the DMSO+ control mean value (100 %). The DMSO- control replicates are provided as a reference. There was high standard deviation between the replicates and therefore no differences in viability could be seen between the concentrations.

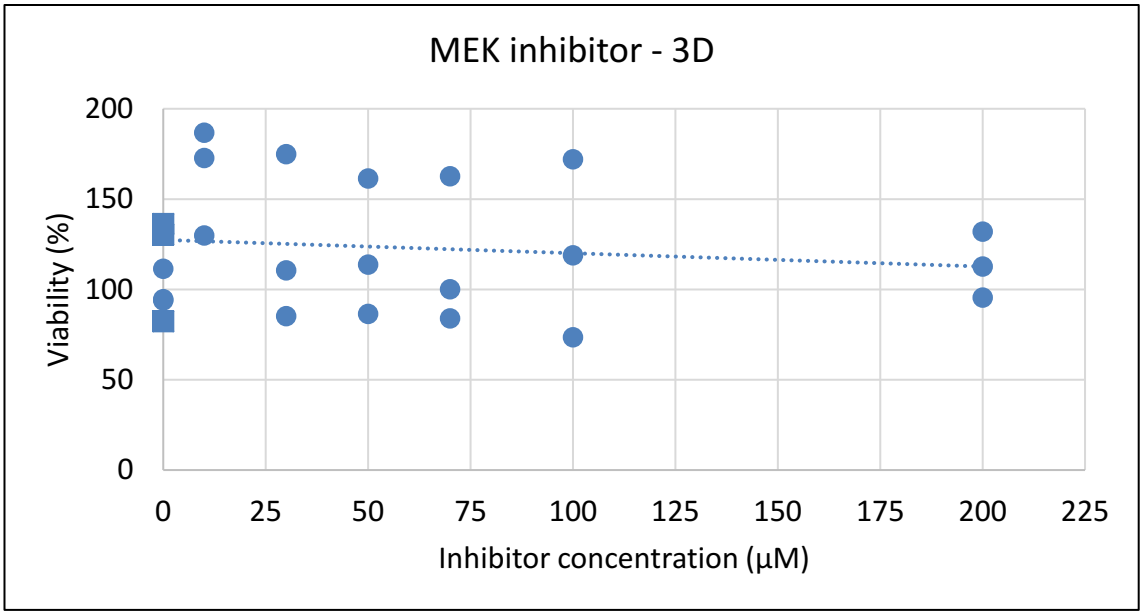

Figure 5. *MEK inhibitor viability results from the 3D model. CCK-8 assay results presented as percent viability vs. inhibitor concentration, after 48 h of exposure with one inhibitor dose. The DMSO+ control mean value is taken as a comparison (100 %) and DMSO- is presented as a square. Each data point represents a single replicate, due to the high standard deviation, and a trend line is shown.*

When comparing the chosen set-up from the 2D viability assay with the 3D results, no correlation can be seen (Figure 6). However, if the 2D assay for the 48 hour exposure with one dose is considered as unsuccessful and 3D assay as successful experiment, the results show that the inhibitor does not affect the viability of the cells, even with higher concentrations.

Representative bright field images were taken from both TCP and glass coverslips in 2D. The results are presented in Figure 7 and Figure 8. No major differences were observed between different concentrations. However, a difference can be seen between the culture surfaces. The MEK inhibitor formed aggregates or crystals when added to the cell culture. These crystals are visible in Figure 5 at 90 µM, shaped like twigs. In order to rule out the possibility that the HS had induced formation of the aggregates, a simple test comparing all different components of the medium was performed. However, crystals formed in all

conditions (data not shown), and warming the solutions did not help to dissolve the crystals, so the aggregates could not be avoided, and were visible at high concentrations.

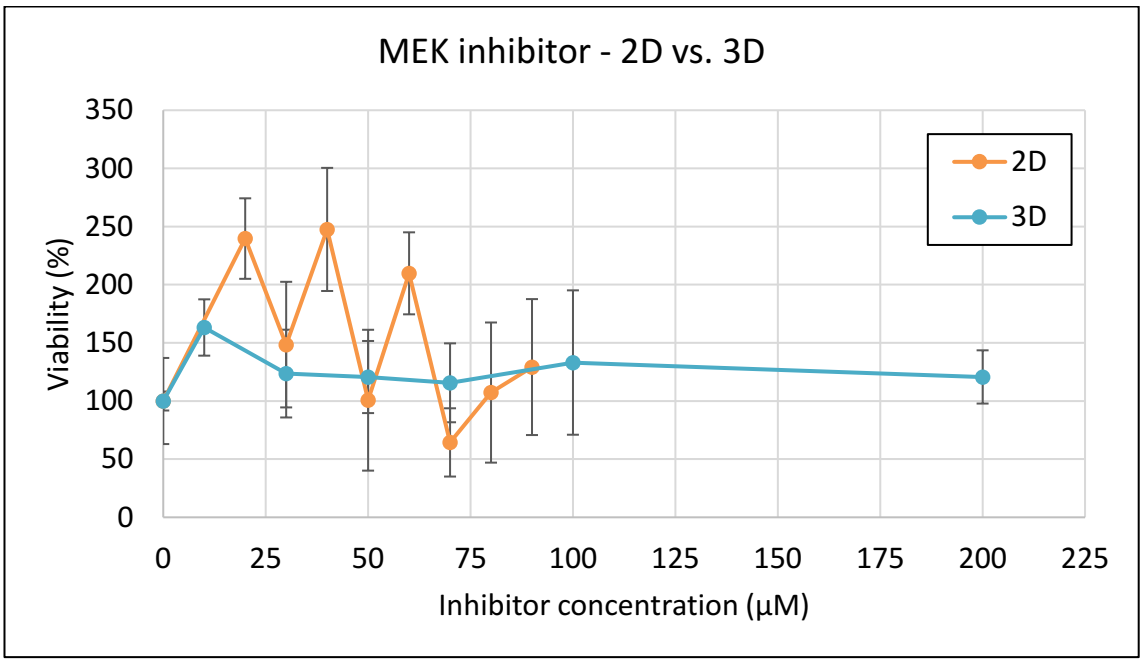

Figure 6. *Comparison of the effect of MEK inhibitor on viability between 2D and 3D models. CCK-8 assay results are presented as percent viability vs. inhibitor concentration. Given results vary in culture models. Both assays were run after 48 h of inhibitor exposure after one dose. The DMSO+ control is taken as a comparison (100 %). Values are presented as mean values, 2D) n=5 and 3D) n=3, with standard deviation.*

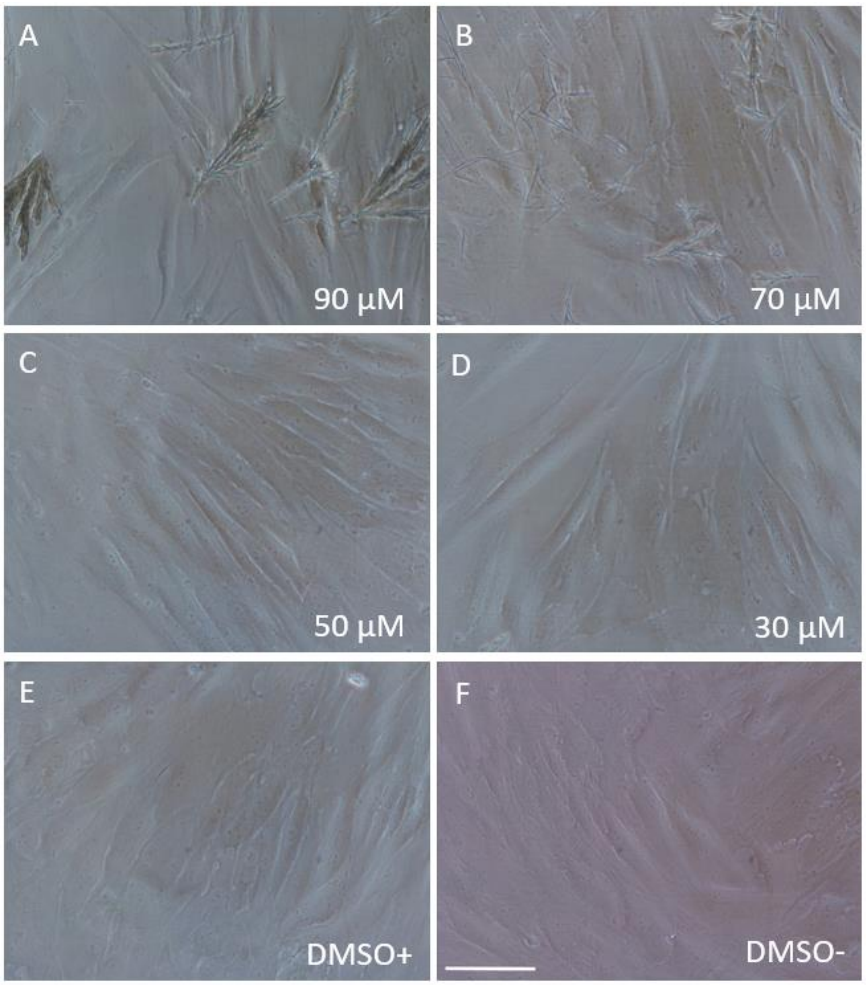

Figure 7. *Brightfield images after 48 h of MEK inhibitor exposure at (A) 90, (B) 70, (C) 50 and (D) 30 µM, (E) 0 µM, with DMSO and (F) 0 µM without DMSO, cultured in a 96 well plate, scale bar 100 µm.*

Fluorescence micrographs of cells exposed to MEK inhibitor are presented in Figure 9. DMSO- controls were imaged for comparison. Some change in morphology and actin intensity can be observed after 30 µM. Moreover, cells treated with 60 µM of the inhibitor seemed to be ruffled from the edges, with a higher intensity of vinculin. In addition, some multi-nucleated cells were visible.

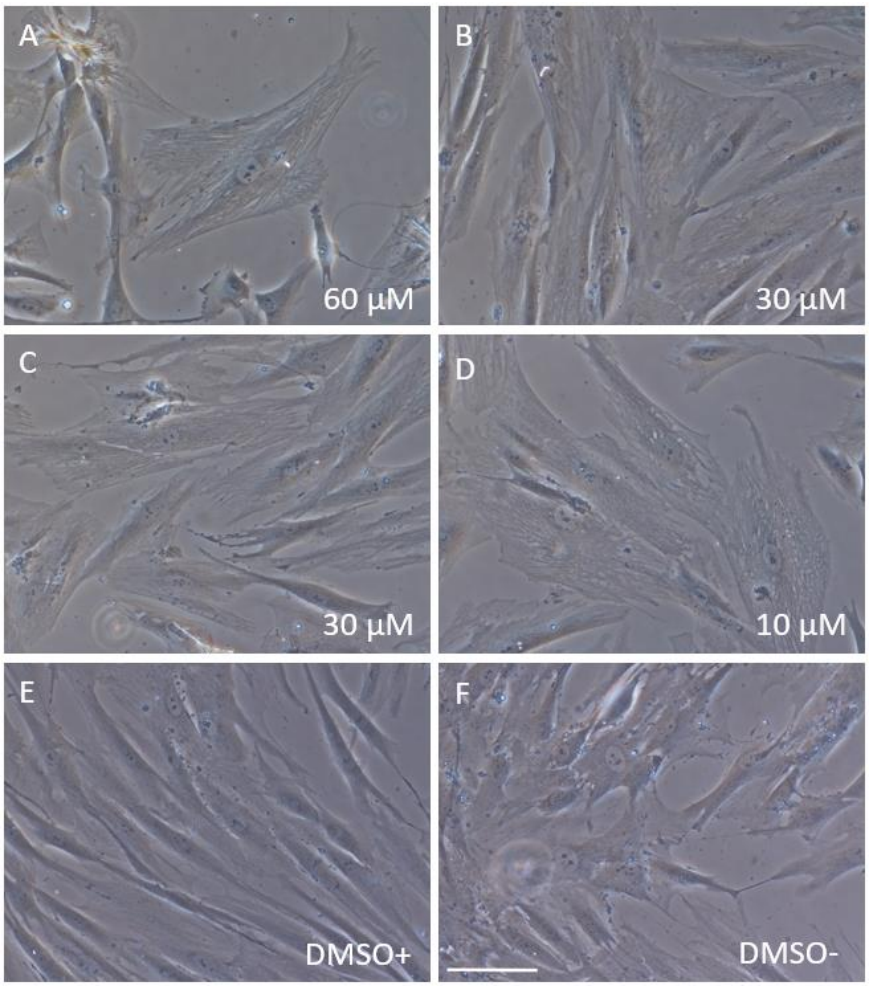

Figure 8. *Brightfield images after 48 h of MEK inhibitor exposure at (A) 60, (B) 30, (C) 30 and (D) 10 µM, (E) 0 µM, with DMSO and (F) 0 µM without DMSO, cultured on glass coverslips in a 24 well plate, scale bar 100 µm.*

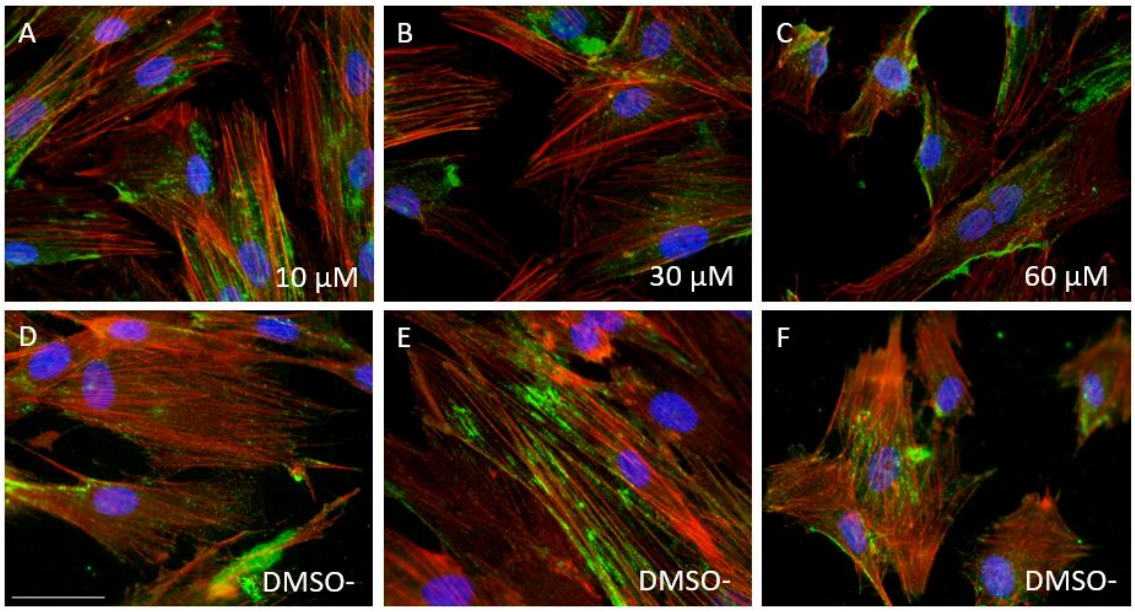

Figure 9. *Fluorescent images of the MEK inhibitor 2D morphology samples. Cells were exposed to MEK inhibitor for 48 h at (A) 10, (B) 30, (C) 60 and (D,E,F) 0 µM without DMSO. F-actin (red), vinculin (green), nucleus (blue), scale bar 50 µm.*

In Figure 10, the 3D control samples from immunostaining and confocal imaging are presented. The images are formed from z-plane images as sums in a z-stack. There is little difference to be detected between the DMSO+ and DMSO- samples. Cells are elongated and reaching through the Col-I matrix in all directions. In the second DMSO- image (Figure 10, C) a z-stack from the bottom of the culture is presented. Here the cells appear to have migrated to the bottom of the samples, to the glass. This apparent durotaxis was observed in all samples.

The MEK inhibitor-treated samples did not change morphology as a response to the exposure. Both high concentration samples, 100 and 200 µM, were imaged (Figure 11). Cells were elongated and presented a similar intensity of both F-actin and vinculin in both samples.

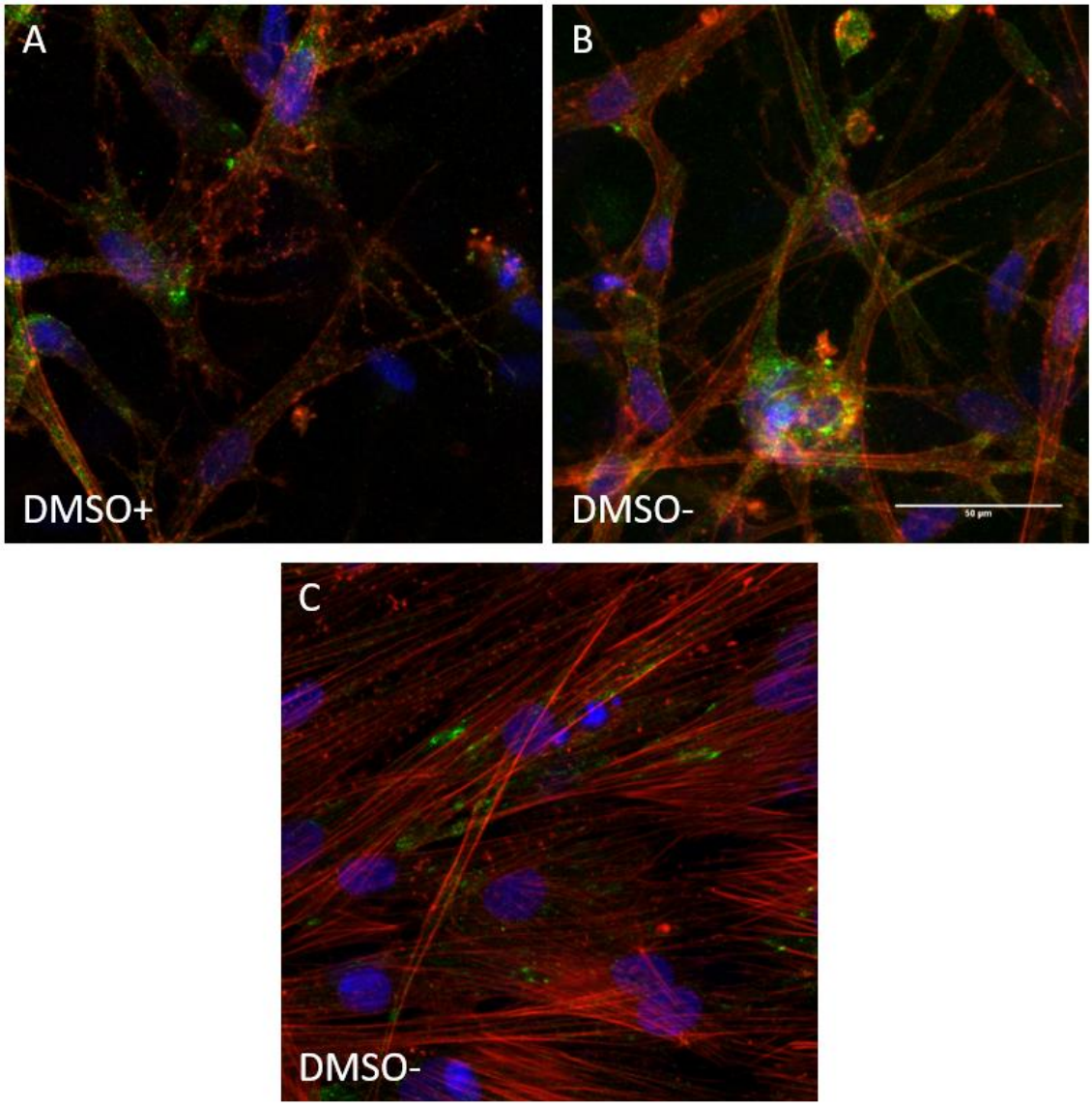

Figure 10. *Fluorescent images of 3D sample controls. Images were formed from confocal microscope z-stacks: (A) DMSO+, 11 z-planes (B) DMSO-, 32 z-planes and (C) DMSO-, 11 z-planes, shift between planes 0.82 µm. The z-stack is a sum of all z-planes. Cells were exposed to the ROCK inhibitor for 48 h. F-actin (red), vinculin (green), nucleus (blue), scale bar 50 µm.*

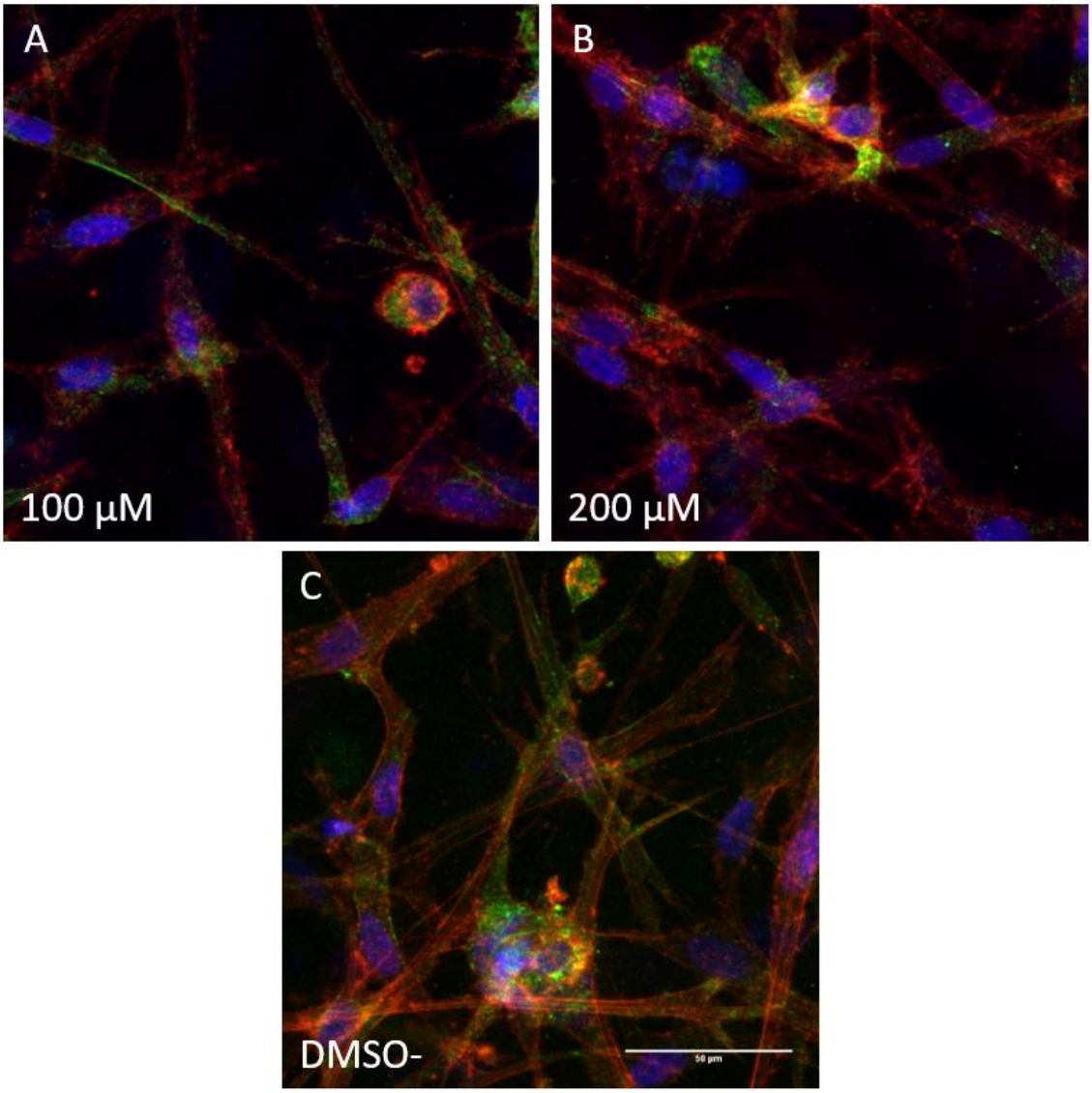

Figure 11. *Fluorescent images of a MEK inhibitor exposed 3D samples. Images were formed from confocal microscope z-stacks: (A) 100 µM, 15 z-planes, (B) 200 µM, 42 z-planes, (C) DMSO-, 32 z-planes, shift between planes 0.82µm. The z-stack is a sum of all z-planes. Cells were exposed to the MEK inhibitor for 48h. F-actin (red), vinculin (green), nucleus (blue), scale bar 50 µm*

The inhibitor crystal aggregates caused significant background staining with the DAPI dye, even though they were on top of the gel and far from the cells being imaged. These aggregates of butterfly-shape are presented in Figure 12. In this z-stack, no nuclei were distinguishable from the intense staining of the aggregates. This could not be corrected with brightness alterations without over-exposing the images.

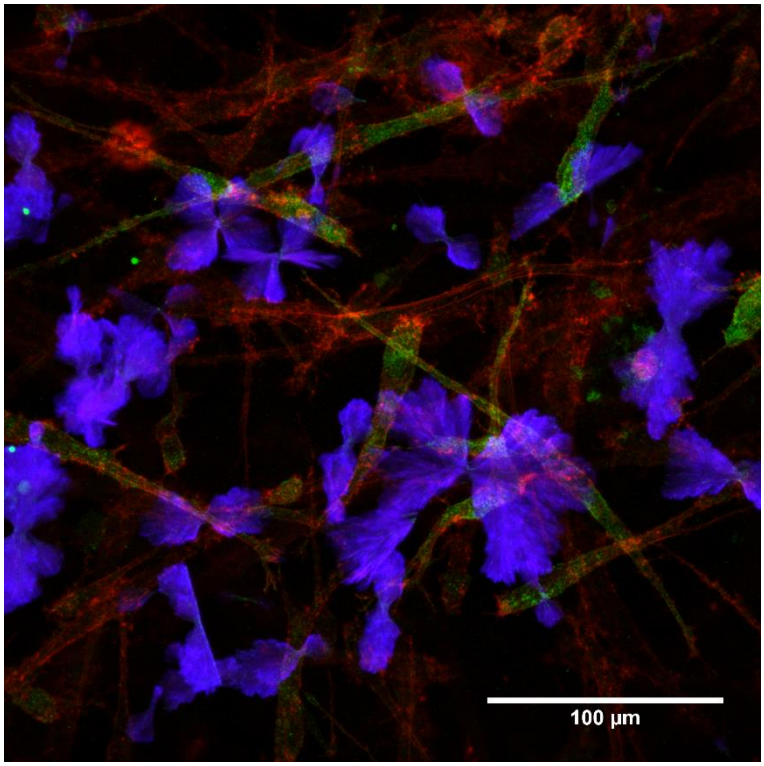

Figure 12. *Fluorescent image of a MEK inhibitor-exposed 3D sample, presenting inhibitor aggregates. Images were formed from confocal microscope z-stacks: nine z-planes, shift between planes 0.82 µm. The z-stack is a sum of all z-planes. Cells were exposed to 200 µM of MEK inhibitor for 48 h. F-actin (red), vinculin (green), aggregates (blue), scale bar 100 µm.*

7.2 ROCK inhibitor induced significant changes in morphology

For ROCK inhibitor the viability assay was performed with two set-ups: after 24 and 48 hour exposure. In addition, the 48 hour exposure was executed with two different inhibitor ranges, first with two-fold dilutions and then with a range with 10 µM intervals. The viability results are presented in Figure 13. Although no visible changes in the viability were detected, a correlation between exposure time and cell viability was visible. Although the second 48 hour range appears to indicate cell proliferation, this is more likely to be due to inaccurate preparation of different concentration solutions, caused by not using the twofold dilution method.

For the 3D viability assay, higher concentrations were chosen to achieve maximum effect. The results with ROCK inhibitor are presented in Figure 14. As with the MEK inhibitor, the 3D results are presented with one data point per replicate. All samples in 2D and 3D were normalized relative to the DMSO+ control mean value (100 %). The DMSO-

controls are provided as a reference. There was some variation between the replicates, but a descending trend can be detected. However, this decrease in viability only reaches about 80 % compared to the control, even though the concentration of the inhibitor is extremely high.

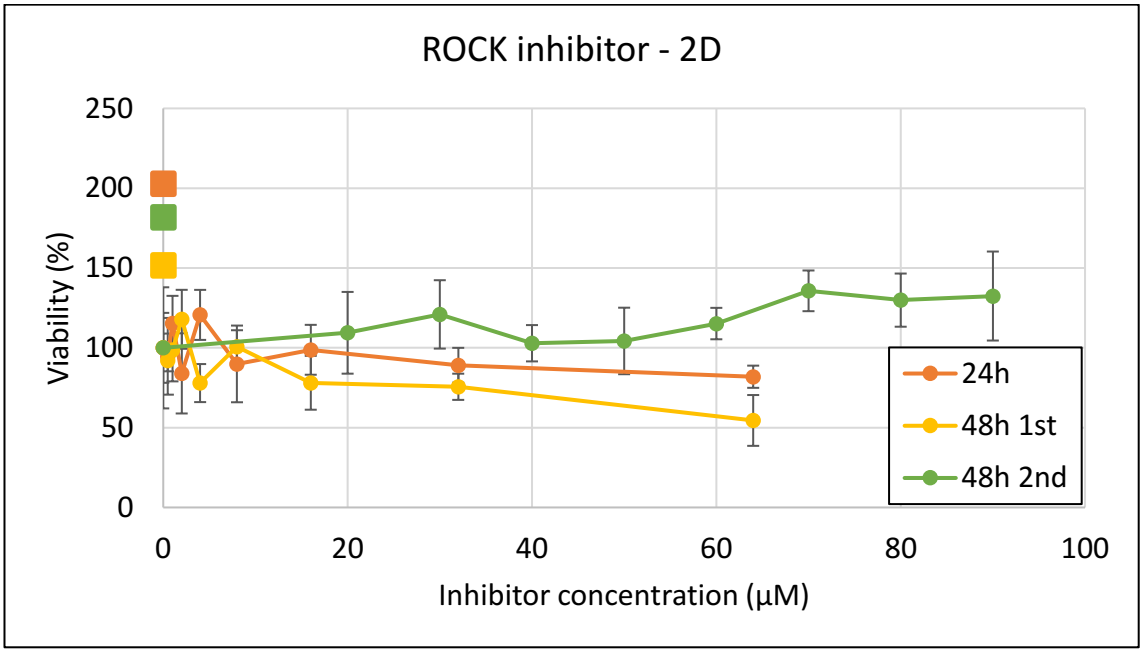

Figure 13. *ROCK inhibitor viability results from 2D model. CCK-8 assay results presented as percent viability vs. inhibitor concentration. Given results vary in time-points. DMSO+ control is taken as a comparison (100 %) and DMSO- is presented as a mean value, a color coordinated square. Values are presented as mean values (n=5) with standard deviation.*

For the comparison between the two models, the successful twofold dilution range (1st 48 hour range) assay was chosen to present the 2D model. As can be seen from Figure 15, there are no similarities between the two models. The 2D model inhibitor treatment seems to cause a decrease in viability, whereas the 3D model shows no clear trend.

The representative brightfield images of both TCP and glass cultures are presented in Figure 16 and Figure 17. In addition to morphological changes corresponding to surface type and possibly stiffness, the cells seemed to be leaving or forming protrusions in all directions in a dose-dependent manner. The morphological changes were detectable at ≥8 µM and clearly visible after 10 µM.

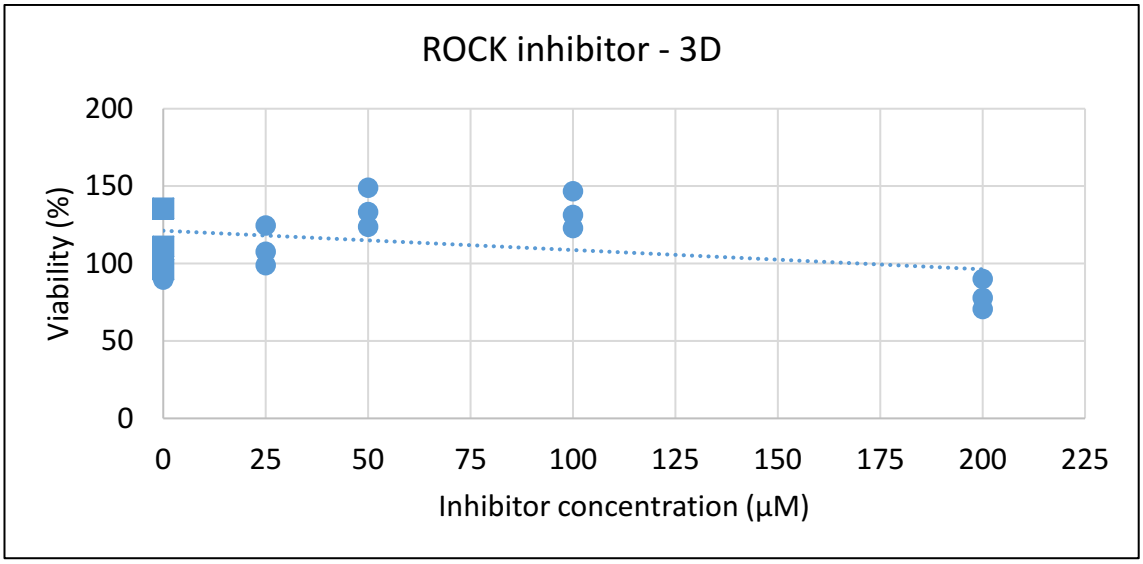

Figure 14. *ROCK inhibitor viability assay results from 3D model. CCK-8 assay results presented as percent viability vs. inhibitor concentration, after 48 h of exposure with one inhibitor dose. The DMSO+ control mean value is taken as a comparison (100 %) and DMSO- is presented as a square. Values are presented as individual data point for each replicate, with a trend line.*

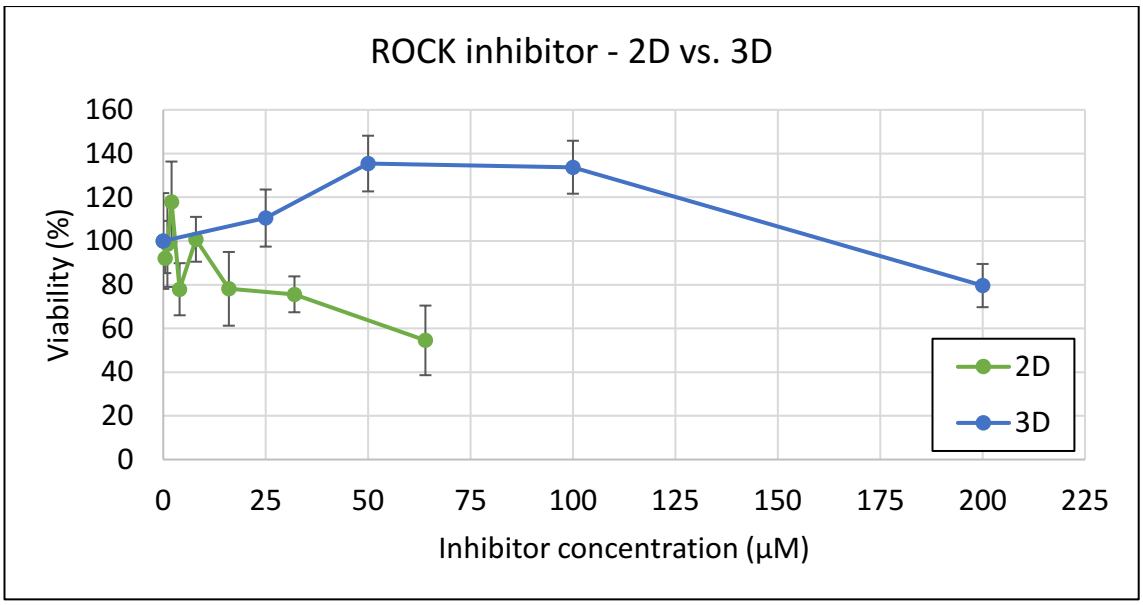

Figure 15. *ROCK inhibitor viability assay result comparison between 2D and 3D models. CCK-8 assay results are presented as viability-% vs. inhibitor concentration. Both assays were run after 48 h of inhibitor exposure. Given results vary in culture models. The DMSO+ control is taken as a comparison (100 %). Values are presented as mean values, 2D) n=5 and 3D) n=3, with standard deviation.*

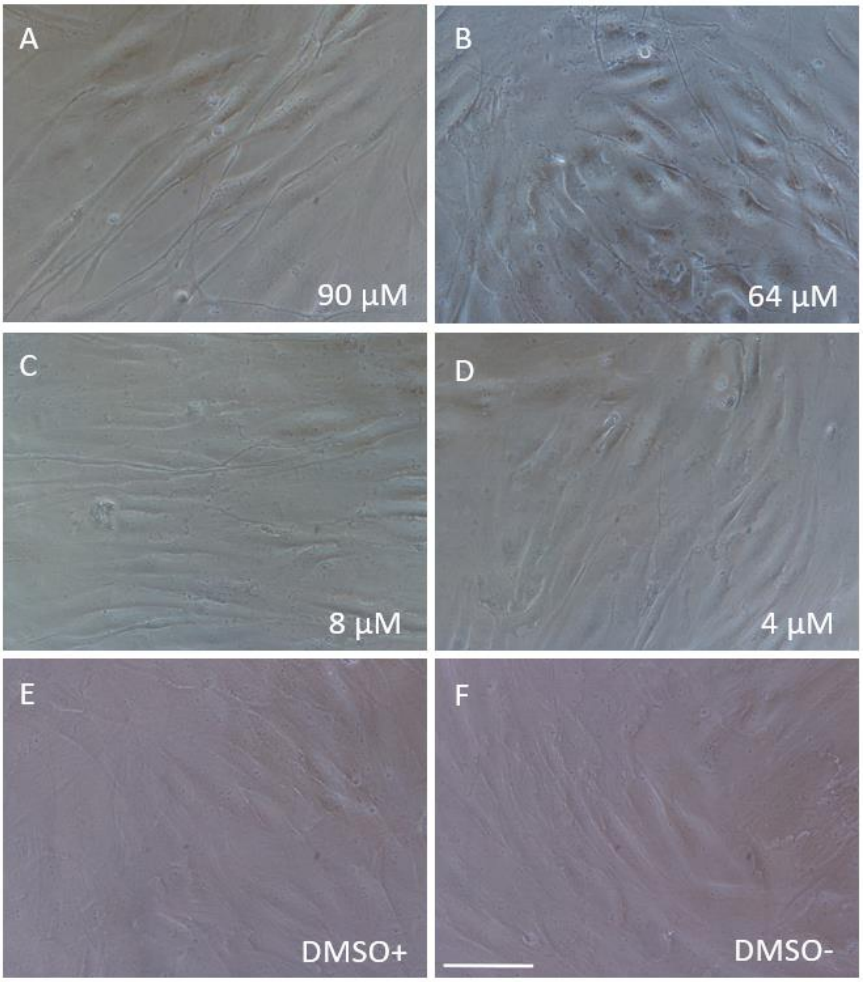

Figure 16. *Brightfield images after 48 h of ROCK inhibitor exposure at (A) 90, (B) 64, (C) 8 and (D) 4 µM, (E) 0 µM, with DMSO and (F) 0 µM without DMSO, cultured in a 96 well plate, scale bar 100 µm.*

The protrusion formation can be seen clearly from the fluorescent images taken from immuno-stained samples. These images are presented in Figure 18. The 10 µM exposure still maintains a morphology close to the control, but the actin bundles seem to have decreased. In 40 µM exposure the protrusions are very visible and polarization is lost in the cells. The size of cells varied greatly at ≥90 µM exposure. It should also be noted that in the 90 µM culture, multi-nucleated cells were present. At the very high concentration of 200 µM, the cells were rounded and no cytoskeletal organization could be recognized. Vinculin is very much centered according to the nucleus. In addition, the protrusions seem to be more like tails and could possibly be the result of the cell retracting, rather than intentional formation.

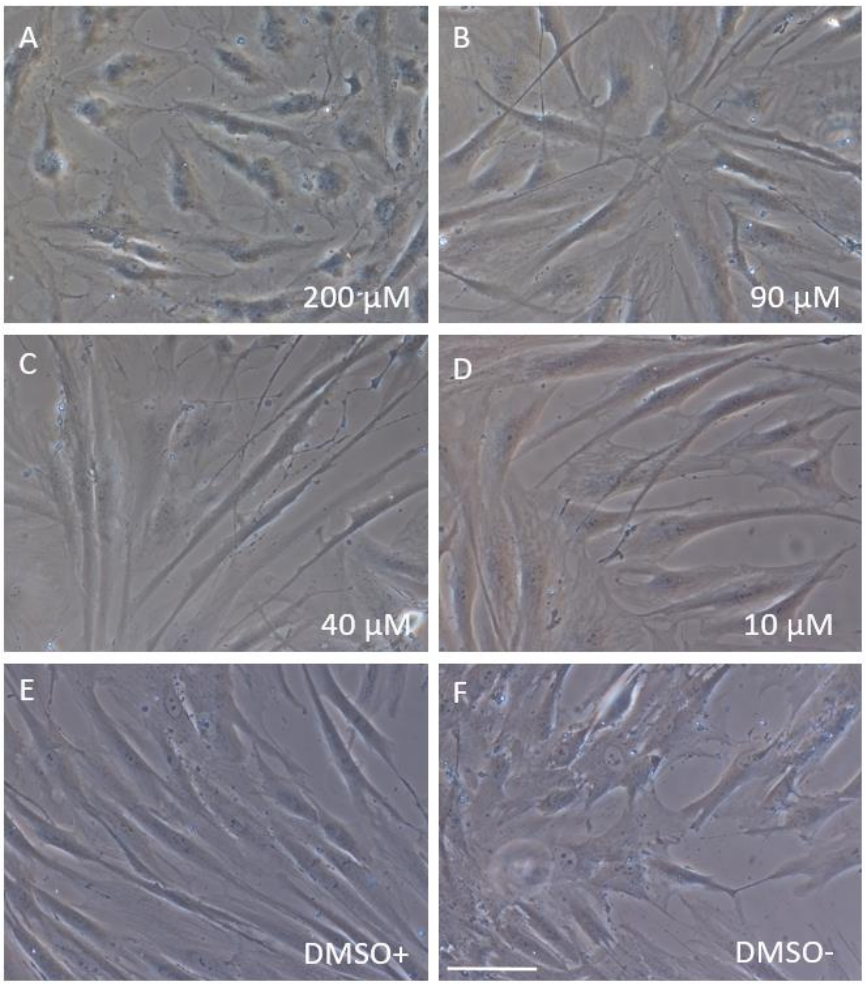

Figure 17. *Brightfield images after 48 h of ROCK inhibitor exposure at (A) 200, (B) 90, (C) 40 and (D) 10 µM, (E) 0 µM, with DMSO and (F) 0 µM without DMSO, cultured on glass coverslips in a 24 well plate, scale bar 100 µm.*

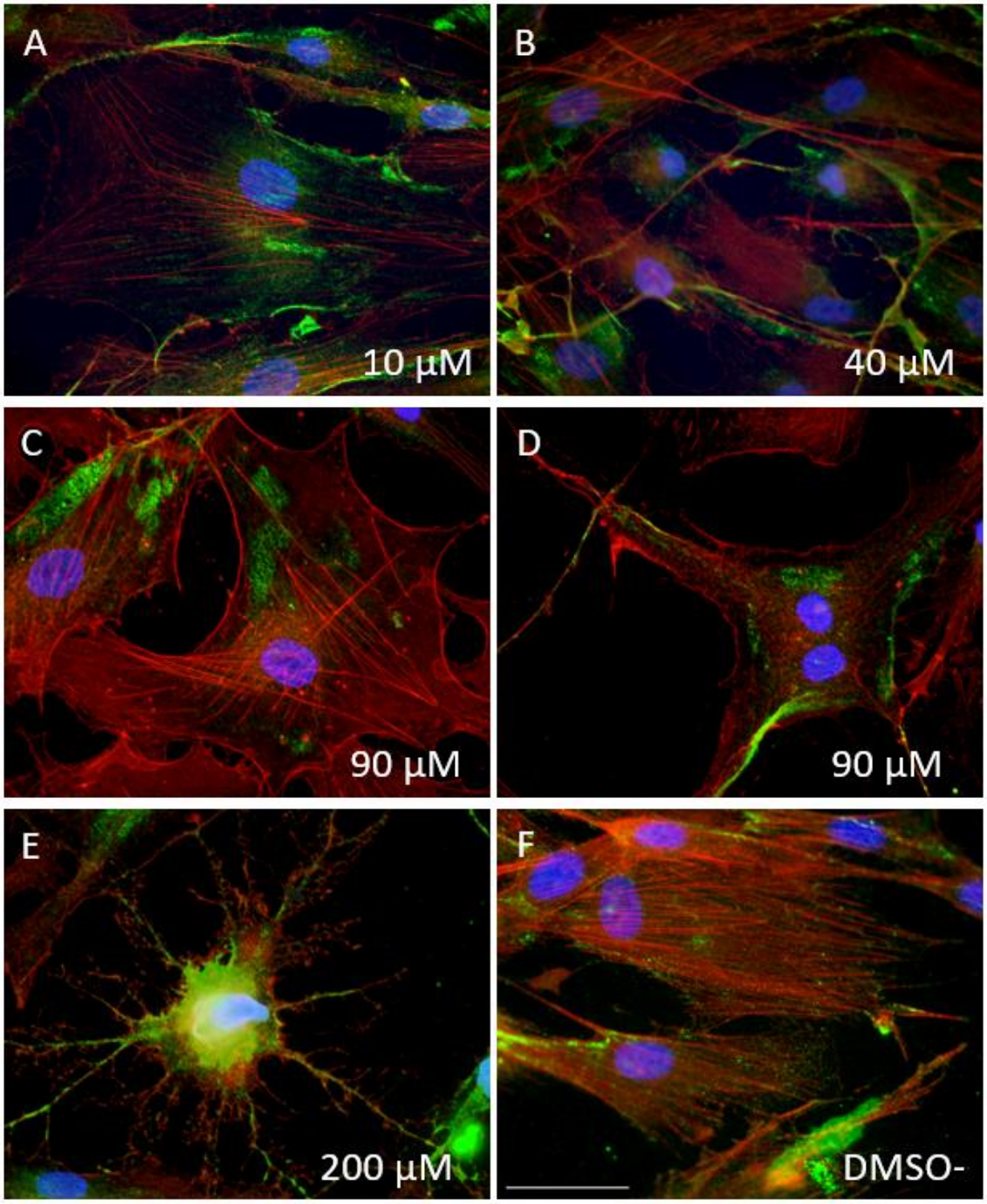

Figure 18. *Fluorescent images of the ROCK inhibitor 2D morphology assay. Cells were exposed to ROCK inhibitor for 48 h at (A) 10, (B) 40, (C) 90, (D) 90 and (E) 200 µM, (F) 0 µM without DMSO. F-actin (red), vinculin (green), nucleus (blue), scale bar 50 µm.*

Similar morphological changes were also visible in 3D. In Figure 19, a fluorescent image of confocal z-stacks are presented. Long protrusions reach inside the gel, but very little F-actin is visible, whereas vinculin was stained very strongly.

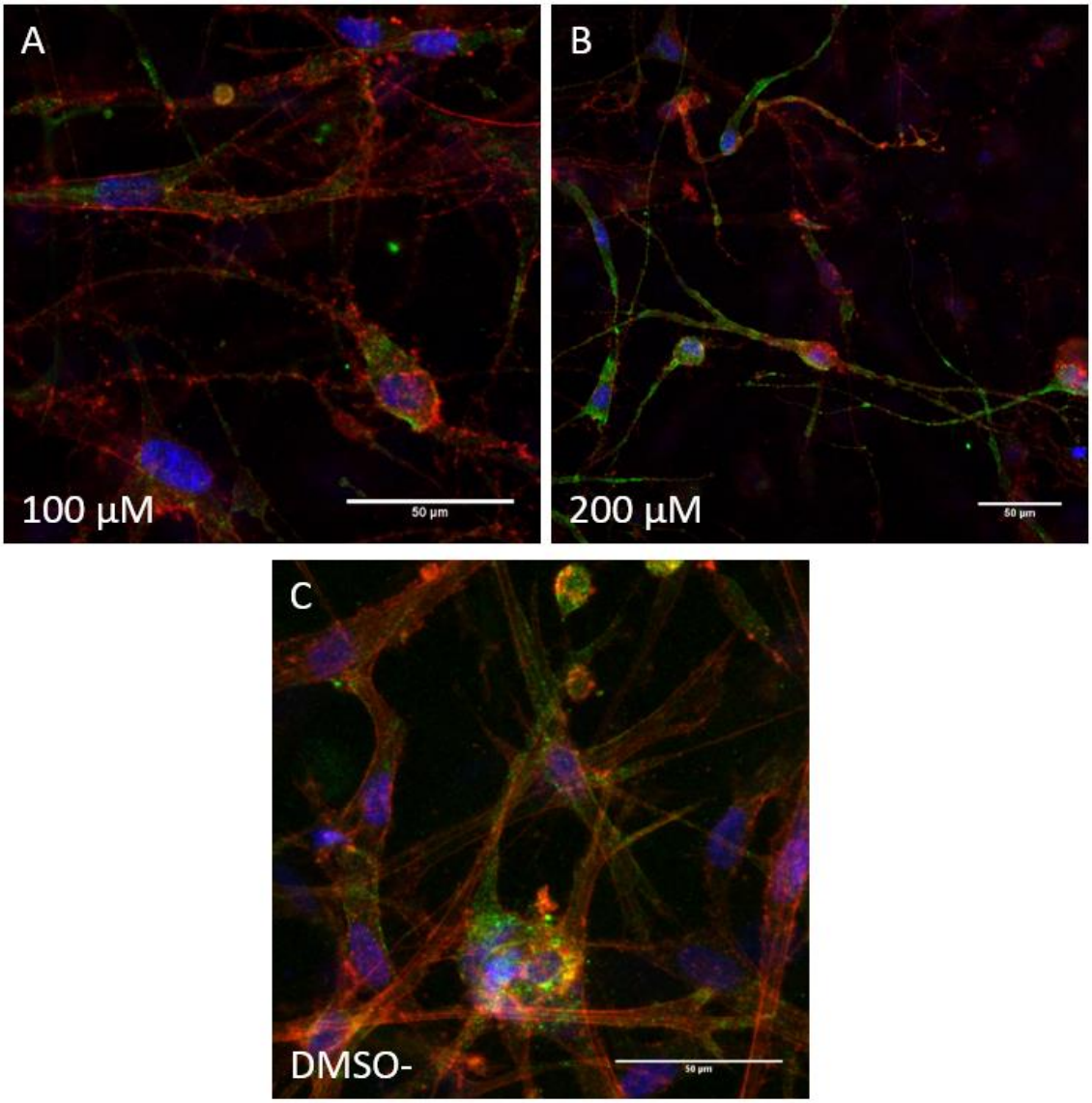

Figure 19. *Fluorescent images of a ROCK inhibitor exposed 3D sample. Images were formed from confocal microscope z-stacks: (A) 100 µM, seven z-planes, (B) 200 µM, eight z-planes and (C) DMSO-, 32 z-planes, shift between planes 0.82µm. The z-stack is a sum of all z-planes. Cells were exposed to the ROCK inhibitor for 48 h. F-actin (red), vinculin (green), nucleus (blue), scale bar 50 µm.*

7.3 Blebbistatin affected both viability and morphology

The 2D viability results with Blebbistatin are presented in Figure 20. Blebbistatin was experimented at 24 hours and twice at 48 hours. The results were in alignment between the 24 hour and the first 48 hour experiment, but was less successful in the second range as the dilutions were not executed in twofold dilutions. With Blebbistatin there is a clear change in viability, determining a critical threshold affecting viability between 16 and 32 µM.

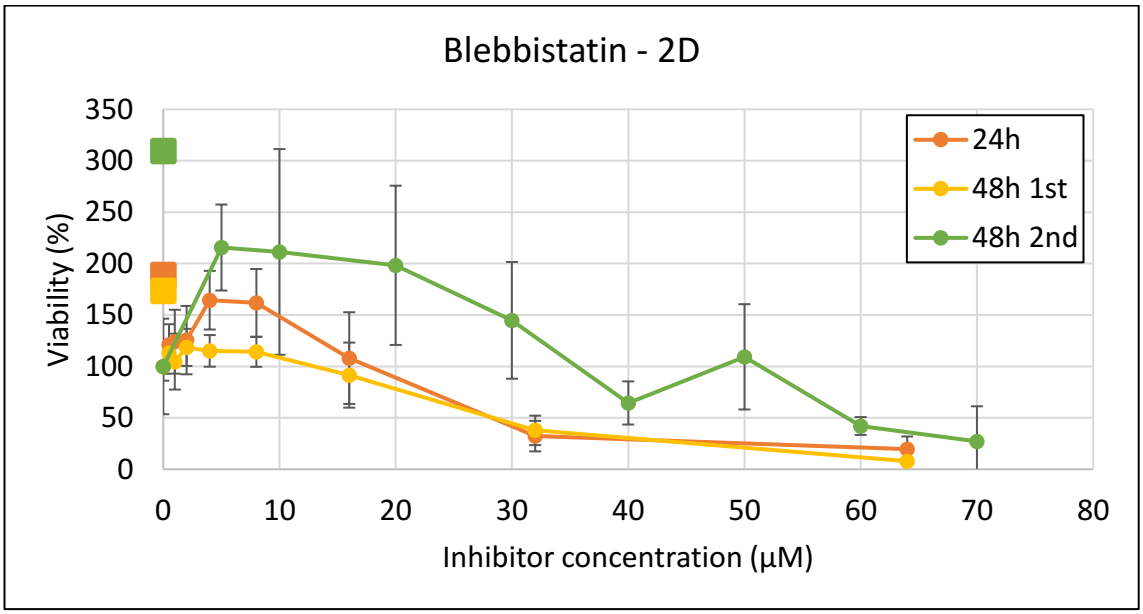

Figure 20. *Blebbistatin treatment viability assay results from 2D model. CCK-8 assay results presented as percent viability vs. inhibitor concentration. Given results vary in time-points. The DMSO+ control is taken as a comparison (100 %) and DMSO- is presented as a mean value, a color coordinated square. Values are presented as mean values (n=5) with standard deviation.*

In 3D the change in viability after Blebbistatin treatment was not as marked as in 2D. The results are illustrated in Figure 21. The used concentrations were quite close to the concentrations used in the 2D model. The replicates had little variation, excluding the 10 µM samples and therefore it appears that there was a decreasing trend in a dose-dependent manner.

The first range of 48 hour exposure with twofold dilutions was chosen to be the most insightful assay. The results were compared with the 3D viability assay results (Figure 22). Both models show a similar decrease in viability in a dose-dependent manner, when excluding the high standard deviation of the 10 µM (3D) and 16 µM (2D) samples. However, the decreasing effect is more subtle in 3D and does not reach greater than 50 % viability loss, whereas in 2D over 90 % is achieved.

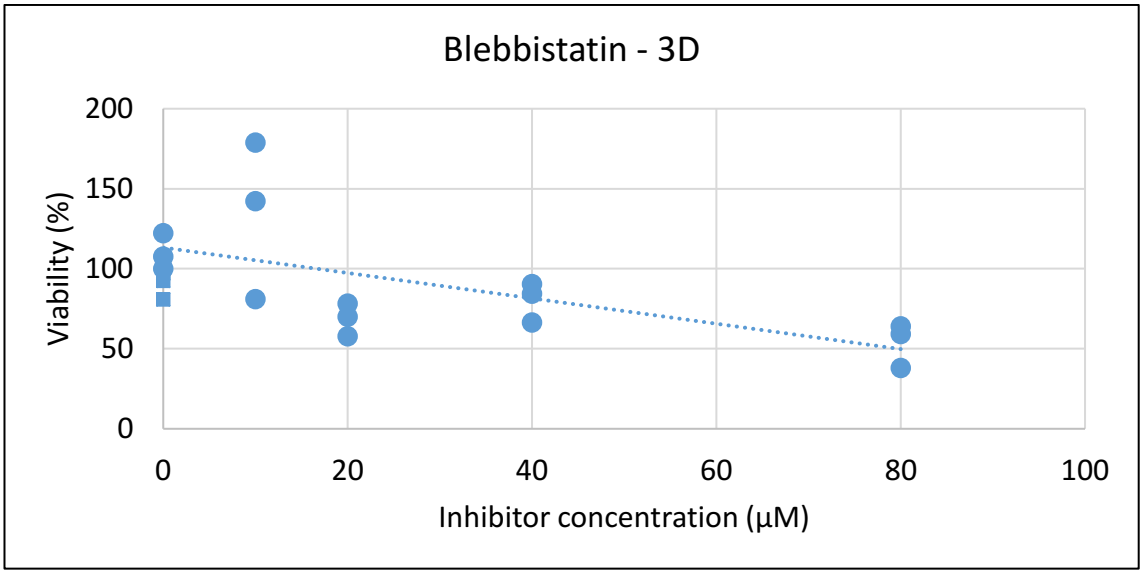

Figure 21. *Blebbistatin treatment viability assay results from 3D model. CCK-8 assay results presented as percent viability vs. inhibitor concentration, after 48 h of exposure with one inhibitor dose. The DMSO+ control mean value is taken as a comparison (100 %) and DMSO- is presented as a square. Each data point represents one replicate, with a trend line.*

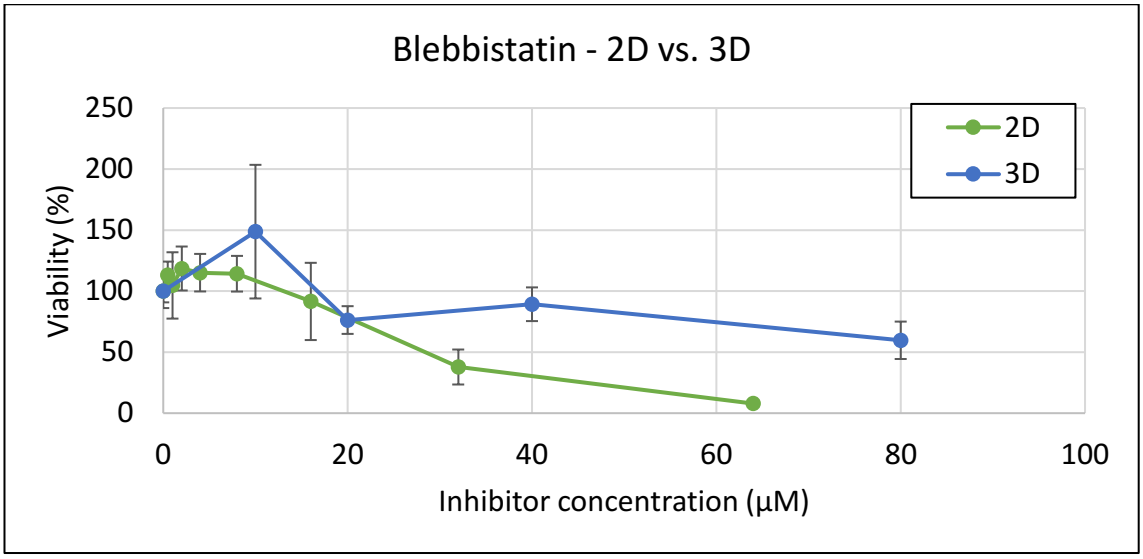

Figure 22. *Blebbistatin treatment viability assay result comparison 2D vs. 3D. CCK-8 assay results are presented as percent viability vs. inhibitor concentration. Both assays were run after 48 h of inhibitor exposure. Given results vary in culture models. The DMSO+ control is taken as a comparison (100 %). Values are presented as mean values, 2D) n=5 and 3D) n=3, with standard deviation.*

The corresponding images of Blebbistatin-treated cultures on TCP and glass are presented in Figure 23 and Figure 24, respectively. Morphological changes were visible on both materials. With higher concentrations, the cells seem more round and retracting. This is visible at ≥16 µM treatment. Much like with MEK inhibitor, Blebbistatin formed aggregates at higher concentrations. These aggregates, shaped as rods, can be seen in Figure 24 at 60 µM.

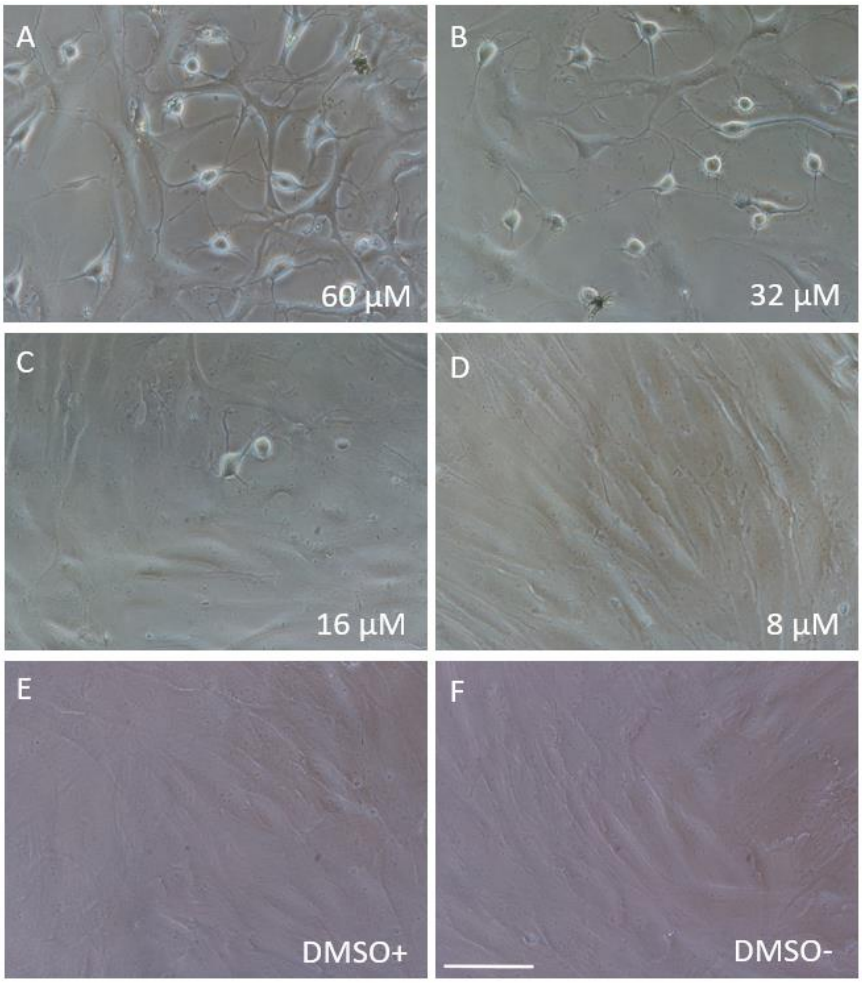

Figure 23. *Brightfield images after 48 h of Blebbistatin exposure at (A) 60, (B) 32, (C) 16 and (D) 8 µM, (E) 0 µM, with DMSO and (F) 0 µM without DMSO, cultured in a 96 well plate scale bar 100 µm.*

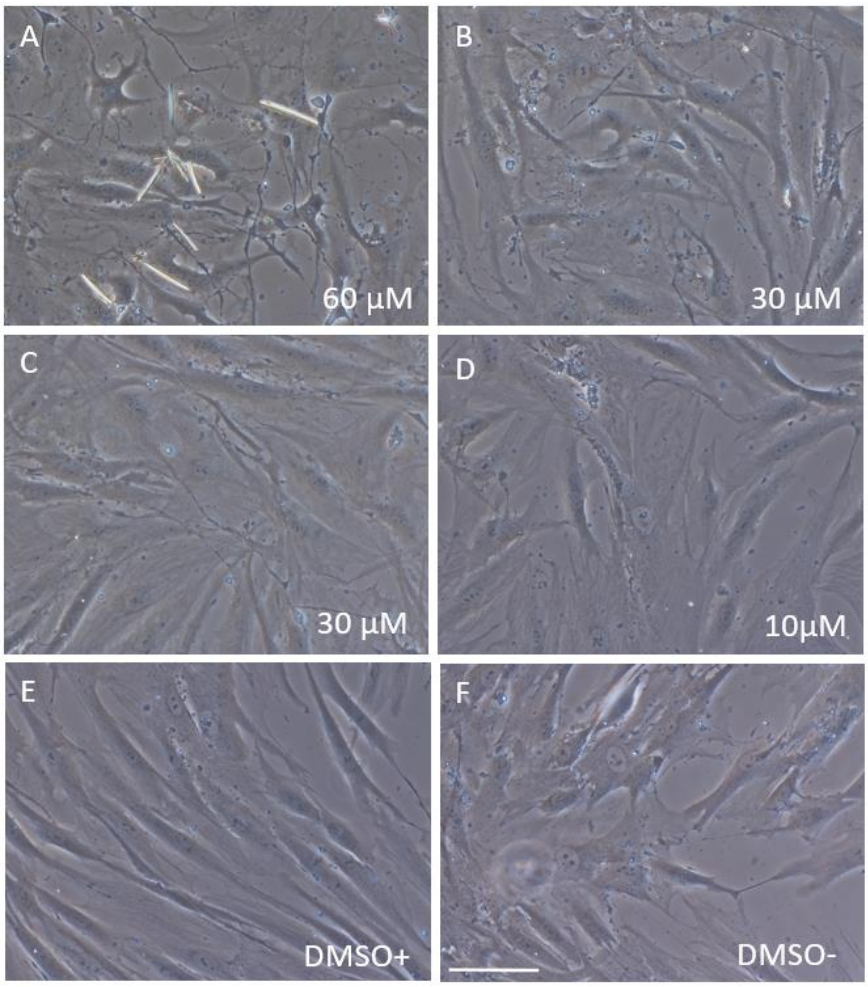

Figure 24. *Brightfield images after 48h of Blebbistatin exposure at (A) 60, (B) 30, (C) 30 and (D) 10 µM, (E) 0 µM, with DMSO and (F) 0 µM without DMSO, cultured on a glass covers in a 24-well plate, scale bar 100 µm*

The samples cultured on glass covers were immunostained and assessed for cytoskeletal organization or FA changes. These fluorescent images are presented in Figure 25. When compared to the DMSO- control, the cells treated with 10 µM of the inhibitor showed no difference in morphology. However, at the two higher concentrations, F-actin bundles appeared to be less dense and sparser. Moreover, the cells were larger in size and at 60 µM exposure, some of the cells were multi-nucleated.

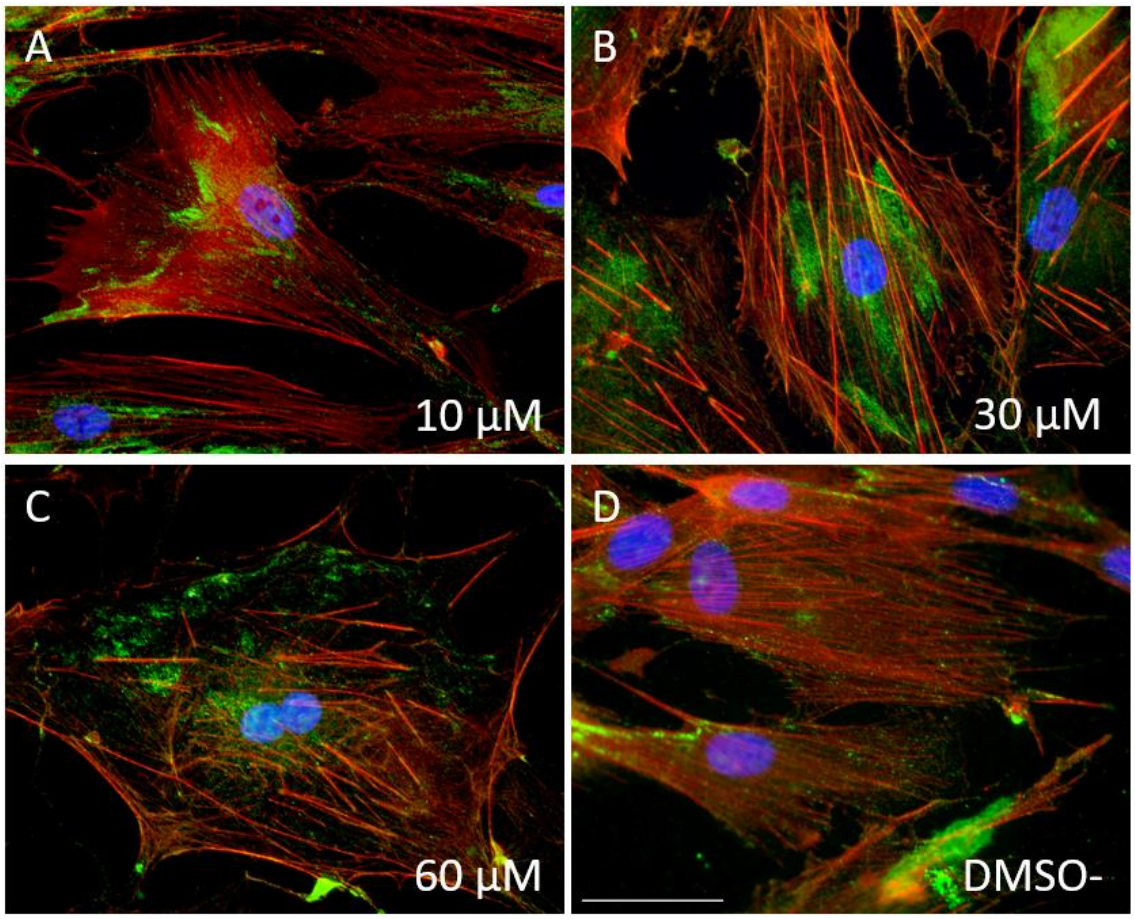

Figure 25. *Fluorescent images of the Blebbistatin-treated 2D morphology assay. Cells were exposed to Blebbistatin for 48 h at (A) 10, (B) 30 and (C) 60 µM, (D) 0 µM without DMSO. F-actin (red), vinculin (green), nucleus (blue), scale bar 50 µm*

When cultured in Col-I, the Blebbistatin-treated cells showed neuronal resemblance. The confocal imaging results are presented in Figure 26. The cells showed round somata with protrusions in several directions. In addition, the cells had minimal actin organization with dense vinculin formation around the nucleus.

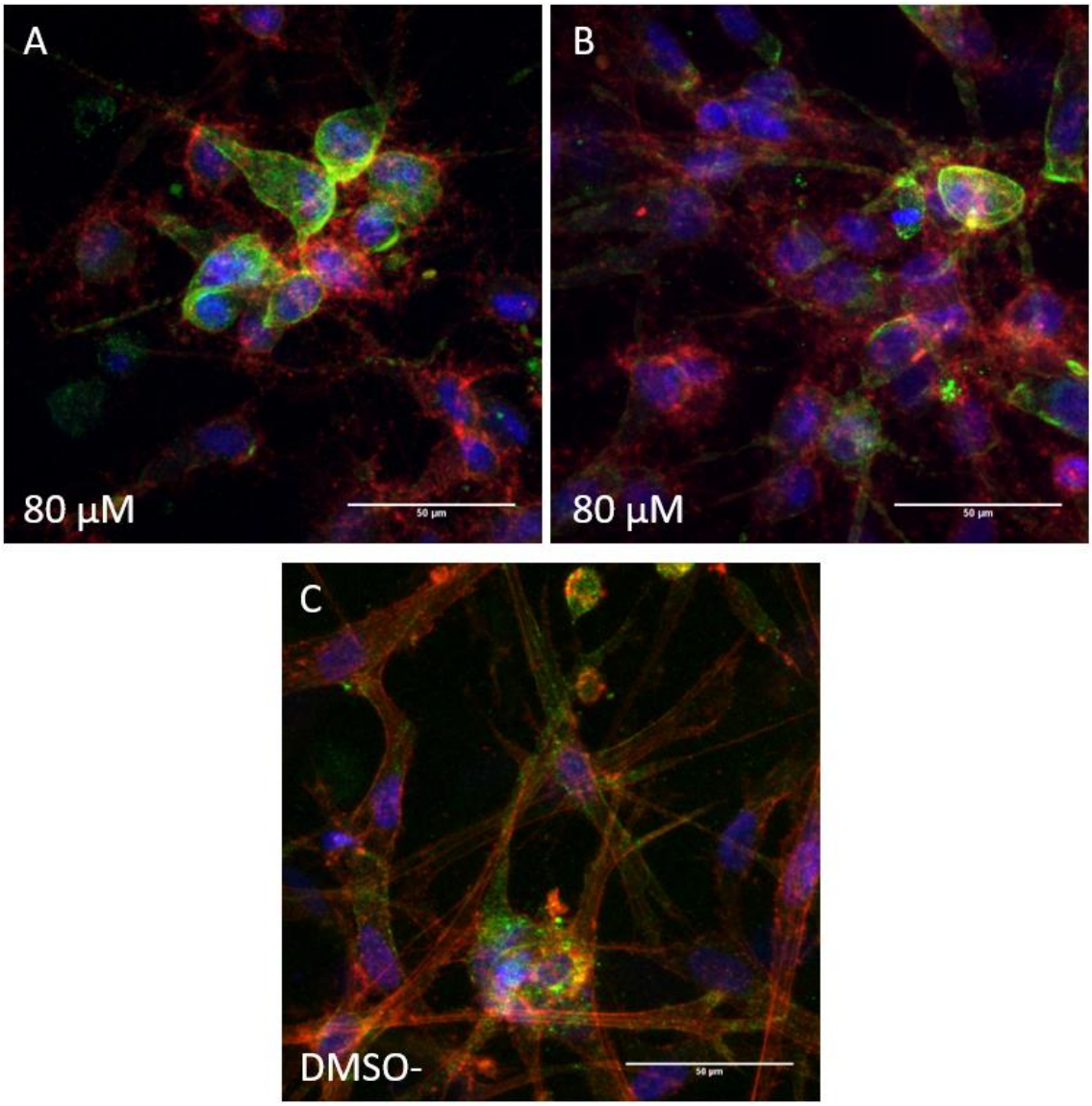

Figure 26. *Fluorescent images of Blebbistatin exposed 3D samples after 48 h. Images were formed from confocal microscope z-stacks: (A, B) 80 µM, 11 z-planes, and (C) DMSO-, 32 z-planes, shift between planes 0.82µm. The z-stack is a sum of all z-planes. F-actin (red), vinculin (green), nucleus (blue), scale bar 50 µm.*

7.4 A critical point was determined for FAK inhibitor

The FAK inhibitor was tested with the viability assay only once in 2D. The representative viability curve is presented in Figure 27. As was with the other inhibitors, DMSO+ was used as the reference value (100 %). The different cultures were exposed to eight concentrations of the inhibitor, performed in twofold dilutions, for 48 hours before the

assay was executed. The graph has the typical shape expected. The viability decreased by almost 40 % at the lowest used concentration (0.1 µM) and reached full apoptosis at a concentration of only 6.4 µM.

In the 3D viability assay, the same concentration range was used as in 2D, but with regular intervals between concentrations (Figure 28). Full apoptosis was not achieved at the highest concentration (10 µM), but the dose-dependent viability loss is clearly visible. The drop in viability after the lowest concentration (2 µM) is not as sharp as in 2D, but takes place in all replicates. It should be noted, that between 7 µM and 10 µM there is little to no difference in viability change.

When comparing the two models it is clear that FAK inhibitor indeed affects the cell culture viability (Figure 28). However, slightly higher concentrations are needed in 3D to achieve the same results as in 2D. Nevertheless, the most drastic drop in viability takes place in the range of ~4–8 µM in both models.

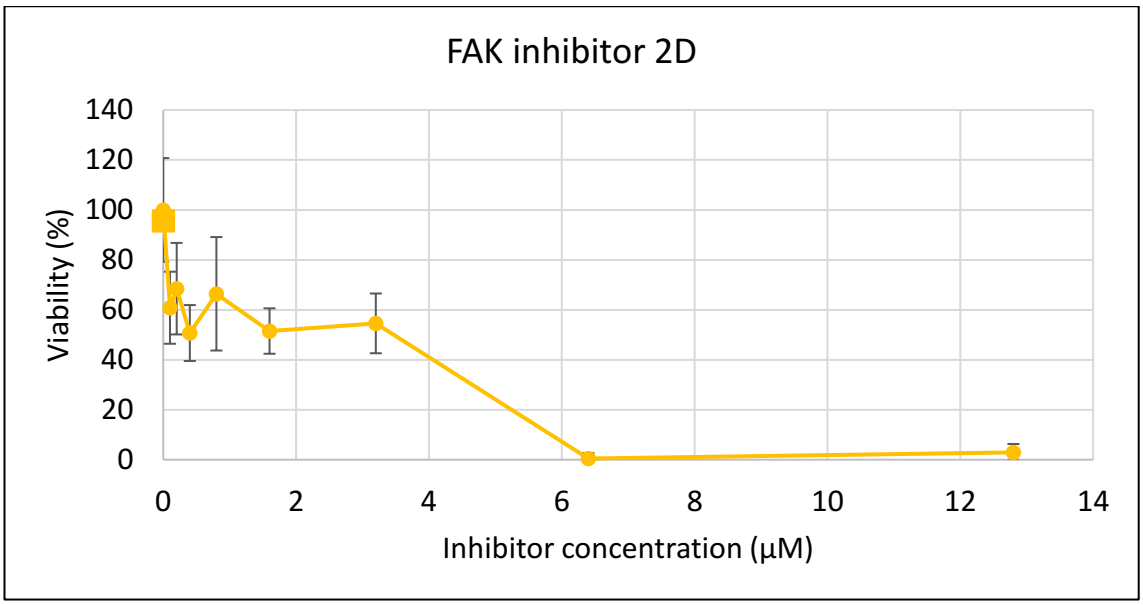

Figure 27. *FAK inhibitor viability assay results 2D. CCK-8 assay results presented as percent viability vs. inhibitor concentration. Exposure time 48 h. The DMSO+ control is taken as a comparison (100 %) and DMSO- is presented as a mean value (square). Values are presented as mean values (n=5) with standard deviation.*

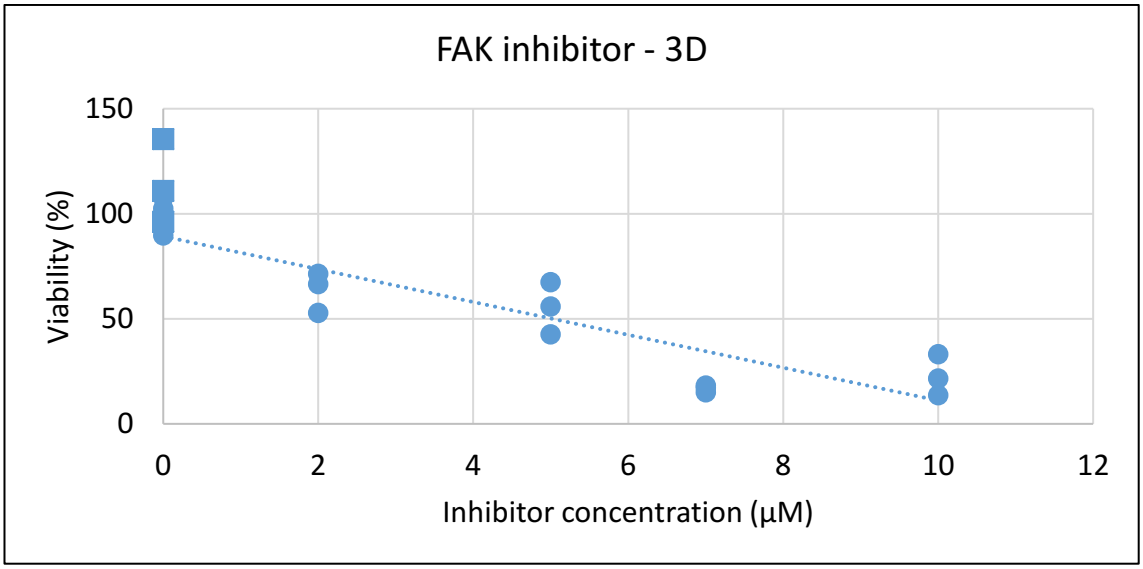

Figure 28. *FAK inhibitor treatment viability assay results from 3D model. CCK-8 assay results presented as percent viability vs. inhibitor concentration, after 48 h of exposure with one inhibitor dose. The DMSO+ control mean value is taken as a comparison (100 %) and DMSO- control is presented as a square for comparison. Each data point represents a single replicate, with a trend line.*

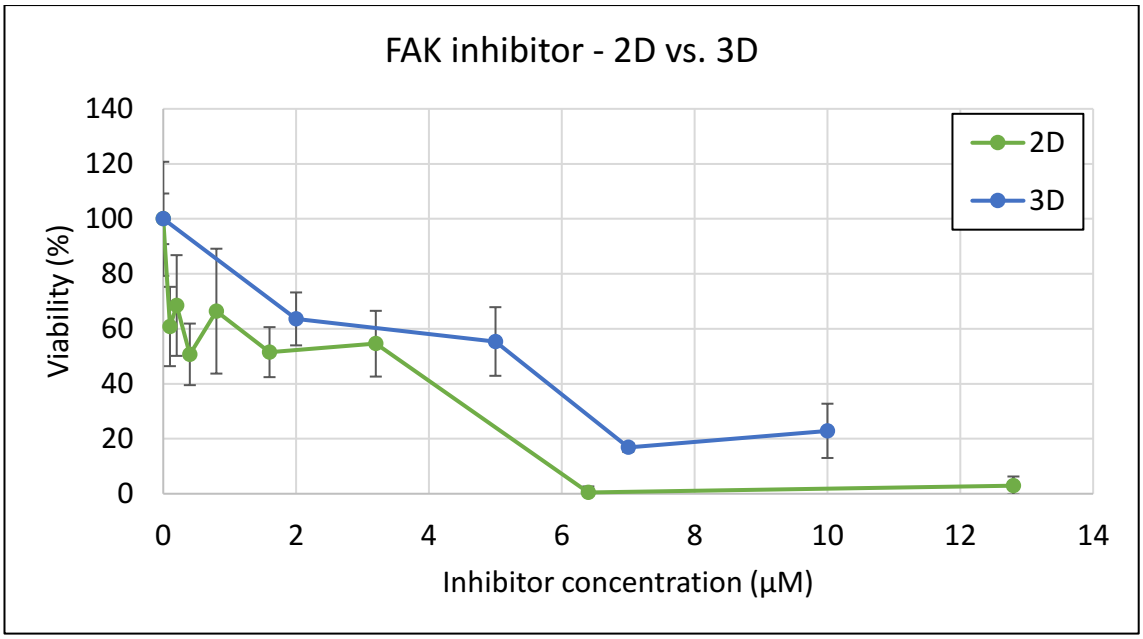

Figure 29. *FAK inhibitor treatment viability assay result comparison 2D vs. 3D. CCK-8 assay results are presented as percent viability vs. inhibitor concentration. Given results vary in culture models. The DMSO+ control (mean value) is taken as a comparison (100 %). Values are presented as mean values, 2D) n=5 and 3D) n=3, with standard deviation.*

The 2D model morphology assay brightfield images from TCP are presented in Figure 30. Here the radical morphological change correlates with the viability tests; there is a clear difference between concentrations 3.2 µM and 6.4 µM. At the two highest inhibitor concentrations, the cells retracted and adopted a rounded morphology, whereas at the lower concentrations, the cells remained in spindle form, as in the controls.

Cells cultured on glass coverslips and treated with FAK inhibitor did not survive, although the DMSO- controls seeded in parallel did survive. Therefore, no immunostaining images are provided from the 2D model. It may have been that the DMSO reacted with the glass, causing the cells to die. The experiment was not repeated due to limited time resources.

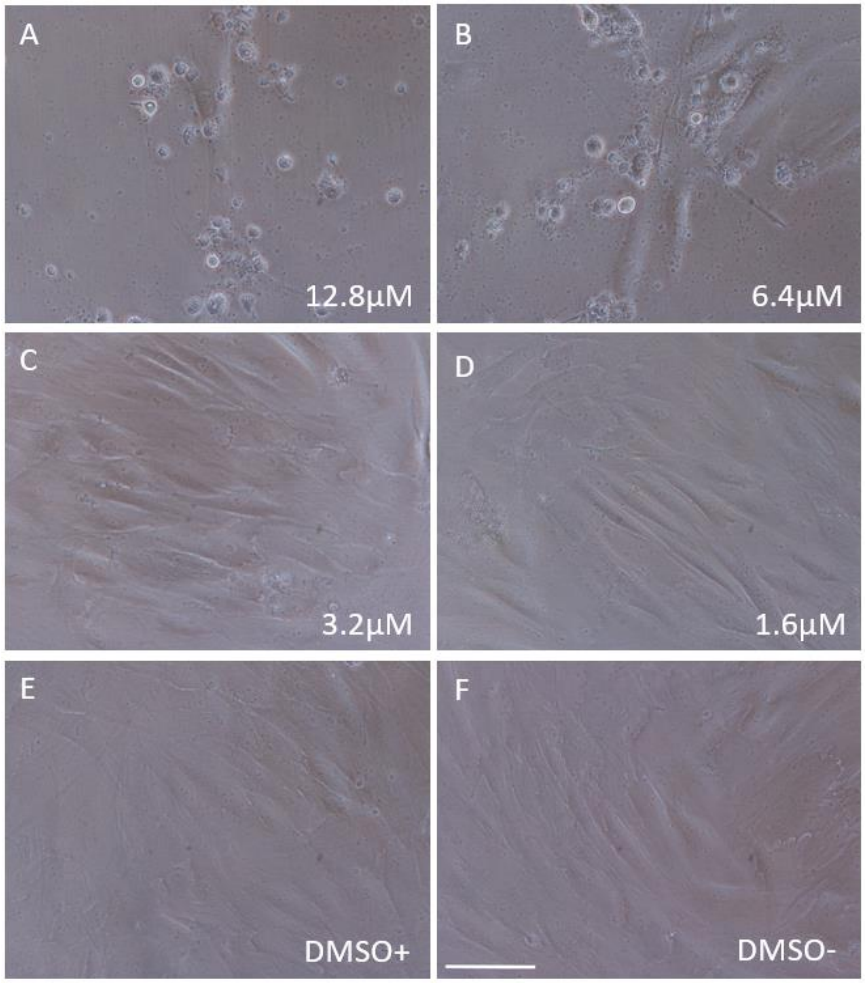

Figure 30. *Brightfield images after 48 h of FAK inhibitor exposure at (A) 12.8, (B) 6.4, (C) 3.2 and (D) 1.6 µM, (E) 0 µM, with DMSO and (F) 0 µM without DMSO, cultured in a 96 well plate scale bar 100 µm.*

The fluorescent images from the 3D confocal imaging are presented in Figure 31. Only the highest 3D model inhibitor concentration was stained for the morphological assessment. The results correlate with the 2D brightfield images, as the cells have very round somata with retracting tails following them. In addition, some apoptotic debris was visible in the samples, showing as vinculin clusters without the nucleus (Fig. 31, 10 µM, right). This correlates with the viability assays.

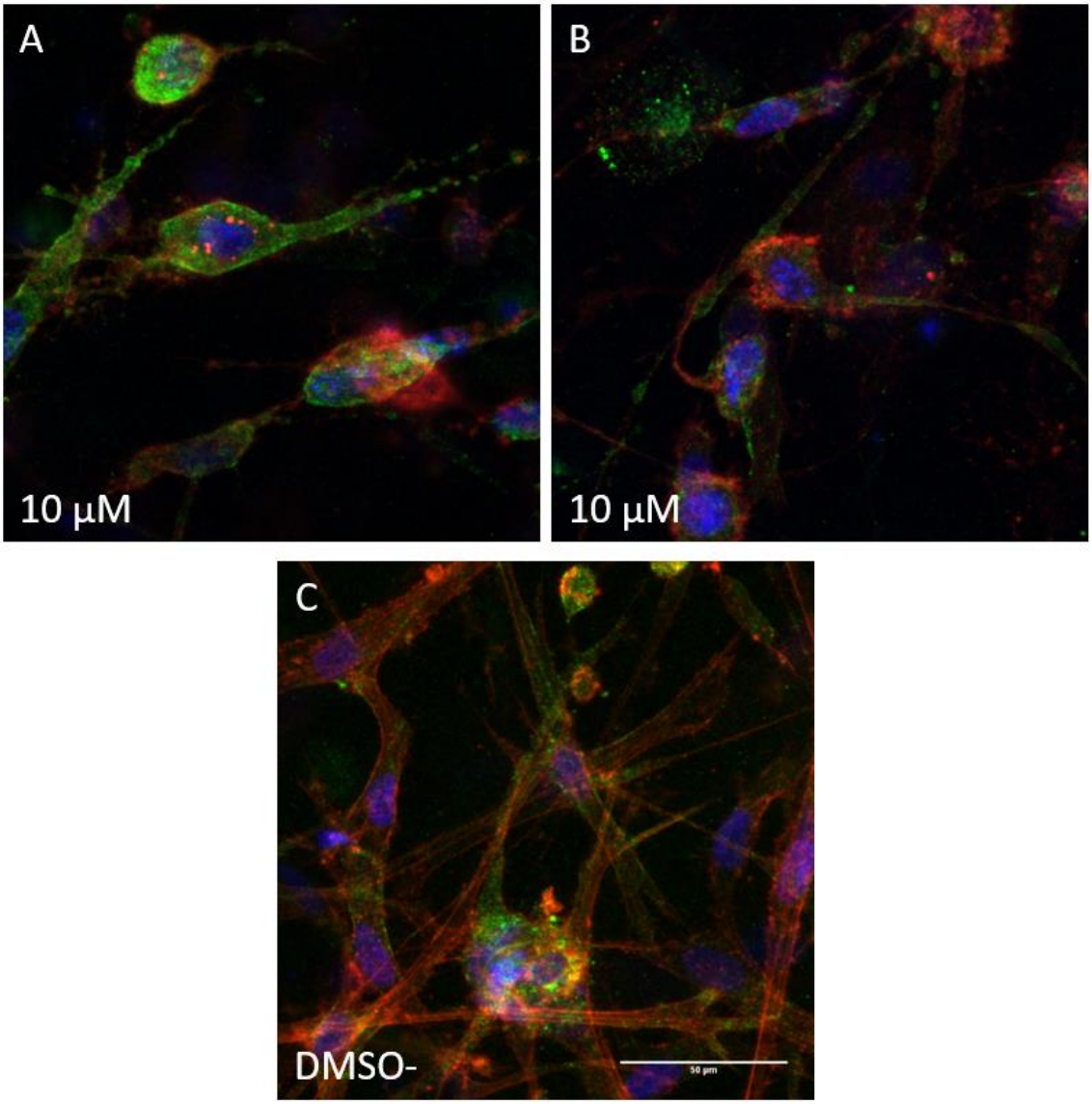

Figure 31. *Fluorescent images of FAK inhibitor-exposed 3D samples. Images were formed from confocal microscope z-stacks: (A) 10 µM, 10 z-planes, (B) 10 µM, 9 z-planes, and (C) DMSO-, 32 z-planes, shift between planes 0.82 µm. The z-stack is a sum of all z-planes. Cells were exposed to the FAK inhibitor for 48 h. F-actin (red), vinculin (green), nucleus (blue), scale bar 50 µm.*

7.5 Determining IC50 values

As a clear decreasing viability was detected in the 2D model of Blebbistatin and both models of FAK inhibitor, the IC50 values can be determined. The effect on viability was plotted against the logarithmic scale of inhibitor concentrations and the values were recorded at 50 % of effect. The plotting is presented in Figure 32 and the calculated values are stated in Table 18.

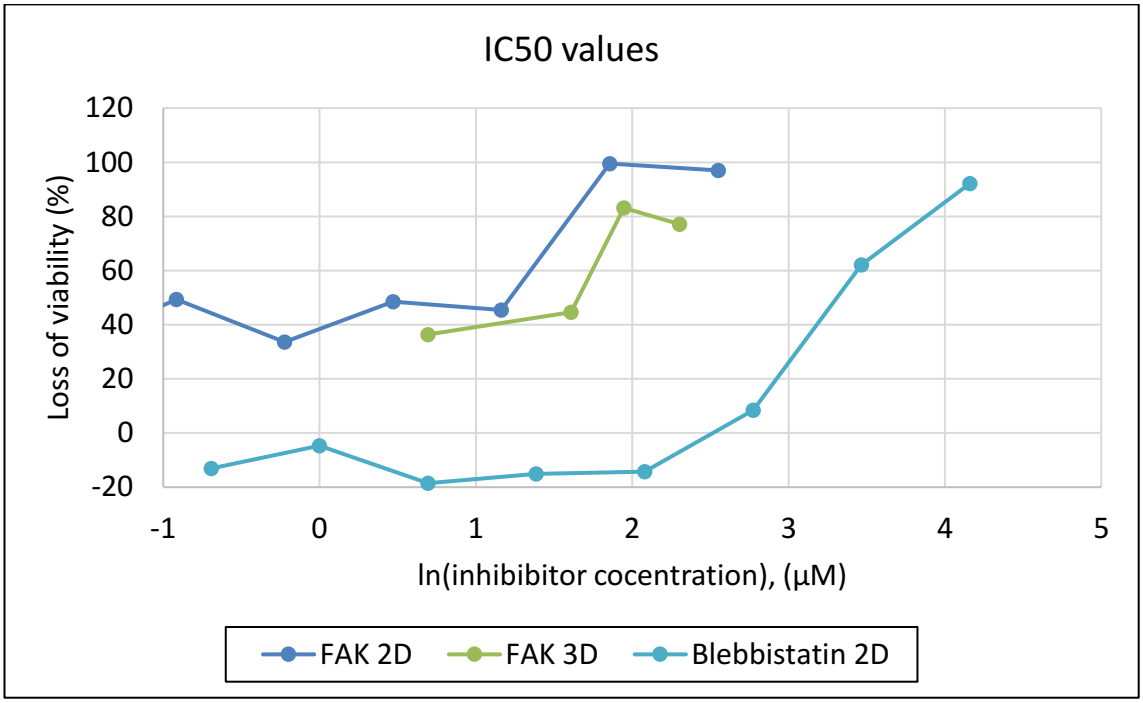

Figure 32. *IC50 calculations for Blebbistatin in 2D and FAK inhibitor in both models. Results are presented as mean values without standard deviation and plotted as loss of viability against logarithmic concentration values (µM). Here the results were read at 50 % loss of viability. All results were achieved through 48 h exposure and one inhibitor dose.*

Table 18. *Calculated IC50 values for the successful viability assays*

Inhibitor and model	*Read value at 50 % viability loss*	***IC50***
Blebbistatin 2D	3.35	~28.5 µM
FAK inhibitor 2D	1.25	~3.5 µM
FAK inhibitor 3D	1.65	~5.2 µM

8. DISCUSSION

8.1 MEK inhibitor

The viability assay with MEK inhibitor gave inconclusive results. The first two set-ups in 2D – 24 hour exposure and 48 hour exposure with two doses – seemed to have a declining trend (Figure 4). However, both barely reached 50 % viability loss and the standard deviation is high, especially after 24 hour exposure. The results achieved after 48 hour exposure with one dose were unsuccessful. It may be considered that some secondary signaling pathways were trying to balance and overrule the effect of the inhibited MEK, but such an effect might not expected to be as strong and fluctuating throughout different concentrations. It is therefore more likely that there was pipetting error in the inhibitor dilutions. The volumes used in the dilutions were extremely small and therefore the probability of manual error was high. In 3D, there was still no strong evidence of the MEK inhibitor affecting cell viability (Figure 5). In addition, the variability between replicates was high. Based on these results, it could be suggested that the MEK-ERK pathway does not directly regulate the viability of cells. Yet, the pathway is a key signaling pathway for several cell functions. Thus, the critical point of the MEK inhibitor should be estimated through other means.

The results are in agreement with the morphological assessment. Small changes were detected in the 2D model in a dose-dependent manner as the actin intensity decreased at ≥30 µM and vinculin build-up was visible at the ruffled edges of the cells at ≥60 µM (Figure 9). This was supported by the confocal images, where there are only mild differences between the MEK treated cultures and the DMSO- control. The vinculin intensity decreased and the cells looked a bit more ruffled from the edges, but the elongated network of cells still remained. The results indicate that there are no major morphological effects resulting from MEK inhibitor treatment and no clear critical point can be determined.

Previously, MEK inhibitor has mostly studied for its effects on differentiation. The connection to osteogenesis has been demonstrated on several occasions (Table 5). Thus, as the results of the present study do not provide information on the critical point, the effects in differentiation could be measured instead. This is supported by the fact that in the present study, only a mild change was detected at concentrations of 30 and 60 µM, whereas in the literature, significant changes were detected with 50 µM (Table 5).

The crystal formation of the inhibitor caused challenges throughout the project. The crystals in the 2D assays could not be rinsed from the culture and caused background staining in the brightfield imaging. The crystals also attached to the tops of the hydrogels,

causing strong background staining and illuminating throughout the gel. This complicated the imaging process. It should therefore be considered that the inhibitor may not have reached the cells in the 3D culture, due to its aggregation outside the gels. In conclusion, due to the contradicting results and problems with the inhibitor aggregates, no conclusion concerning the effects of MEK can be made with any confidence. Instead, the crystal formation issue should be solved and the assays should be performed again. As the medium components and heating were already tested as a solution, the next step should be to test a fresh batch of the MEK inhibitor.

8.2 ROCK inhibitor

For the ROCK inhibitor, the viability results in 2D showed closer correlation than for the MEK inhibitor. Again, there was some decline in cell viability in the 24 hour and the first 48 hour assay. In contradiction, the second 48 hour showed no decrease in viability. There also seemed to be some proliferation at the lower concentrations in comparison to the DMSO+ control. The second assay with the 48 hour exposure could be considered to be unsuccessful, since twofold dilution was not used to prepare the samples, resulting in likely pipetting error. In 3D, an increase in viability was recorded at lower concentrations, with a greater decline at higher concentrations. This could indicate that there is, in fact, an effect on viability, but that higher concentrations are needed than in 2D. Nevertheless, as the highest used concentration was quite high, the effects would most likely be due to toxicity, rather than being due to the effect of inhibiting the signaling pathway. Based on these results it is suggested that the ROCK inhibitor does not affect the viability of the cells.

By contrasts, the morphological assay showed a change in cell morphology in a dose-dependent manner, and the critical point, an IC50 of ~6 µM, could be estimated from the images. This value was estimated based on the fact that clear morphological changes were detected at 8 µM, but not at 4 µM (Figure 16). This IC50 value is rather small when compared to the values referred to in the literature, which most commonly ranging from 10-100 µM. However, downregulation of pFAK and pERK was reported after 5 µM inhibitor treatment on hBMSCs [85] and abrogation of osteogenesis at 10 µM in hMSCs [18]. In addition, 10 µM inhibitor treatment of mMPC leading to ruffling of the cell edges was detected only after 1 hour [81]. Therefore, it could be concluded that the estimated IC50 correlates with the literature. Higher concentrations on other studies could be due to the difference in cell type.

The morphological changes were observed in both models, although the concentrations affecting morphology were threefold higher in 3D. The expected loss of actin fibers was visible throughout the images (Figure 18). In addition, the inhibitor likely caused loss of intracellular tension, as multinucleated cells are present (Figure 18, D). FA formation

seemed to be presented in bundles and mostly at the edges of the cells. At the highest concentration, the cell appeared to be retracting and rounding, and therefore the intensity of vinculin was high (Figure 18, 200 µM). The protrusions can be described as resembling tails. In agreement, it has been hypothesized in the literature that ROCK inhibition induces cell migration [82]. The observable tail has been explained as being an effect of inhibited tail detachment and depolymerization of the stress fibers. On the other hand, ROCK has been described as being a regulator of imbalance in polarity, controlling the fact that there is only one edge leading in the migration, or that cells can have basal and apical sides to them. In this sense, these processes could be the result of polarity regulation and protrusions are therefore created without control. The results in this study are compatible with either theory (Figure 18).

The ROCK inhibitor has been connected to the differentiation potential of stem cells in several studies (Table 9). Typically, differentiation has been linked with osteogenesis, but due to the protrusions, there has been some suggestion that there is an association with neurogenesis. The neurogenic induction demonstrated by Neuhuber et al. changed the morphology of the MSCs, but the effect was reversed after the induction was finished [93]. The neurogenic resemblance both in 2D and 3D environment could be tested in future. In addition, the reversibility of this morphological change could be studied after inhibitor removal.

8.3 Blebbistatin

The viability study on Blebbistatin showed the expected trend in 2D and the 3D model correlates well. It was possible to calculate a critical point from the 2D assay of the first 48 hour exposure, with an IC50 of 28.5 µM. This falls within the range of concentrations investigated in the literature. For Blebbistatin the most commonly stated concentrations have been 50 µM and 5 µM, indicating that perhaps a too high or a too low concentrations have been used, respectively.

There are several reasons why the reliability of the 3D results are questionable, including the variability between replicates and the anomaly at 40 µM. Another reason is that the viability does not decrease enough to confirm the critical point. Therefore, it is either the case that higher concentrations must be investigated in 3D in order for reliable results to be achieved, or that cells are less affected in 3D by Blebbistatin than in 2D.

The morphology of the Blebbistatin-treated cells correlated with the critical point calculated from the viability results in 2D. The morphology of the cells was round in the brightfield images (Figure 23, A, B, C) and they were larger in size, as indicated by the immunostaining (Figure 25, C). The loss of stress fibers indicated changes in other pathways such as ROCK and MEK-ERK as explained by [89]. Moreover, intracellular

contractility and tension was lost in the higher concentrations as multinucleated cells were present and, hence, cytokinesis was likely disabled (Figure 25, C). In 3D, the morphology of the cells was quite different. The somata of the cells were rounding as in 2D, but the cells seemed to aggregate and create networks of processes. As was stated with the ROCK inhibitor, these processes could be intentional protrusions or the result of inhibited tail retraction. Nevertheless, the resemblance to neuronal morphology cannot be discarded and adipogenic and chondrogenic differentiation has been previously observed, so differentiation down various lineages should therefore be tested in future.

8.4 FAK inhibitor

The FAK inhibitor provided the most insightful and conclusive results in the present study. Based on the viability results, a critical point was determined for both models, with IC50 values of ~3.5 µM and ~5.2 µM in 2D and 3D, respectively. In addition, as expected from the hypothesis, there was a difference between the two models, with a higher IC50 in 3D. Few *in vitro* experiments have previously been conducted, but the concentrations that were found in the literature were quite high (10 µM). It should, however, be noted that the treated cells were of cancer lineage. Interestingly, Roberts et al. demonstrated cell cycle inhibition at 3.3 µM, which is extremely close to the IC50 value obtained in the present research. [64]

The morphology changes of the FAK treated cells were in agreement with the viability result, supporting the stated IC50 values. The rounding of the cells indeed correlates with the loss of FAs, which is demonstrated in the literature [62]. Moreover, the loss of FAs likely led to the detachment of the cells and subsequent anoikis, as detected by the viability assay. Unfortunately, the 2D immunostaining was unsuccessful and, thus, the loss of FAs cannot be confirmed without further investigation. In the 3D model it is thought that too high a concentration was used to demonstrate the morphological changes, as the viability was quite low at 10 µM. The cells seemed apoptotic and a lot of cell debris was visible around the stained cells. A lower concentration of 7 µM could have demonstrated the morphological changes more efficiently.

There were no signs from the morphological changes that indicated possible stem cell fate commitment. However, as FAK is upstream in the mechanotransductive signaling in the present study, and a key effector in mechanotransductive response, it is likely that when inhibited, the effects diminish ECM-induced differentiation. Hence, differentiation should in future be studied in matrices of various stiffnesses at the calculated IC50.

8.5 Material speculation

Several improvements could be made to the culturing conditions. For example the hydrogel material could have been replaced with a non-expired hydrogel. On the other hand, the controls were performed with the same material and used as a baseline in the expired material. Another addition to the material studies could have been a Col-I coated 2D experiment. However, the 3D material was chosen after the 2D studies were finished and due to limited time resources the experiment was not executed.

To improve the experiments with the hydrogel, the samples could have been taller. As the samples were quite low, the cells may have been able to sense the stiff glass cover at the bottom of the hydrogel and migrate via durotaxis. This sensing through a thin ECM was stated by Tusan et al. demonstrating that cells sense the stiffness of the underlying material ≤15 μm [94]. As was estimated with the confocal microscope, the height of the used hydrogels were at maximum 30 μm. Therefore, the sensing and possible durotaxis might have been avoided with a different mold and increase in height.

The last material related speculation should be directed to the permeability of the hydrogel. No tests were executed to ensure that the inhibitors reached the cells inside the gels. Yet, changes were detected in all inhibitors except MEK inhibitor. Suspending might have helped. For example, to retrieve the viability assay's yellow hue entrapped in the gels, the solution was pipetted up and down. A similar process could be applied to the inhibitors. In addition, the permeability of the material could be tested through a separate assay. However, the issue of permeability is inherent when working with 3D matrices.

8.6 Assessment of the study

The results of the study may not be accurate due to the limited number to experimental repeats and high variability between the groups. This is especially the case with the 3D experiments which were not tested with several experiment set-ups and different exposure times. Moreover, there were only three replicates.

The results on morphology can be taken as indicators of the possible effects. The morphological changes depend much on the provided ECM as was already demonstrated between the TCP and glass covers and, hence, the differences are expected in 3D, as well. The material properties can vary greatly in stiffness, degradation and ligand presentation, as stated in chapter 3.4. The morphological changes demonstrated here apply only at these concentrations in this material, until proven otherwise.

The first hypothesis of the study was partially proved, as the critical point could be calculated for two inhibitors, FAK inhibitor and Blebbistatin. It was concluded that the ROCK and MEK inhibitors are not directly implicated in affecting cell viability, based

on the achieved results. The second hypothesis was proven via the morphological analysis and the correlation between cell shape and the critical inhibitor concentrations. In addition, with ROCK inhibitor, morphological changes brought additional information, a possible critical point, where the viability assay did not. The third hypothesis of this study predicted a difference between the two models. This was confirmed to be true in the case of all the inhibitors tested, indicating that a higher concentration is required for a similar effect in 3D compared to 2D. Moreover, new information or at least indications of all inhibitors were created throughout this project and study.

8.7 Conclusions

The calculated and estimated IC50 values demonstrate the signaling pathway hierarchy in mechanotransduction. FAK being the upstream signaling protein, regulator of FAs and an activator of the downstream signaling proteins needs only a small concentration (3.5 μM) of inhibitor to cause significant changes in the mechanotransductive pathway in 2D. The disturbance in the pathway caused changes both in viability and morphology. ROCK has a key role in the actin stress fiber regulation and is downstream of FAK. In correlation, an inhibitor concentration of 6 μM was estimated based on the morphological changes. NMMII, being at the very end of mechanotransductive signaling pathways, required the highest concentration. The IC50 of 28.5 μM was enough to affect viability and morphology of hBMSCs in 2D. The effects of disrupting MEK on mechanotransduction were inconclusive and require further investigation.

8.8 Future outlook

To conclude on the weak links of the project, in the future, the study could be improved by four aspects: dilution, repetition, material and assays. As the great variation between the replicates and the unexpected fluctuation in the viability response was most likely due to pipetting error, the dilutions could be performed in stages, in order to pipet larger volumes. The dilutions should also be performed in two-fold dilutions as this was demonstrated to be most reliable. Furthermore, automated pipetting technology could be used to prepare the inhibitor solutions from the stock solutions, almost entirely removing human error. Repetitions should be performed on all inhibitors to confirm the results, but the emphasis should be on the 3D material, which was only tested once. To define the critical point more accurately, various twofold dilutions providing different concentrations could be used.

Another aspect to be added, is to follow the changes in the material during the study. The collagen fibers could be stained and imaged before and after the inhibitor exposure. Here, not only the morphological changes in the cells could be followed stage by stage, but also

the changes in cells ability to reform their surrounding could be assessed, as both are stated as effects of mechanotransduction.

As mechanotransduction and the used inhibitors are connected to differentiation of stem cells, the differentiational assays should be added to the study. These studies could be performed through mineralization or lipid staining to detect osteogenic or adipogenic indication, respectively. The studies could also be taken further by measure the mRNA expression of known proteins as stated in chapter 2. For example, Runx2, PPARγ and Sox9 expression could be tested for osteogenesis, adipogenesis and chondrogenesis, respectively. In addition, the expression of nestin could be tested for neurogenic commitment.

The most important improvement to the present study is to follow the decrease in the active forms of the targeted signaling proteins. Through Western blot the decrease in the activated forms could be detected and, therefore, the functionality of the inhibitors confirmed, both in 2D and 3D. It would also be highly interesting to measure the indirect effects the inhibitors might have on the other signaling proteins.

REFERENCES

[1] A.C. Brignier, A.M. Gewirtz, Embryonic and adult stem cell therapy, The Journal of Allergy and Clinical Immunology, Vol. 125, Iss. 2 Suppl 2, 2010, pp. 336.

[2] I. Ullah, R. Subbarao, G. Rho, Human mesenchymal stem cells - current trends and future prospective, Bioscience Reports, Vol. 35, Iss. 2, 2015.

[3] A.J. Friedenstein, K.V. Petrakova, A.I. Kurolesova, G.P. Frolova, Heterotopic of bone marrow. Analysis of precursor cells for osteogenic and hematopoietic tissues, Transplantation, Vol. 6, Iss. 2, 1968, pp. 230-247.

[4] P.A. Zuk, M. Zhu, H. Mizuno, J. Huang, J.W. Futrell, A.J. Katz, P. Benhaim, H.P. Lorenz, M.H. Hedrick, Multilineage cells from human adipose tissue: implications for cell-based therapies, Tissue Engineering, Vol. 7, Iss. 2, 2001, pp. 211-228.

[5] X. Zhang, M. Yang, L. Lin, P. Chen, K.T. Ma, C.Y. Zhou, Y.F. Ao, Runx2 overexpression enhances osteoblastic differentiation and mineralization in adipose--derived stem cells in vitro and in vivo, Calcified Tissue International, Vol. 79, Iss. 3, 2006, pp. 169-178.

[6] H. Wang, S. Hung, S. Peng, C. Huang, H. Wei, Y. Guo, Y. Fu, M. Lai, C. Chen, Mesenchymal Stem Cells in the Wharton's Jelly of the Human Umbilical Cord, Stem Cells, Vol. 22, Iss. 7, 2004, pp. 1330-1337.

[7] S. Gronthos, M. Mankani, J. Brahim, P.G. Robey, S. Shi, Postnatal human dental pulp stem cells (DPSCs) in vitro and in vivo, Proceedings of the National Academy of Sciences of the United States of America, Vol. 97, Iss. 25, 2000, pp. 13625-13630.

[8] C.M. Raynaud, M. Maleki, R. Lis, B. Ahmed, I. Al-Azwani, J. Malek, F.F. Safadi, A. Rafii, Comprehensive characterization of mesenchymal stem cells from human placenta and fetal membrane and their response to osteoactivin stimulation, Stem Cells International, Vol. 2012, 2012, pp. 658356.

[9] M.F. Pittenger, A.M. Mackay, S.C. Beck, R.K. Jaiswal, R. Douglas, J.D. Mosca, M.A. Moorman, D.W. Simonetti, S. Craig, D.R. Marshak, Multilineage potential of adult human mesenchymal stem cells, Science (New York, N.Y.), Vol. 284, Iss. 5411, 1999, pp. 143-147.

[10] W. Wagner, F. Wein, A. Seckinger, M. Frankhauser, U. Wirkner, U. Krause, J. Blake, C. Schwager, V. Eckstein, W. Ansorge, A.D. Ho, Comparative characteristics of

mesenchymal stem cells from human bone marrow, adipose tissue, and umbilical cord blood, Experimental Hematology, Vol. 33, Iss. 11, 2005, pp. 1402-1416.

[11] W. Xu, X. Zhang, H. Qian, W. Zhu, X. Sun, J. Hu, H. Zhou, Y. Chen, Mesenchymal stem cells from adult human bone marrow differentiate into a cardiomyocyte phenotype in vitro, Experimental Biology and Medicine (Maywood, N.J.), Vol. 229, Iss. 7, 2004, pp. 623-631.

[12] K. Igura, X. Zhang, K. Takahashi, A. Mitsuru, S. Yamaguchi, T.A. Takashi, Isolation and characterization of mesenchymal progenitor cells from chorionic villi of human placenta, Cytotherapy, Vol. 6, Iss. 6, 2004, pp. 543-553.

[13] K. Lee, T.K. Kuo, J. Whang-Peng, Y. Chung, C. Lin, S. Chou, J. Chen, Y. Chen, O.K. Lee, In vitro hepatic differentiation of human mesenchymal stem cells, Hepatology (Baltimore, Md.), Vol. 40, Iss. 6, 2004, pp. 1275-1284.

[14] S.M. Phadnis, M.V. Joglekar, M.P. Dalvi, S. Muthyala, P.D. Nair, S.M. Ghaskadbi, R.R. Bhonde, A.A. Hardikar, Human bone marrow-derived mesenchymal cells differentiate and mature into endocrine pancreatic lineage in vivo, Cytotherapy, Vol. 13, Iss. 3, 2011, pp. 279-293.

[15] C.M. Kolf, E. Cho, R.S. Tuan, Mesenchymal stromal cells. Biology of adult mesenchymal stem cells: regulation of niche, self-renewal and differentiation, Arthritis Research & Therapy, Vol. 9, Iss. 1, 2007, pp. 204.

[16] L. MacQueen, Y. Sun, C.A. Simmons, Mesenchymal stem cell mechanobiology and emerging experimental platforms, Journal of the Royal Society, Interface, Vol. 10, Iss. 84, 2013, pp. 20130179.

[17] F. Matsuoka, I. Takeuchi, H. Agata, H. Kagami, H. Shiono, Y. Kiyota, H. Honda, R. Kato, Morphology-based prediction of osteogenic differentiation potential of human mesenchymal stem cells, PloS One, Vol. 8, Iss. 2, 2013, pp. e55082.

[18] R. McBeath, Cell shape, cytoskeletal tension, and RhoA regulate stem cell lineage commitment, Developmental cell, Vol. 6, Iss. 4, 2004, pp. 483.

[19] M. Ross, W. Pawlina, Histology and a Text Atlas with Correlated Cell and Molecular Biology, 6th ed. Lippincott Williams & Wilkins, 2011, .

[20] L.E. Clements, E.R. Garvican, J. Dudhia, R.K. Smith, Modulation of mesenchymal stem cell genotype and phenotype by extracellular matrix proteins, Connective tissue research, Vol. 57, Iss. 6, 2016, pp. 443-453.

[21] J.C. Chen, C.R. Jacobs, Mechanically induced osteogenic lineage commitment of stem cells, Stem cell research & therapy, Vol. 4, Iss. 5, 2013, pp. 107.

[22] J. Hao, Y. Zhang, D. Jing, Y. Shen, G. Tang, S. Huang, Z. Zhao, Mechanobiology of mesenchymal stem cells: Perspective into mechanical induction of MSC fate, Acta Biomaterialia, Vol. 20, 2015, pp. 1-9.

[23] C. Frantz, K.M. Stewart, V.M. Weaver, The extracellular matrix at a glance, Journal of cell science, Vol. 123, Iss. 24, 2010, pp. 4195-4200.

[24] M.A. Schwartz, Integrins and extracellular matrix in mechanotransduction, Cold Spring Harbor perspectives in biology, Vol. 2, Iss. 12, 2010, pp. a005066.

[25] T.D. Ross, B.G. Coon, S. Yun, N. Baeyens, K. Tanaka, M. Ouyang, M.A. Schwartz, Integrins in mechanotransduction, Current opinion in cell biology, Vol. 25, Iss. 5, 2013, pp. 613-618.

[26] C. Huang, J. Dai, X.A. Zhang, Environmental physical cues determine the lineage specification of mesenchymal stem cells, Biochimica et biophysica acta, Vol. 1850, Iss. 6, 2015, pp. 1261-1266.

[27] D.J. Lee, C. Ho, F. Grinnell, LPA-stimulated fibroblast contraction of floating collagen matrices does not require Rho kinase activity or retraction of fibroblast extensions, Experimental Cell Research, Vol. 289, Iss. 1, 2003, pp. 86-94.

[28] J. Glowacki, S. Mizuno, Collagen scaffolds for tissue engineering, Biopolymers, Vol. 89, Iss. 5, 2008, pp. 338-344.

[29] S. Khetan, M. Guvendiren, W.R. Legant, D.M. Cohen, C.S. Chen, J.A. Burdick, Degradation-mediated cellular traction directs stem cell fate in covalently crosslinked three-dimensional hydrogels, Nature materials, Vol. 12, Iss. 5, 2013, pp. 458-465.

[30] J.P. Jung, M.K. Bache-Wiig, P.P. Provenzano, B.M. Ogle, Heterogeneous Differentiation of Human Mesenchymal Stem Cells in 3D Extracellular Matrix Composites, BioResearch open access, Vol. 5, Iss. 1, 2016, pp. 37-48.

[31] Y. Du, E. Lo, S. Ali, A. Khademhosseini, Directed assembly of cell-laden microgels for fabrication of 3D tissue constructs, Proceedings of the National Academy of Sciences of the United States of America, Vol. 105, Iss. 28, 2008, pp. 9522-9527.

[32] C. Tu, Q. Cai, J. Yang, Y. Wan, J. Bei, S. Wang, The fabrication and characterization of poly(lactic acid) scaffolds for tissue engineering by improved solid–liquid phase separation, Polymers for Advanced Technologies, Vol. 14, Iss. 8, 2003, pp. 565-573.

[33] H. Geckil, F. Xu, X. Zhang, S. Moon, U. Demirci, Engineering hydrogels as extracellular matrix mimics, Nanomedicine (London, England), Vol. 5, Iss. 3, 2010, pp. 469-484.

[34] B. Alberts, J. Wilson, T. Hunt, Molecular biology of the cell, 5. ed. ed. Garland Science, New York, 2008, 90 s p.

[35] Q. Chen, T.H. Lin, C.J. Der, R.L. Juliano, Integrin-mediated activation of MEK and mitogen-activated protein kinase is independent of Ras [corrected, The Journal of biological chemistry, Vol. 271, Iss. 30, 1996, pp. 18122-18127.

[36] J. Jokinen, E. Dadu, P. Nykvist, J. Kapyla, D.J. White, J. Ivaska, P. Vehvilainen, H. Reunanen, H. Larjava, L. Hakkinen, J. Heino, Integrin-mediated cell adhesion to type I collagen fibrils, The Journal of biological chemistry, Vol. 279, Iss. 30, 2004, pp. 31956-31963.

[37] M. Barczyk, S. Carracedo, D. Gullberg, Integrins, Cell and tissue research, Vol. 339, Iss. 1, 2009, pp. 269-280.

[38] C. Le Clainche, M.F. Carlier, Regulation of actin assembly associated with protrusion and adhesion in cell migration, Physiological Reviews, Vol. 88, Iss. 2, 2008, pp. 489-513.

[39] Y.R. Shih, K.F. Tseng, H.Y. Lai, C.H. Lin, O.K. Lee, Matrix stiffness regulation of integrin-mediated mechanotransduction during osteogenic differentiation of human mesenchymal stem cells, Journal of bone and mineral research : the official journal of the American Society for Bone and Mineral Research, Vol. 26, Iss. 4, 2011, pp. 730-738.

[40] J.C. Kuo, Mechanotransduction at focal adhesions: integrating cytoskeletal mechanics in migrating cells, Journal of Cellular and Molecular Medicine, Vol. 17, Iss. 6, 2013, pp. 704-712.

[41] M.C. Brown, C.E. Turner, Paxillin: Adapting to Change, Physiol Rev, Vol. 84, Iss. 4, 2004, pp. 1315.

[42] S. Pellegrin, H. Mellor, Actin stress fibres, Journal of cell science, Vol. 120, Iss. Pt 20, 2007, pp. 3491-3499.

[43] K.A. Kilian, B. Bugarija, B.T. Lahn, M. Mrksich, Geometric cues for directing the differentiation of mesenchymal stem cells, Proceedings of the National Academy of Sciences of the United States of America, Vol. 107, Iss. 11, 2010, pp. 4872-4877.

[44] A.J. Engler, S. Sen, H.L. Sweeney, D.E. Discher, Matrix elasticity directs stem cell lineage specification, Cell, Vol. 126, Iss. 4, 2006, pp. 677-689.

[45] K.E. Kubow, S.K. Conrad, A.R. Horwitz, Matrix microarchitecture and myosin II determine adhesion in 3D matrices, Current biology: CB, Vol. 23, Iss. 17, 2013, pp. 1607-1619.

[46] N. Huebsch, P.R. Arany, A.S. Mao, D. Shvartsman, O.A. Ali, S.A. Bencherif, J. Rivera-Feliciano, D.J. Mooney, Harnessing traction-mediated manipulation of the cell/matrix interface to control stem-cell fate, Nature Materials, Vol. 9, Iss. 6, 2010, pp. 518-526.

[47] Y.S. Pek, A.C.A. Wan, J.Y. Ying, The effect of matrix stiffness on mesenchymal stem cell differentiation in a 3D thixotropic gel, Biomaterials, Vol. 31, Iss. 3, 2010, pp. 385-391.

[48] S.K. Mitra, D.A. Hanson, D.D. Schlaepfer, Focal adhesion kinase: in command and control of cell motility, Nature reviews.Molecular cell biology, Vol. 6, Iss. 1, 2005, pp. 56-68.

[49] J.M. Dunty, V. Gabarra-Niecko, M.L. King, D.F. Ceccarelli, M.J. Eck, M.D. Schaller, FERM domain interaction promotes FAK signaling, Molecular and cellular biology, Vol. 24, Iss. 12, 2004, pp. 5353-5368.

[50] A.P. Gilmore, Anoikis, Cell death and differentiation, Vol. 12 Suppl 2, 2005, pp. 1473-1477.

[51] X. Zhao, J.L. Guan, Focal adhesion kinase and its signaling pathways in cell migration and angiogenesis, Advanced Drug Delivery Reviews, Vol. 63, Iss. 8, 2011, pp. 610-615.

[52] V.M. Golubovskaya, C. Nyberg, M. Zheng, F. Kweh, A. Magis, D. Ostrov, W.G. Cance, A small molecule inhibitor, 1,2,4,5-benzenetetraamine tetrahydrochloride, targeting the y397 site of focal adhesion kinase decreases tumor growth, Journal of medicinal chemistry, Vol. 51, Iss. 23, 2008, pp. 7405-7416.

[53] S.T. Lim, D. Mikolon, D.G. Stupack, D.D. Schlaepfer, FERM control of FAK function: implications for cancer therapy, Cell cycle (Georgetown, Tex.), Vol. 7, Iss. 15, 2008, pp. 2306-2314.

[54] R.W. Tilghman, J.T. Parsons, Focal adhesion kinase as a regulator of cell tension in the progression of cancer, Seminars in cancer biology, Vol. 18, Iss. 1, 2008, pp. 45-52.

[55] A.B. Castillo, J.T. Blundo, J.C. Chen, K.L. Lee, N.R. Yereddi, E. Jang, S. Kumar, W.J. Tang, S. Zarrin, J.B. Kim, C.R. Jacobs, Focal adhesion kinase plays a role in osteoblast mechanotransduction in vitro but does not affect load-induced bone formation in vivo, PloS one, Vol. 7, Iss. 9, 2012, pp. e43291.

[56] J.A. McCubrey, L.S. Steelman, W.H. Chappell, S.L. Abrams, E.W. Wong, F. Chang, B. Lehmann, D.M. Terrian, M. Milella, A. Tafuri, F. Stivala, M. Libra, J. Basecke, C. Evangelisti, A.M. Martelli, R.A. Franklin, Roles of the Raf/MEK/ERK pathway in cell growth, malignant transformation and drug resistance, Biochimica et biophysica acta, Vol. 1773, Iss. 8, 2007, pp. 1263-1284.

[57] F. Chang, L.S. Steelman, J.T. Lee, J.G. Shelton, P.M. Navolanic, W.L. Blalock, R.A. Franklin, J.A. McCubrey, Signal transduction mediated by the Ras/Raf/MEK/ERK pathway from cytokine receptors to transcription factors: potential targeting for therapeutic intervention, Leukemia, Vol. 17, Iss. 7, 2003, pp. 1263-1293.

[58] J.H. Hwang, M.R. Byun, A.R. Kim, K.M. Kim, H.J. Cho, Y.H. Lee, J. Kim, M.G. Jeong, E.S. Hwang, J.H. Hong, Extracellular Matrix Stiffness Regulates Osteogenic Differentiation through MAPK Activation, PloS one, Vol. 10, Iss. 8, 2015, pp. e0135519.

[59] R.K. Jaiswal, N. Jaiswal, S.P. Bruder, G. Mbalaviele, D.R. Marshak, M.F. Pittenger, Adult human mesenchymal stem cell differentiation to the osteogenic or adipogenic lineage is regulated by mitogen-activated protein kinase, The Journal of biological chemistry, Vol. 275, Iss. 13, 2000, pp. 9645-9652.

[60] J.K. Liao, M. Seto, K. Noma, Rho Kinase (ROCK) Inhibitors, Journal of cardiovascular pharmacology, Vol. 50, Iss. 1, 2007, pp. 17-24.

[61] M. Amano, M. Nakayama, K. Kaibuchi, Rho-Kinase/ROCK: A Key Regulator of the Cytoskeleton and Cell Polarity, Cytoskeleton (Hoboken, N.j.), Vol. 67, Iss. 9, 2010, pp. 545-554.

[62] D. Lagares, O. Busnadiego, R.A. García-Fernández, M. Kapoor, S. Liu, D.E. Carter, D. Abraham, X. Shi-Wen, P. Carreira, B.A. Fontaine, B.S. Shea, A.M. Tager, A. Leask, S. Lamas, F. Rodríguez-Pascual, Inhibition of focal adhesion kinase prevents

experimental lung fibrosis and myofibroblast formation, Arthritis and Rheumatism, Vol. 64, Iss. 5, 2012, pp. 1653-1664.

[63] Selleckchem.com - Inhibitor expert: PF-562271 - FAK inhibitor, Selleckchem.com, web page. Available (accessed 04.09.2017): http://www.selleckchem.com/products/pf-562271.html.

[64] W.G. Roberts, E. Ung, P. Whalen, B. Cooper, C. Hulford, C. Autry, D. Richter, E. Emerson, J. Lin, J. Kath, K. Coleman, L. Yao, L. Martinez-Alsina, M. Lorenzen, M. Berliner, M. Luzzio, N. Patel, E. Schmitt, S. LaGreca, J. Jani, M. Wessel, E. Marr, M. Griffor, F. Vajdos, Antitumor activity and pharmacology of a selective focal adhesion kinase inhibitor, PF-562,271, Cancer Research, Vol. 68, Iss. 6, 2008, pp. 1935-1944.

[65] H. Sun, S. Pisle, E.R. Gardner, W.D. Figg, Bioluminescent imaging study: FAK inhibitor, PF-562,271, preclinical study in PC3M-luc-C6 local implant and metastasis xenograft models, Cancer Biology & Therapy, Vol. 10, Iss. 1, 2010, pp. 38-43.

[66] H. Yoon, Y. Choi, J. Song, I. Do, S.Y. Kang, Y. Ko, S. Song, B. Kim, Targeted inhibition of FAK, PYK2 and BCL-XL synergistically enhances apoptosis in ovarian clear cell carcinoma cell lines, PloS One, Vol. 9, Iss. 2, 2014, pp. e88587.

[67] Y. Nakashima, S. Takahashi, Induction of cysteine-rich motor neuron 1 mRNA expression in vascular endothelial cells, Biochemical and biophysical research communications, Vol. 451, Iss. 2, 2014, pp. 235-238.

[68] A.P. Gilmore, L.H. Romer, Inhibition of focal adhesion kinase (FAK) signaling in focal adhesions decreases cell motility and proliferation, Molecular biology of the cell, Vol. 7, Iss. 8, 1996, pp. 1209-1224.

[69] R.M. Salasznyk, R.F. Klees, W.A. Williams, A. Boskey, G.E. Plopper, Focal adhesion kinase signaling pathways regulate the osteogenic differentiation of human mesenchymal stem cells, Experimental Cell Research, Vol. 313, Iss. 1, 2007, pp. 22-37.

[70] A.P. Gilmore, L.H. Romer, Inhibition of focal adhesion kinase (FAK) signaling in focal adhesions decreases cell motility and proliferation, Molecular biology of the cell, Vol. 7, Iss. 8, 1996, pp. 1209-1224.

[71] Selleckchem.com - Inhibitor expert: PD98059 - MEK inhibitor, Selleckchem.com, web page. Available (accessed 04.09.2017): http://www.selleckchem.com/products/PD-98059.html.

[72] P.J. Roberts, C.J. Der, Targeting the Raf-MEK-ERK mitogen-activated protein kinase cascade for the treatment of cancer, Oncogene, Vol. 26, Iss. 22, 2007, pp. 3291-3310.

[73] Q. Liu, L. Cen, H. Zhou, S. Yin, G. Liu, W. Liu, Y. Cao, L. Cui, The role of the extracellular signal-related kinase signaling pathway in osteogenic differentiation of human adipose-derived stem cells and in adipogenic transition initiated by dexamethasone, Tissue Engineering. Part A, Vol. 15, Iss. 11, 2009, pp. 3487-3497.

[74] D.F. Ward, R.M. Salasznyk, R.F. Klees, J. Backiel, P. Agius, K. Bennett, A. Boskey, G.E. Plopper, Mechanical strain enhances extracellular matrix-induced gene focusing and promotes osteogenic differentiation of human mesenchymal stem cells through an extracellular-related kinase-dependent pathway, Stem Cells and Development, Vol. 16, Iss. 3, 2007, pp. 467-480.

[75] A.W. Lund, J.P. Stegemann, G.E. Plopper, Inhibition of ERK Promotes Collagen Gel Compaction and Fibrillogenesis to Amplify the Osteogenesis of Human Mesenchymal Stem Cells in Three-Dimensional Collagen I Culture, Stem Cells and Development, Vol. 18, Iss. 2, 2009, pp. 331-341.

[76] T. Cui, J.J. Jimenez, N.L. Block, E.V. Badiavas, L. Rodriguez-Menocal, A.V. Granda, R. Cai, W. Sha, M. Zarandi, R. Perez, A.V. Schally, Agonistic analogs of growth hormone releasing hormone (GHRH) promote wound healing by stimulating the proliferation and survival of human dermal fibroblasts through ERK and AKT pathways, Oncotarget, Vol. 7, Iss. 33, 2016, pp. 52661-52672.

[77] J.K. Liao, M. Seto, K. Noma, Rho kinase (ROCK) inhibitors, Journal of Cardiovascular Pharmacology, Vol. 50, Iss. 1, 2007, pp. 17-24.

[78] Selleckchem.com - Inhibitor expert: Y-27632 2HCl - ROCK inhibitor, Selleckchem.com, web page. Available (accessed 04.09.2017): http://www.selleckchem.com/products/Y-27632.html.

[79] T. Ishizaki, M. Uehata, I. Tamechika, J. Keel, K. Nonomura, M. Maekawa, S. Narumiya, Pharmacological properties of Y-27632, a specific inhibitor of rho-associated kinases, Molecular Pharmacology, Vol. 57, Iss. 5, 2000, pp. 976-983.

[80] R.A. Worthylake, S. Lemoine, J.M. Watson, K. Burridge, RhoA is required for monocyte tail retraction during transendothelial migration, The Journal of Cell Biology, Vol. 154, Iss. 1, 2001, pp. 147-160.

[81] E.J. Arnsdorf, P. Tummala, R.Y. Kwon, C.R. Jacobs, Mechanically induced osteogenic differentiation--the role of RhoA, ROCKII and cytoskeletal dynamics, Journal of cell science, Vol. 122, Iss. Pt 4, 2009, pp. 546-553.

[82] E. Novozhilova, U. Englund-Johansson, A. Kale, Y. Jiao, P. Olivius, Effects of ROCK inhibitor Y27632 and EGFR inhibitor PD168393 on human neural precursors co-cultured with rat auditory brainstem explant. Neuroscience, Vol. 287, 2015, pp. 43-54.

[83] M. Maldonado, R.J. Luu, M.E. Ramos, J. Nam, ROCK inhibitor primes human induced pluripotent stem cells to selectively differentiate towards mesendodermal lineage via epithelial-mesenchymal transition-like modulation, Stem cell research, Vol. 17, Iss. 2, 2016, pp. 222-227.

[84] C. Wu, Focal Adhesion: A Focal Point in Current Cell Biology and Molecular Medicine, Cell Adhesion & Migration, Vol. 1, Iss. 1, 2007, pp. 13-18.

[85] Y.V. Shih, K. Tseng, H. Lai, C. Lin, O.K. Lee, Matrix stiffness regulation of integrin-mediated mechanotransduction during osteogenic differentiation of human mesenchymal stem cells, Journal of Bone and Mineral Research: The Official Journal of the American Society for Bone and Mineral Research, Vol. 26, Iss. 4, 2011, pp. 730-738.

[86] E. Maharam, M. Yaport, N.L. Villanueva, T. Akinyibi, D. Laudier, Z. He, D.J. Leong, H.B. Sun, Rho/Rock signal transduction pathway is required for MSC tenogenic differentiation, Bone Research, Vol. 3, 2015, pp. 15015.

[87] Selleckchem.com - Inhibitor expert: (-)-Blebbistatin, Selleckchem.com, web page. Available (accessed 04.09.2017): http://www.selleckchem.com/products/blebbistatin.html.

[88] M.A. Ngo, A. Müller, Y. Li, S. Neumann, G. Tian, I.M.C. Dixon, R.C. Arora, D.H. Freed, Human mesenchymal stem cells express a myofibroblastic phenotype in vitro: comparison to human cardiac myofibroblasts, Molecular and Cellular Biochemistry, Vol. 392, Iss. 1-2, 2014, pp. 187-204.

[89] S.R. Caliari, B.A.C. Harley, Structural and Biochemical Modification of a Collagen Scaffold to Selectively Enhance MSC Tenogenic, Chondrogenic, and Osteogenic Differentiation, Advanced healthcare materials, Vol. 3, Iss. 7, 2014, pp. 1086-1096.

[90] T. Sharma, P. Kumari, N. Pincha, N. Mutukula, S. Saha, S.S. Jana, M. Ta, Inhibition of non-muscle myosin II leads to G0/G1 arrest of Wharton's jelly-derived mesenchymal stromal cells, Cytotherapy, Vol. 16, Iss. 5, 2014, pp. 640-652.

[91] A.F. Straight, A. Cheung, J. Limouze, I. Chen, N.J. Westwood, J.R. Sellers, T.J. Mitchison, Dissecting temporal and spatial control of cytokinesis with a myosin II Inhibitor, Science (New York, N.Y.), Vol. 299, Iss. 5613, 2003, pp. 1743-1747.

[92] ThermoFisher Scientific: Collagen I Rat Protein, Tail, ThermoFisher Scientific, web page. Available (accessed 24.07.2017): https://www.thermofisher.com/order/catalog/product/A1048301.

[93] B. Neuhuber, G. Gallo, L. Howard, L. Kostura, A. Mackay, I. Fischer, Reevaluation of in vitro differentiation protocols for bone marrow stromal cells: disruption of actin cytoskeleton induces rapid morphological changes and mimics neuronal phenotype, Journal of neuroscience research, Vol. 77, Iss. 2, 2004, pp. 192-204.

[94] C.G. Tusan, E. Gentleman, S. Yang, B. Senger, N.D. Evans, The effect of extracellular matrix stiffness and dimensions in collective cellular mechanosensing, International journal of experimental pathology, 111 River St, Hoboken 07030-5774, NJ USA, Wiley, pp. A8.